

Department of Aeronautics and Astronautics
Stanford University
Stanford, California

CONTROL OF THE RELATIVE MOTION BETWEEN SATELLITES
IN NEIGHBORING ELLIPTIC ORBITS

by
William R. Davis

SUDAAR No. 274
May 1966

This work was performed in association with research sponsored by the
National Aeronautics and Space Administration
under Research Grant NsG 582

FOREWORD

The research described in this report is the result of an effort which started about November 1964. Since that time the work has been sponsored by three different means. After the initial idea, the first organized impetus came from a Lockheed Independent Research effort which resulted in a proposal to the Air Force. This in turn resulted in three contract change notices that included an initial feasibility study followed by a laboratory development and test phase, and culminated in a hardware flight-test phase which is just now coming to fruition.

The work covered in Chapter 4 and Appendices B and C was mainly supported by the Air Force. The author's time for the remainder of the effort was supported by the Lockheed Independent Research Program and by Lockheed Aerospace Sciences Laboratory overhead budget. The computer effort of Chapter 3 was carried out on the Burroughs 5500 digital machine at Stanford University and was supported there through NASA Contract NsG 582.

This report was submitted to the Department of Electrical Engineering at Stanford University as a dissertation in partial fulfillment of the requirements for a degree of Doctor of Philosophy.

PRECEDING PAGE BLANK NOT FILMED.

ABSTRACT

The relative motion between satellites in neighboring orbits is of interest in three different missions namely rendezvous, station keeping, and dispersion (including orbit prediction). Although both rendezvous and dispersion missions can be treated by the techniques developed, the emphasis in this dissertation is on the "drag make-up satellite" in which satellite air drag is compensated for by continuously thrusting an "outer" satellite so that it never touches an "inner proof mass." The following specific problems are treated: The nature of the relative motion; the control of relative translative motion for an arbitrarily tumbling outer vehicle and also for a completely attitude controlled outer vehicle; and the problem of minimizing limit cycle fuel consumption in the presence of noise in the relative position sensor.

The nature of the motion is investigated in terms of transition matrices. The relative translative motion is typically that between an idealized and a perturbed orbit. Linearized equations are used in which the relative motions are considered small compared to orbit radius and velocity.

The approach to the solution of minimum limit cycle fuel consumption is to compare the performance of three control mechanizations by digital computer simulation. The impulse required to just compensate for drag is known and serves as an ultimate bound on the performance.

A solution to the translative control of a satellite that is attitude controlled to local level is presented in a system which actively controls the relative translative motion of the vehicle relative to the proof mass along one axis only. The proof mass is constrained mechanically transverse to the controlled axis. An error analysis is made of this system by computing bounds on disturbing forces

and by treating these forces as small perturbations. The efficacy of this system is scheduled to be tested in an Agena satellite. Flight hardware has been built and tested.

The nature of the translative motion is expressed in the fundamental matrix solution to the differential equations of motion. This matrix is obtained through the use of a theorem which states that for systems described by the matrix differential equation $F' = FQ$, the relation $Q^\dagger K Q = C$ where K and C are constants, is valid if and only if $F^\dagger K + KF = 0$. This relation gives $Q^{-1} = C^{-1} Q^\dagger K$. The availability of the inverse as a direct product allows expeditious construction of the fundamental matrix $X(\tau_2, \tau_1) = Q(\tau_2) Q^{-1}(\tau_1)$. Fundamental matrices are given. These are in closed form for orbits of arbitrary eccentricity.

The fundamental matrix for the orientation of a free body in terms of Euler parameters is developed and presented. It has the simple form $Q = e^{\frac{\varphi}{2} A} e^{\frac{\psi}{2} C}$ where φ and ψ are standard Euler angles and A and C are particular constant 4×4 skew symmetric matrices.

The results of the investigation of the limit cycle fuel consumption in the presence of position sensor noise are displayed in a series of graphs. The total impulse required for control increased markedly as the ratio of rms noise to dead band was increased to 1. A PWPF control with lead lag derived rate was the least susceptible to noise followed by one using pseudo rate and bang-bang control. A simple lead-lag bang-bang control was the poorest.

The system for single axis control of a drag make-up satellite uses measured position information and pseudo rate for translation control. An error analysis on the effects of the side-wall ball constraints indicates that the root sum square of all effects is less than 0.2% of the effect of the drag force.

ACKNOWLEDGMENT

I would like to thank my advisor Professor B. O. Lange for his help and guidance during these investigations and especially his many helpful suggestions on the first draft of this dissertation. I wish also to thank my colleagues at Lockheed Research Laboratories, especially Professor J. V. Breakwell and Dr. C. M. Petty for their suggestions and stimulating discussions, J. K. Matsunaga who performed the laboratory simulations of Chapter 4 and who was project leader of the hardware fabrication effort, and G. R. Chippendale, M. E. Stickney, and R. L. McKenzie for numerous discussions on the single axis system problem. I am indebted to B. W. Parkinson for many helpful discussions on Algol programming. I would like to thank Mrs. Phyllis Hecht who typed much of the original draft and also Jarvis Todd, my technical editor, and his staff in Lockheed Research Publications for their many extra efforts in producing the final manuscript.

I would also like to thank my supervision at Lockheed and the graduate study program for encouraging and supporting me in these investigations and allowing me the flexibility necessary to satisfy the academic requirements. Finally I would like to thank my neighbor Mr. D. L. Legg and my wife Catherine for their assistance in final proofreading of the manuscript.

W. R. Davis
Menlo Park, Calif.
May 8, 1966

NOMENCLATURE

Symbols (identifiers)

\bar{A}, \bar{B}	2×2 matrices
A, B, G, J	4×4 skew symmetric matrices
b	angular velocity
c	constant column matrix
c_i, f_i, r_i, p_i	2×2 matrices
d	distance
E	expected value operator, eccentric anomaly
e	eccentricity
f	1×2 column matrix
\vec{F}, \vec{f}	specific force
F	system matrix
i, j	2×2 matrices
I	identity matrix
K, N, C	4×4 constant matrix
k	constant
L	vehicle lengths
n, M	mass
P, Q, R, D	4×4 matrices
p, q, r, s	generalized coordinates
t, T, T_1, T_2	time; period; lag- and lead-time constants
x, y, z	local level coordinate system
x, y, q	1×4 column matrices
V_i, u_i, w_i, V_{B-W}	Ball-Wall relative velocity
$u_0, u_1, u_2, V_0, V_1, V_2$	elements in transition matrix
X, Y	fundamental matrices

α	angle of thrust misalignment
β	angle of attack
β_0	4×4 constant matrix
γ	thrust ratio, Euler angle
$\vec{\delta}$	normalized difference vector
Δ	incremental
ϵ	$\sqrt{1 - e^2}$
ξ, η, ξ	components of $\vec{\delta}$
θ	angle
$\vec{\xi}$	position difference vector
σ	standard deviation, inertia ratio
τ	true anomaly
φ	Euler angle, matrizant
ξ, η, ξ, χ	Euler parameters
ψ, Ψ	4×4 matrices
ω	scalar angular velocity
$\vec{\omega}$	vector angular velocity
Ω	matrix angular velocity (4×4) skew symmetric
μ	coefficient of friction, gravitation constant
Λ	diagonal matrix

Indices (subscript)

i, j, k, n

TABLE OF CONTENTS

Chapter		Page
	FOREWORD	iii
	ABSTRACT	v
	ACKNOWLEDGMENTS	vii
	NOMENCLATURE	ix
	LIST OF ILLUSTRATIONS	xiii
1	INTRODUCTION	1
	1.1 Statement of Problem	1
	1.2 Approach to Solution	3
	1.3 Previous Work	5
	1.4 New Results	8
2	SOLUTIONS TO THE EQUATIONS OF RELATIVE MOTION AND THEIR INVERSION	11
	2.1 The Differential Equations of Relative Motion	11
	2.2 The Solution to the Equations of Relative Motion	12
	2.3 The Fundamental Matrix	14
	2.4 Symplectic Matrices	15
	2.5 Theorem on K-Orthogonality	16
	2.6 Inversion of the Tschauner-Hempel Matrizant	19
	2.7 Fundamental Matrix for a Non-Canonical State Vector	31
	2.8 The Fundamental Matrix of the Orientation of a Free Body in Euler Parameters	35
	2.8.1 The Form of the Matrizant Solution	41
	2.8.2 Theorem on the Form of the Angular Rotation Matrix	44
	2.8.3 Exponential Form of the Matrizant Q	45
	2.8.4 Geometric Interpretation of the Exponents of Q	47
	2.8.5 Explicit Form of the Fundamental Matrix Q	50
3	EVALUATION OF THRUST CONTROL SYSTEMS FOR A TUMBLING VEHICLE	53
	3.1 Precise Statement of Limit Cycle Fuel Consumption Problem	54
	3.2 The Dynamic Characteristics of the System (Plant)	55
	3.3 Actual Rate Systems	58
	3.3.1 Proportional Control	58

Chapter		Page
	3.3.2 On-Off Control	60
	3.3.3 Limit Cycle Performance With Bang-Bang Control	62
	3.4 Derived Rate Systems	65
	3.4.1 Pseudo Rate With Bang-Bang Control	68
	3.4.2 Lead-Lag With Bang-Bang Control	73
	3.4.3 Lead-Lag With Pulse Width Pulse Frequency Modulation Control	
	3.5 System Performance With Position Measurement Noise	76
4	THE SINGLE AXIS DRAG MAKE-UP CONTROL SYSTEM	92
	4.1 System Components	92
	4.2 Sensor Theory of Operation	96
	4.3 Control System Dynamics	97
	4.4 Laboratory Simulation of the Control System	98
	4.5 System Error Analysis	101
	4.5.1 End Wall Hit	104
	4.5.2 Side Wall Contact	105
	4.5.3 Vehicle Gravity Force	123
	4.5.4 Perturbation Due to Vehicle Magnetic Fields	126
	4.5.5 Perturbations Due to Electric Forces	127
	4.5.6 Perturbations Due to Misalignment of Attitude Control Jets	127
5	CONCLUSIONS AND RECOMMENDATIONS	129
Appendix		
A	LINEARIZED EQUATIONS OF RELATIVE MOTION FOR SATELLITES IN NEIGHBORING ELLIPTIC ORBITS	131
B	FOLLOW THE BOUNCING BALL	145
C	PSEUDO RATE LIMIT CYCLE PERFORMANCE	159
D	PWPF Control	163
	REFERENCES	165

LIST OF ILLUSTRATIONS

Figure		Page
2-1	Rotation of a Rigid Body in Terms of Euler Angles	47
3-1	Block Diagram of Relative Translational Motion	56
3-2	X Channel (Typical): Actual Rate With Linear Control	59
3-3	Y-Axis Capture With Actual Rate and Proportional Control	61
3-4	Y-Axis Capture With Actual Rate and Bang-Bang Control	61
3-5	Y-Axis Capture With Actual Rate and Proportional Control With Dead Band and Hysteresis	63
3-6	Y-Axis Capture With Actual Rate and Bang-Bang Control With Dead Band and Hysteresis	64
3-7	Y-Axis Limit Cycle Performance Actual Rate	66
3-8	X Jet Thrust in Orbit Frame	67
3-9	X Channel (Typical) Pseudo-Rate Control System	69
3-10	Pseudo Rate Capture Performance	70
3-11	Pseudo Rate Limit Cycle Performance	71
3-12	Y-Axis Capture Partial Pseudo Rate	72
3-13	X Channel (Typical) Lead-Lag With Bang-Bang Control	74
3-14	Y-Axis Capture Lead-Lag With Bang-Bang Control	75
3-15	X Channel (Typical) Lead-Lag With PWPF Control	77
3-16	Y-Axis Capture LL-PWPF Control	78
3-17	Y-Axis Limit Cycle LL-PWPF Control	79
3-18	Limit Cycle Fuel Consumption in the Presence of Noise: Actual Rate With Bang-Bang Control	82
3-19	Limit Cycle Fuel Consumption in the Presence of Noise: Pseudo Rate With Bang-Bang Control	83
3-20	Limit Cycle Fuel Consumption in the Presence of Noise: Pseudo Rate With Bang-Bang Control	84
3-21	Limit Cycle Fuel Consumption in the Presence of Noise: Pseudo Rate With Bang-Bang Control	85
3-22	Limit Cycle Fuel Consumption in the Presence of Noise: Pseudo Rate With Bang-Bang Control	86
3-23	Limit Cycle Fuel Consumption in the Presence of Noise: Partial Pseudo Rate With Bang-Bang Control	87
3-24	Limit Cycle Fuel Consumption in the Presence of Noise: Partial Pseudo Rate With Bang-Bang Control	88

Figure		Page
3-25	Limit Cycle Fuel Consumption in the Presence of Noise: Lead-Lag Rate With Bang-Bang Control	89
3-26	Limit Cycle Fuel Consumption in the Presence of Noise: Lead-Lag Rate With Bang-Bang Control	90
3-27	Limit Cycle Fuel Consumption in the Presence of Noise: Lead-Lag With PWPF	91
4-1	Drag Make-Up System	93
4-2	Position Sensor	93
4-3	Position Sensor Optical Components	94
4-4	Ball-In-Cage Mechanization	94
4-5	Block Diagram of Electronics Package	95
4-6	Single Axis Control System Block Diagram	97
4-7	Laboratory Test Fixture	97
4-8	Acquisition Behavior	100
4-9	Trajectory Perturbation Due to In-Track Force	103
4-10	Trajectory Perturbation Due to Cross-Track Force	103
4-11	Position Versus Time Under Constant Drive Force	106
4-12	Thrust Misalignment	108
4-13	Wall-Ball Relative Velocity	109
4-14	Wall-Ball Relative Velocity With Contact	111
4-15	Angle of Attack	112
4-16	Vehicle Mass Distribution	124
C-1	Limit Cycle Phase Plane Diagram	159

Chapter 1

INTRODUCTION

1.1 STATEMENT OF THE PROBLEM

The relative motion between satellites in neighboring orbits is of interest in three different types of missions. These are (1) rendezvous, in which the objective is to bring two satellites from slightly different orbits into close proximity in the same orbit and possibly to maintain some specified relative position; (2) station keeping, in which the objective is to maintain a satellite on some particular trajectory; and (3) dispersion, in which the objective is to separate two objects, which were once in identical orbits (perhaps attached), according to some particular schedule. This latter category also includes the ephemeris-prediction type problem in the sense that one may postulate a satellite in some idealized, nominal orbit and study the ephemeris of an actual satellite in terms of its relative displacement from the idealized one.

By directing attention to the relative motion between the satellites one sees that the differential equations of the relative motion are the same for all three types of missions. This equivalence offers the possibility that solutions to problems presented by one mission may have direct application to the others.

The dynamical system whose control problem will be investigated in this dissertation is represented by these differential equations of relative motion. An important part of this (control) problem is the response of the unforced part of these equations, or equivalently the computation of the state transition matrix, which gives the nature of the relative motion between satellites under no differential forces. Knowledge of the nature of the unforced motion is essential to solving the problem of control of the motion under various differential forces.

Although both rendezvous and dispersion missions can be treated by the techniques developed in this dissertation, the principal problem which will be discussed is the station keeping mission or more specifically the so-called

zero-g or "drag-make-up" satellites.* In these missions the objective is to maintain two distinct objects, subject to various differential forces, the most significant being drag, in close proximity and in identical orbits for extended periods of time.

Thus, the following specific problems are addressed:

- The nature of the relative motion between satellites that can be considered quite close, (i.e., in nearly the same orbits) but with no restriction as to the eccentricity of the orbits (the form which the solution of this problem takes makes it especially useful for computing orbit perturbations due to disturbing forces which persist over very long periods i.e., months to years)
- The control of the relative translative (center of mass) motion by active means for two important special cases of relative angular motion – namely, for the case in which the angular motion of the controlled vehicle is completely and continuously controlled resulting in the translative (center of mass) motion being essentially one-dimensional along the direction of the instantaneous drag force** and, at the other extreme, the case in which the vehicle experiencing the translative control is allowed to tumble freely and arbitrarily in attitude
- The so-called "limit-cycle" fuel-consumption problem – in which it is desired to design a gas expulsion control system which maintains the desired vehicle-ball state within some specified distance of the origin in the presence of noise in the measurement of the state with a minimum expenditure of fuel

*Drag make-up is the preferred terminology and in this dissertation refers to the concept of continuously compensating for satellite air drag by thrusting an "outer" satellite so that it never touches an inner "proof mass" at least in the direction of the drag force. Since the inner mass is shielded from the air stream, it experiences no drag and to the extent that the outer vehicle does not perturb it, it will proceed on a purely gravitational trajectory.

**This "single-axis drag make-up satellite" is especially simple to mechanize in satellites which control their attitude relative to a locally-level reference frame. It is only necessary to provide one thruster which fires always to oppose the drag. The proof mass or "ball" is located in a tube or "cage" which constrains the ball mechanically in the directions transverse to the controlled axis. This concept which was originated and developed by the author is in the final stages of hardware development and will soon be flown on an Agena satellite.

- The determination of trajectory perturbations which result from the disturbing forces associated with the "single axis drag make-up satellite" as a consequence of the transverse constraint on the ball by the vehicle (cage)

Several applications for low-altitude zero-drag satellites have already been stated. These include geodesy, aeronomy, orbit sustaining, precision gyroscope development and testing, scientific experiments including the gyroscope precession predicted by general relativity (Pugh-Schiff), time dependence of the gravitational constant (Dicke), and others in which a zero or near zero acceleration field is necessary.

1.2 APPROACH TO SOLUTION

One can separate methods of problem solution into two basic categories: theoretical and experimental. Most complex system problems require both. In this dissertation the efforts to define the nature of the relative motion are theoretical, whereas the development of systems for control is both theoretical and experimental.

Much of the investigation on the nature of the motion is carried out in terms of transition matrices which relate the state of the "system" at different values of some independent variable, e.g., time or true anomaly. The state of the system is typically expressed as a column matrix (or vector). In the case of the relative motion between the center of masses of the two satellites, for example, the state vector is of even dimension, half referring to the relative displacement and half to the relative velocity.

Several methods are available for getting appropriate equations of relative motion. The approach taken here follows most closely that of G. W. Hill who first used relative displacement between the actual and an ideal orbit of the moon to improve the knowledge of the moon's actual orbit.

The technique of using linearized approximate equations to get closed form solutions is standard. The major approximation used herein for investigating the nature of the motion is that the relative motion (e.g., position and/or velocity) is very small compared to the corresponding orbit elements. No limitation is

explicitly placed on the eccentricity. However, since the major interest is in satellite trajectories, some of the expressions are valid only for eccentricity less than 1.

The approach taken in the study of the means of controlling the translative motion between satellites was to compare several different control mechanizations by digital computer simulation. This technique is becoming more common with the ready availability of high speed digital computers and the requirement for investigating complex, often nonlinear, systems. The system which emerges as preferred from this approach is in a sense optimum, i.e., in comparison to the others evaluated. However, for the criterion of limit-cycle fuel consumption, the absolute optimum performance is not known, and one is not able to assess a given system on an absolute scale.

In drag-make up satellites the requirement for thrust in opposition to drag for extended periods of time in light of the limited propulsive energy storage capability on board a satellite suggests fuel consumption as a major optimization criterion. Thus, with some deference to system simplicity for reliability, the approach taken in this study was to assess control systems primarily in terms of fuel economy. Furthermore since initial capture will occur only once during the mission (or in the presence of disturbances only a few times) the important problem is to minimize the consumption of on-board propellant during the control limit cycles.

In making this assessment one is confronted on the one hand with the fact that there is no known method available for synthesizing a control system which minimizes the limit-cycle fuel consumption; however, for any drag make-up system the best one could ever expect in fuel consumption is that just necessary to provide a thrust force equal (and opposite) to the drag force. This provides a reference for assessing a system on an absolute scale. However, the choice of a given control mechanization over another can only be determined on a relative basis at the present time.

Because of undetermined force interactions between the two vehicles the proof mass will not follow a "purely-gravitational" orbit. In order to analyze the effect of these "errors" the approach will be to first compute bounds on their magnitudes and then to treat these errors as small perturbations driving the linearized equations of relative motion. When it is appropriate the errors will be considered to be uncorrelated and their effects determined individually. The combined effects are then viewed in terms of appropriate statistics.

The ultimate test of any system is in actual operation. For satellite systems this is a very expensive proposition. However, the author is fortunate to be associated with a program in which the single-axis thrust system described in this dissertation will be flown. Although the flight results will not be available in time for publication in this dissertation. The error analyses in this dissertation will be used in the interpretation of the flight results.

1.3 PREVIOUS WORK

The present effort is derived from and is an extension of work at Stanford on drag make-up satellites. Lange (Ref. 1) indicated several applications for drag make-up satellites, obtained the equations of motion referenced to a circular orbit, proposed and investigated several control schemes, and identified significant errors in a trajectory error analysis. The problem of trajectory analysis and associated transition (or covariance) matrices by which the future state of a gravitational trajectory can be computed from a present known state has received considerable attention in recent years especially with the advent of numerical solutions with digital computers. The area of special interest here, that of closed form solutions for the transition matrices, is generally viewed to have started with Hill in 1878 in which he studied the ephemeris of the moon in terms of the relative motion between the moon and a reference system which was located at the center of the earth and moving in orbit around the sun. More recently numerous workers Danby (Ref. 2), deVries (Ref. 3), Clohessy and Wiltshire (Ref. 4), Battin (Ref. 5), and finally Tschauner and Hempel (Ref. 6), to name a few, have presented transition matrices in various forms. The work of Tschauner and Hempel, which came from the search for optimum acceleration programs for rendezvous, was particularly useful in that by choosing the true anomaly as the independent variable and by appropriate normalization, they were able to give a very simple closed-form solution in the form of a position/velocity state transition matrix for reference orbits of arbitrary eccentricity.

These solutions are often formulated as a "fundamental" transition matrix which defines the state of the system (relative displacement and velocity between an actual and a reference orbit) at an arbitrary future time in terms of the initial state.

As presented by Tschauner and Hempel these solutions are for the homogeneous or force free case. They were used by Lange and Smith (Ref. 7) for getting long term propagation of certain periodic perturbations of drag-free satellites in eccentric orbits.

In order for the homogeneous solutions to be generally useful for the case in which perturbing forces are present one needs not only a transition matrix that goes in one direction but also its inverse (which corresponds to the reverse transition). The equivalence between canonical transformations and certain transition matrices has been discussed by several authors especially Wintner (Ref. 8), Battin (Ref. 5), Synge (Ref. 9), Siegel (Ref. 10), and Garfinkel (Ref. 11). Transition matrices which are "equivalent" to canonical transformations, (in a sense to be defined precisely later) turn out to also be symplectic. They have a special symmetry which allows their inverse to be obtained through a direct matrix multiplication involving only knowledge of the transpose. These authors have primarily been interested in transitions between states in mechanical systems (i.e., mechanics and dynamics).

The concept of using a state vector to describe the condition of a system is of course not confined to dynamics. It is a very useful concept for treating all systems equally without regard to their particular function. Pease (Ref. 12) has found it useful, in dealing with the "states" of interacting electron beams in traveling wave electron tubes, to search for special symmetry in the state transition matrices that in essence provides a basis or "metric" in which the matrix is symmetric. In particular he calls a matrix M K -Hermitian (K -symmetric) if, for some constant Hermitian (symmetric) matrix K , the matrix formed by the matrix product KM is skew-Hermitian (symmetric). He then points out that if the (system) coefficient matrix (in a list order linear differential equation) is K -Hermitian (K -symmetric) then the matrizant* is K -unitary (K -orthogonal)** This of course leads to a direct method of computing the inverse. A generalization of this concept can be applied to the transition matrices between states of satellite relative motion.

*In this dissertation matrizant will refer to an integral solution to a first order matrix differential equation. The term fundamental matrizant will be used for a particular matrizant (see p. 12).

**A matrix M is said to be K -orthogonal if $M^\dagger KM = K$ where M^\dagger denotes the transpose of M .

In analyzing the performance of the translation control system of an arbitrarily tumbling satellite, it is necessary to be able to compute its orientation given the initial attitude and rate. Euler, Gayley, Klein and many others have presented several ways of describing the motion of a rigid body. See Refs. 13 through 15. In this dissertation we will use the Euler symmetric parameters first proposed by Euler.

The relation between Euler's symmetric parameters and Euler angles can be found in most modern dynamics texts (e.g., see Goldstein). Interest in the symmetric parameters has revived with the emergence of the digital computer since there are several advantages, including fewer integrations, to doing numerical computations on rigid body rotations in terms of these parameters. The recent treatment by Weiten (Ref. 16), in which the four Euler parameters were used to define the "state" (vector) of the system suggested the possibility of obtaining a general formulation of the transition matrix between arbitrary states.

The basic drag-make up control problem is to maintain the position of the outer satellite relative to a reference (proof mass) by measuring the relative displacement and applying a control force. For the case of uniaxial thrust applied to a very slowly rotating vehicle it reduces to a classical second order $1/s^2$ control problem. For the arbitrarily tumbling outer vehicle, however, the problem is complicated by the rotation, especially since the position measurements and control forces are most conveniently mechanized in a tumbling reference frame (fixed in the vehicle) whereas air drag, the major perturbing force to be countered, is an approximately constant vector in a reference which remains locally level and hence rotates once per orbit.

One is faced with three interdependent major system problems, the control law to use, the measurements to make, and the control actuators to use. Previous experience (Refs. 17 through 19) with control systems for long-term space systems especially in terms of component reliability and gas leakage strongly suggests the use of on-off type actuators. For this reason the use of on-off actuators was stipulated in the present work.

The knowledge of the state of the system which will be necessary for the translation control system can be acquired either by direct measurement or by interference from certain "derived states." Lange (Ref. 1) has observed that for an arbitrarily tumbling vehicle the relative position and velocity between the vehicle and proof mass coordinated in an inertial frame can be used in linear

combination to effect a simple control law with linear elements. In light of Aizerman's conjecture (Ref. 20) it seems reasonable to believe that on-off controls (thrusters) should also be feasible for this system without compromising stability.

In order to implement such a control law position and/or velocity must be known. One must certainly measure position if long term relative position is to be kept arbitrarily small. In a second order system velocity provides damping. Fortunately it does not have to be known with high precision. This suggests the possibility of deriving velocity. The use of derived states to create quantities necessary for system stability has a history nearly as long as closed loop control systems. The recent work of Luenberger (Ref. 21), however, summarizes the general picture very well. The technique referred to in this thesis as "pseudo rate" follows closely that of Leonard (Ref. 22) in which the output of the switch which turns on the thrust (acceleration) is integrated once to produce a velocity (rate) related signal. See also Nicholas and Vivian (Ref. 23).

Two other systems use lead-lag circuits in the direct signal path to introduce rate information into the system. In one of the systems a simple bang bang control is used. The other identified as PWPF (pulse width, pulse frequency) modulation follows most closely the work of Trimmer (Ref. 24).

A detailed system error analysis is essential not only for giving an indication of how well the system may perform but also to provide a basis for design trade-offs in detailed system (e.g., component) decisions. Lange (Ref. 1) presents quite a complete error analysis on the effect of various possible perturbations on the trajectory of a drag free satellite. It is predicated on the assumption that the outer vehicle never touches the reference (proof) mass. As such it provides a reference performance against which to compare the system proposed in Chapter 4.

1.4 NEW RESULTS

In Chapter 2, a basic theorem relating the K-symmetry of the coefficient matrix in a first order linear differential equation to the K-orthogonality of a matrizant solution to the equation is presented and proved. In the event of

certain "K" symmetry in the coefficient matrix it turns out that the inverse of the matrizant can be obtained by a simple matrix product which includes the transpose of the matrizant. The implication of this is that the matrizant is orthogonal in a sense which will be defined precisely in Chapter 2. It is closely related to the symplectic property of canonical transformations, which itself is a special case of K-orthogonality.

This theorem is similar to a relation noted by Pease (Ref. 12), but is somewhat more general in that it requires no constraint on the symmetry of the K and also that it can accommodate directly a matrizant corresponding to arbitrary initial conditions.

This theorem is used to get a general inverse to the matrizant of Tschauner and Hempel for the relative motion of two satellites in neighboring elliptical orbits. Fundamental matrizants for both canonical and non-canonical state transitions are given.

This theorem also has important application in the analysis of translation control systems for tumbling symmetric vehicles. Basic Floquet factorization, valid for periodic coefficient matrices, is used to arrive at an interesting insight into the structure of the "fundamental matrizant" for the transition between states of a rigid free body (i. e., subject to no external torques) having two equal principal moments of inertia. A condition (theorem) on the nature of the coefficient matrix which leads to the unique form of the fundamental matrizant is stated and proved. The fundamental matrix for a free body (of two equal inertias) is computed and presented.

In Chapter 3, an "experimental" evaluation of three different systems for translative control of a tumbling satellite is presented. The feasibility of using on-off controls with the control law proposed by Lange (Ref. 1) was established by simulation of the basic system (i. e., using actual rate for damping) on a Burroughs 5500 digital computer. Following this, the limit-cycle fuel consumption and capture properties of three different systems with on-off controls including dead band and hysteresis were compared by digital simulations. The systems

are identified by the method of obtaining rate information and by actuator modulation technique as (1) lead lag with bang-bang, (2) pseudo rate with bang-bang, and (3) lead lag with PWPF modulation.

Random noise corresponding to uncertainty in the relative position measurements was introduced to investigate the effect of sensor noise on system performance.

In Chapter 4, an original design of a sensor for use in the flight test of a single axis system conceived by the author is presented. A first model of the sensor identified as a "ball-in-cage accelerometer"* has been built and tested. This system takes advantage of satellite attitude control which maintains one vehicle axis along the nominal velocity vector. This axis coincides with the sensor axis, the direction of control thrust, and, of course, the nominal direction of the drag force.

The flight test is planned to evaluate the efficacy of the drag make-up concept in general and the single axis system in particular. The flight test, which will be the first continuous drag make-up system to fly is planned to last for only 2 to 3 days (30 to 40 orbits). System performance will be checked by monitoring the sensor signals via tape/telemetry and by closely monitoring the satellite ephemeris for verification of the effective drag cancellation.

A detailed error analysis of the effect of constraining the ball (by the cage) transverse to the direction of drag force is presented. The analysis indicates that the ball-in-cage should allow compensation of drag to better than 1 percent for satellites in low altitude orbits.

*Patent applied for.

Chapter 2

SOLUTIONS TO THE EQUATIONS OF RELATIVE MOTION AND THEIR INVERSION

In those missions where the primary goal of the drag-free satellite is to eliminate all forces on the proof mass other than gravity it is necessary to investigate the effects of small nongravitational forces which arise due to interactions between the outer vehicle and the proof mass or which may possibly penetrate the shield.

Since the answer is desired in a form which compares the actual motion of the vehicle with an ideal motion where only gravitational forces act, it is convenient to use the technique of "perturbation of the coordinates." In this method the linear differential equations of the relative motion between the actual and the ideal orbit are derived and the disturbances (forces other than gravity acting on the proof mass) are treated as driving or forcing terms for these equations.

2.1 THE DIFFERENTIAL EQUATION OF RELATIVE MOTION

Formally one can express these linearized error equations quite simply. If an even dimensional state vector $x(\tau)^*$ is defined which is composed of two parts namely the components of the relative position $\bar{\delta}r$ and the components of the relative velocity $\delta\dot{r}$ viz $x^\dagger(\tau) = (\delta\dot{r}, \bar{\delta}r)^{**}$, then the linearized equation of relative motion (see Appendix A) can be expressed in the form

$$x' \equiv \frac{dx(\tau)}{d\tau} = F(\tau) x(\tau) + D(\tau)f(\tau) \quad (2.1)$$

*The independent variable τ will stand for the true anomaly in this dissertation.

**The superscript \dagger indicates transpose, thus x^\dagger is a row vector.

where $F(\tau)$ is the coefficient (or system) matrix and expresses the system dynamics, i. e., the basic constraint on the nominal orbit provided by the central attracting mass, $f(\tau)$ is a vector containing the perturbing and/or control forces, and $D(\tau)$ is a matrix which expresses the way the forces are distributed among the states and is called the "distribution matrix."

2.2 THE SOLUTION TO THE EQUATIONS OF RELATIVE MOTION

For $f(\tau) = 0$, the situation of no perturbing forces, we may write a formal solution to Eq. (2.1) as

$$x(\tau) = X(\tau, \tau_0) x(\tau_0) \quad (2.2)$$

in which the "fundamental matrix" $X(\tau, \tau_0)$ satisfies the matrix equation

$$X' = FX \quad (2.3)$$

where $[]' \equiv d[]/d\tau$ and $X(\tau_0, \tau_0) = I$ the identity matrix. From Eq. (2.2) one can obtain the state of the system $x(\tau)$ at some argument τ by having the state $x(\tau_0)$ at the argument τ_0 . That is to say, if we have the solution matrix $X(\tau, \tau_0)$, we need only the initial relative displacement and velocity to be able to compute directly the relative displacement (and velocity) at an arbitrary future time. The simplest example of this form of solution is for the case in which F is a constant. In that case we have simply

$$X(\tau, \tau_0) = \exp [F(\tau - \tau_0)] \quad (2.4)$$

where $\exp [F(\tau - \tau_0)]$ has the usual interpretation viz:

$$\exp [F(\tau - \tau_0)] = I + F(\tau - \tau_0) + \frac{1}{2} F^2(\tau - \tau_0)^2 + \dots \frac{1}{n!} F^n(\tau - \tau_0)^n + \dots \quad (2.5)$$

This simple situation arises in the problem at hand for the case in which the "reference" vehicle is in a circular orbit (Ref. 1).

For general $F(\tau)$ there is not necessarily a closed form solution. However, for the present problem in which the $F(\tau)$ for an eccentric orbit is periodic and the equations are written in terms of the true anomaly as the independent variable a closed form solution has been found in terms of simple transcendental functions (Appendix A).

Irrespective of the form of $X(\tau, \tau_0)$ we may formally write down to quadrature the solution to Eq. (2.1) in the case in which $f(\tau) \neq 0$. That this solution is

$$x(\tau) = X(\tau, \tau_0) \left[x(\tau_0) + \int_{\tau_0}^{\tau} X^{-1}(\theta, \tau_0) D(\theta) f(\theta) d\theta \right] \quad (2.6)$$

can be verified by direct substitution into Eq. (2.1).

This solution can, in general, only be evaluated numerically. This is, of course, feasible and is done quite often. However, if one wishes to investigate solutions in which τ is allowed to get very large (corresponding to several hundred orbits), round off errors and prohibitive machine time limit the utility of direct numerical calculation of the perturbations. Computation of the perturbations over thousands of orbits is necessary when the operating lifetime of the satellite approaches a year or more. Now for cases in which X and Df are either constant or periodic with commensurate periods (e. g., all periodic at orbit period), the solution [Eq. (2.6)] can be evaluated with good accuracy over an arbitrarily large number of periods. This somewhat special case, however, is quite important to orbit ephemeris problems since many of the significant perturbations are periodic at orbit period.

2.3 THE FUNDAMENTAL MATRIX

In Appendix A the fundamental matrix $X(\tau, \tau_0)$ for the F (see Eq. A-70) representing a reference orbit of eccentricity e is developed in terms of a matrix $P(\tau)$, viz.,

$$X(\tau, \tau_0) = P(\tau) P^{-1}(\tau_0) \quad (2.7)$$

in which $P' = F(\tau)P$, and the columns of P were independent solutions (i. e., $|P| \neq 0$) to the equation

$$x' = Fx \quad (2.8)$$

The solutions were all in closed form. However, in order to get $X(\tau, \tau_0)$ explicitly one needs not only $P(\tau)$ but $P^{-1}(\tau_0)$. Several methods are available for obtaining $P^{-1}(\tau_0)$ when one has $P(\tau)$. However, most are quite tedious for $P(\tau)$ of dimension 4 or larger. Lange and Smith (Ref. 7) avoided this problem by limiting investigations to a particular argument $\tau_0 = 0$. In their case the 4×4 constant matrix $P(0)$ was easily invertable. Thus they were able to generate the matrix

$$X(\tau, 0) = P(\tau) P^{-1}(0) \quad (2.9)$$

However, they could not easily generate the matrix

$$X^{-1}(\tau, 0) = P(0)P^{-1}(\tau) = X(0, \tau) \quad (2.10)$$

in closed form since $P^{-1}(\tau)$ was not available in closed form. This again limited the possibilities in evaluating the solution, Eq. (2.6).

2.4 SYMPLECTIC MATRICES

Several authors, working on orbit transition matrices and other problems in mechanics, have noted a fundamental property of transition matrices which connect even dimensional state vectors composed of canonical variables (see p. 6). These represent canonical transformations.* The transition matrices in these cases are called symplectic and have the property that

$$\varphi^\dagger J \varphi = J \quad (2.11)$$

where $\varphi = \varphi(\tau)$ is the transition matrix with the property that at some $\tau = \tau_1$

$$\varphi(\tau_1) = I \quad \text{the identity matrix}$$

and

$$J = \begin{bmatrix} 0 & i \\ -i & 0 \end{bmatrix} \quad \text{where } i \text{ is the identity matrix}$$

of half the dimension of φ and J . The usefulness of Eq. (2.11) for obtaining inverses is clear since it is equivalent to

$$\varphi^{-1} = J^\dagger \varphi^\dagger J \quad (2.12)$$

which gives φ^{-1} as a simple matrix product.

*In two dimensions the transformation from coordinates (p, q) to (r, s) is said to be canonical if and only if $s_q = p_r$; $s_p = -q_r$; $r_q = -p_s$; $r_p = q_s$ where $s_p \equiv \partial s / \partial p$ etc. This is identically equivalent to the condition $Q^\dagger J Q = J$, where Q is the Jacobian matrix

$$Q = \begin{bmatrix} s_q & r_q \\ s_p & r_p \end{bmatrix}$$

and J is as defined above.

Battin (Ref. 5) points out that even dimensional transition matrices φ satisfying the equation

$$\frac{d\varphi}{dt} = F(t) \varphi(t) \quad (2.13)$$

where

$$F(t) = \begin{bmatrix} 0 & i \\ G(t) & 0 \end{bmatrix}, \quad \varphi(t_0) = I$$

and $G(t)$ is a symmetrix matrix, are always symplectic. In orbit perburbation problems $G(t)$ arises from the gravitational gradient forces and is always symmetric. The restriction that F have this exact form is unnecessary and the concept can be somewhat generalized.

2.5 THEOREM ON K-ORTHOGONALITY

The following theorem is useful for obtaining inverses to a rather general class of matrizants. It is particularly useful in computing orbit perturbations by the method of "perturbation of coordinates."

Consider the class of systems satisfying the differential equation

$$\frac{d\varphi}{d\tau} \equiv \varphi'(\tau) = F(\tau) \varphi(\tau) \quad (2.14)$$

where φ and F are even dimensioned matrix functions of the variable τ . We state the following theorem:

Theorem: For systems of the class $\varphi' = F\varphi$ with $\det \varphi \neq 0$ the relation $\varphi^\dagger K \varphi = C$ is valid iff* $F^\dagger K + KF = 0$, where K and C are constant matrices.

*iff \equiv if and only if.

Proof: (Only if) For $\varphi' = F\varphi$ and $\varphi^\dagger K\varphi = C$ we have

$$\frac{d}{d\tau} (\varphi^\dagger K\varphi) = 0 \quad (2.15)$$

$$\varphi^{\dagger'} K\varphi + \varphi^\dagger K\varphi' = 0 \quad (2.16)$$

$$\varphi^\dagger (F^\dagger K + KF)\varphi = 0 \quad (2.17)$$

for all τ . For $\det \varphi(\tau) \neq 0$, this yields

$$F^\dagger(\tau) K + KF(\tau) = 0 \quad (2.18)$$

for all τ .

Proof: (If) For $\varphi' = F\varphi$ and $(F^\dagger K + KF) = 0$ we have

$$\varphi^\dagger (F^\dagger K + KF)\varphi = 0 \quad (2.19)$$

$$(\varphi^\dagger)' K\varphi + \varphi^\dagger K\varphi' = 0 \quad (2.20)$$

$$\varphi^\dagger K\varphi = C \quad (2.21)$$

Note that the condition $\det \varphi = |\varphi| \neq 0$ is not necessary here.

Corollary 1: If for some $\tau = \tau_1^*$, $\varphi(\tau_1) = I = \varphi^\dagger(\tau_1)$, then $C = K$ and $\varphi^\dagger K\varphi = K$. In this case φ is called K-orthogonal, i.e., it bears the same relation to the matrix K as an orthogonal matrix does to the identity matrix. This corollary is useful in orbit perturbation calculations since if K^{-1} exists then φ^{-1} is simply $K^{-1}\varphi^\dagger K$.

The problem of inverting φ now reduces to determining whether an appropriate K exists for a particular F . No direct method appears available at this time. The following notes may help in providing an indirect method of finding a suitable K .

*It is not necessary here that the τ_1 be a value which the system can (or does) take on; see discussion on page 28.

Note 2: If $K = -K^\dagger$ (i.e., K is skew-symmetric) then $KF = -F^\dagger K = F^\dagger K^\dagger = (KF)^\dagger$. In this case F is called K -symmetric and $\varphi^\dagger K \varphi = C$.

Note 2a: If $\varphi(\tau_1) = I$ then $\varphi K \varphi = K$.

Note 2b: If for $\varphi(\tau_1) = I$ we find

$$K = J \equiv \begin{bmatrix} 0 & i \\ -i & 0 \end{bmatrix}$$

(notice $J^\dagger = J^{-1} = -J$ and $J^2 = -I$). Then $\varphi^\dagger J \varphi = J$ and φ is called symplectic.

Note 3: If $K = K^\dagger$ is symmetric, then $KF = -F^\dagger K = -(KF)^\dagger$. In this case F is called K -skew symmetric and $\varphi^\dagger K \varphi = C$.

Note 3a*: If $\varphi(\tau_1) = I$ then $\varphi^\dagger K \varphi = K$.

Note 3b: For $K = I$ we have the familiar result $\varphi^\dagger \varphi = I$ iff $F^\dagger + F = 0$ (i.e., φ is orthogonal iff F is skew symmetric).

The case $K = J$ is of particular interest since the F matrix of Tschauner and Hempel (Eq. A-70) is J -symmetric. We can easily compute the explicit restrictions on F imposed by choosing $K = J$. Let us partition F as follows:

$$F = \begin{bmatrix} f_1 & f_2 \\ f_3 & f_4 \end{bmatrix} \quad (2.22)$$

where f_i are matrices of half the order of F . Then $F^\dagger J + JF = 0$, where

$$F^\dagger J = \begin{bmatrix} -f_3^\dagger & f_1^\dagger \\ -f_4^\dagger & f_2^\dagger \end{bmatrix} \quad \text{and} \quad JF = \begin{bmatrix} f_3 & f_4 \\ -f_1 & -f_2 \end{bmatrix} \quad (2.23)$$

*This result is given by Pease (Ref. 12).

implies

$$\begin{aligned} f_3 - f_3^\dagger &= 0 \\ f_2 - f_2^\dagger &= 0 \\ f_4 + f_1^\dagger &= 0 \end{aligned} \tag{2.24}$$

i.e., we require only that f_2 and f_3 be symmetric and that $f_4 = -f_1^\dagger$.
The matrix

$$F = \begin{bmatrix} 0 & i \\ G & 0 \end{bmatrix}$$

(of Battin) is a special case of this.

This theorem and corollaries relating the K-orthogonality of the matrizant to the K-symmetry of the coefficient matrix is of interest here in that it provides a possibility for obtaining the inverse of the matrizant directly. In order to apply these results to a given problem the crux of the matter is clearly associated with finding an appropriate K. Although there is no direct method for obtaining a K for a given system, the K-symmetry associated with the coefficient matrix as developed in the corollaries provides an indirect method for inferring it. As an example of this technique, a K for the system in Appendix A will be obtained and then used for obtaining the inverses of the matrix.

2.6 INVERSION OF THE TSCHAUNER-HEMPEL MATRIZANT

For the system in which the state 4-vector is composed of the position difference $\delta \vec{r}$ and its derivative $\delta \dot{\vec{r}}$, expressed in terms of the true anomaly as the independent variable, we have (Eq. A-69) $x' = Fx$ in which $x^\dagger = (\xi, \eta, \xi', \eta' + 2\xi)$ and

$$F = \begin{bmatrix} 0 & 0 & 1 & 0 \\ -2 & 0 & 0 & 1 \\ q & 0 & 0 & 2 \\ 0 & 0 & 0 & 0 \end{bmatrix}, \quad \text{with } q \equiv \frac{3}{1 + e\tau} - 4^* \quad (2.25)$$

Since it is very easy to do, one first tries

$$K = J = \begin{bmatrix} 0 & i \\ -i & 0 \end{bmatrix}$$

and finds that

$$JF = \begin{bmatrix} q & 0 & 0 & 2 \\ 0 & 0 & 0 & 0 \\ 0 & 0 & -1 & 0 \\ 2 & 0 & 0 & -1 \end{bmatrix} = (JF)^\dagger \text{ is symmetric.}^{**} \quad (2.26)$$

With this result we have, according to theorem (Note 2),

$$P^\dagger J P = C \quad (2.27)$$

for some constant matrix C , where P is the P of Eq. (A-72).

Since $J^\dagger = -J$ is skew symmetric we know from Note 2 that J is an appropriate K for this system.

From Appendix A we have a matrizant solution to the homogeneous equation

$$P'(\tau) - F(\tau) P(\tau) = 0 \quad (2.28)$$

*Note $c\tau \equiv \cos \tau$, etc., throughout.

**This result could be anticipated with the knowledge that the above state vector was comprised of canonical variables.

$$P(\tau) = \begin{bmatrix} 0 & u_0 & u_1 & u_2 \\ 1 & V_0 & V_1 & V_2 \\ 0 & u'_0 & u'_1 & u'_2 \\ 0 & 1 & 0 & 0 \end{bmatrix} \equiv \begin{bmatrix} p_1 & p_2 \\ p_3 & p_4 \end{bmatrix} \quad (2.29)$$

where

$$\left. \begin{aligned} u'_0(\tau) &= -\frac{s\tau}{e} (1 + 2ec\tau) = \frac{1}{e} s\tau - u_1(\tau) \\ u'_1(\tau) &= c\tau + e(c^2\tau - s^2\tau) \\ u'_2(\tau) &= \frac{1}{\epsilon^4} \left[(1 - 4e^2)s\tau + 2e(1 + 2e^2)s\tau c\tau - \frac{3Ee^2 u'_1(\tau)}{\epsilon} \right] \\ u_0(\tau) &= \frac{1}{e} c\tau (1 + ec\tau) \\ u_1(\tau) &= s\tau(1 + ec\tau) \\ u_2(\tau) &= \frac{1}{\epsilon^4} \left[\frac{3e}{2} - \epsilon^2 c\tau - \frac{e}{2} (1 + 2e^2)(c^2\tau - s^2\tau) - \frac{3e^2 E u_1(\tau)}{\epsilon} \right] \\ V_0(\tau) &= -\frac{1}{e} [s\tau + u_1(\tau)] \\ V_1(\tau) &= \frac{1}{e} (1 + ec\tau)^2 \\ V_2(\tau) &= \frac{2}{\epsilon^4} \left[\left(1 + \frac{e^2}{2}\right)s\tau + \frac{e}{2} (1 + 2e^2)s\tau c\tau - \frac{3e^2 E V_1(\tau)}{2\epsilon} \right] \end{aligned} \right\} \quad (2.30)$$

The particular form which C assumes depends on the choice of the arbitrary constants of integration which arise when the u and V functions are evaluated by the technique described in Appendix A. The values for these functions given above were chosen in such a way as to make C have the particularly simple form:

$$C = \begin{bmatrix} 0 & -1 & 0 & 0 \\ 1 & 0 & 0 & 0 \\ 0 & 0 & 0 & 1 \\ 0 & 0 & -1 & 0 \end{bmatrix} \quad (2.31)$$

The reason for this particular choice is that $C^2 = -I$ implying that $C^{-1} = -C$ which is also C^\dagger . With this result P^{-1} has the simple form

$$P^{-1} = C^{-1} P^\dagger J = C^\dagger P^\dagger J \quad (2.32)$$

and may be obtained by direct multiplication.

In order to determine the conditions on the u 's and V 's such that C has the form above, we first multiply out $P^\dagger J P$ giving

$$C = \begin{bmatrix} p_1^\dagger & p_3^\dagger \\ p_2^\dagger & p_4^\dagger \end{bmatrix} \begin{bmatrix} p_3 & p_4 \\ -p_1 & -p_2 \end{bmatrix} = \begin{bmatrix} p_1^\dagger p_3 - p_3^\dagger p_1 & p_1^\dagger p_4 - p_3^\dagger p_2 \\ p_2^\dagger p_3 - p_4^\dagger p_1 & p_2^\dagger p_4 - p_4^\dagger p_2 \end{bmatrix} \quad (2.33)$$

$$\equiv \begin{bmatrix} c_1 & c_2 \\ c_3 & c_4 \end{bmatrix}, \quad c_3 = -c_2^\dagger \quad (2.34)$$

giving the following expressions for the c_i

$$c_1 = \begin{bmatrix} 0 & -1 \\ 1 & 0 \end{bmatrix} \quad (2.35)$$

$$c_4 = \begin{bmatrix} 0 & u_1 u'_2 - u_2 u'_1 \\ u'_1 u_2 - u'_2 u_1 & 0 \end{bmatrix} \quad (2.36)$$

$$c_3 = \begin{bmatrix} 0 & V_1 + u_1 u'_0 - u'_1 u_0 \\ 0 & V_2 + u_2 u'_0 - u'_2 u_0 \end{bmatrix} \quad (2.37)$$

$$c_2 = -c_3^\dagger \quad (2.38)$$

Now C is a constant and Eq. (2.32) is valid for all τ . Thus we see that by appropriate choice of the constants in the solutions u and V the C may be made quite simple. In particular note that the elements of c_4 contain the Wronskian of the solutions u_1 and u_2 (to Eq. A-39). Thus if we take

$$\det \begin{bmatrix} u_1 & u_2 \\ u'_1 & u'_2 \end{bmatrix} = 1 \quad (2.39)$$

we have for c_4

$$c_4 = \begin{bmatrix} 0 & 1 \\ -1 & 0 \end{bmatrix} = -c_1 \quad (2.40)$$

Further, at $\tau = 0$ we have that $u_1(0) = u'_2(0) = 0$ so that from Eq. (2.39) we have

$$u_2(0) u'_1(0) = -1 \quad (2.41)$$

Looking at c_3 at $\tau = 0$ we have [since $u_1(0) = u'_2(0) = 0$]

$$c_3 = \begin{bmatrix} 0 & V_1(0) - u'_1(0) u_0(0) \\ 0 & V_2(0) + u_2(0) u'_0(0) \end{bmatrix} \quad (2.42)$$

Now $u'_0(0) = 0$, $u'_1(0) = 1 + e$ and $u_0(0) = (1 + e)/e$ [see Eq. (2.30)]. Thus if we choose

$$V_2(0) = 0 \quad (2.43)$$

and

$$V_1(0) = \frac{(1 + e)^2}{e} \quad (2.44)$$

we will have that $c_3 = c_2 = 0$. Carrying out the matrix multiplication of Eq. (2.32) we find

$$P^{-1}(\tau) = \begin{bmatrix} -u'_0 & 1 & u_0 & V_0 \\ 0 & 0 & 0 & 1 \\ u'_2 & 0 & -u_2 & -V_2 \\ -u'_1 & 0 & u_1 & V_1 \end{bmatrix} \quad (2.45)$$

$$P^{-1}(0) = \begin{bmatrix} 0 & 1 & \frac{1+e}{e} & 0 \\ 0 & 0 & 0 & 1 \\ 0 & 0 & \frac{1}{1+e} & 0 \\ -(1+e) & 0 & 0 & \frac{(1+e)^2}{e} \end{bmatrix} \quad (2.46)$$

With this result we can now write out the fundamental matrix for the equation, i.e.,

$$X(\tau, \tau_0) = P(\tau) P^{-1}(\tau_0) \quad (2.47)$$

with the properties

$$X^{-1}(\tau, \tau_0) = P(\tau_0) P^{-1}(\tau) = X(\tau_0, \tau) \quad (2.48)$$

$$X(\tau_0, \tau_0) = P(\tau_0) P^{-1}(\tau_0) = I \quad (2.49)$$

Using the notation $u_1(\tau_0) \equiv u_{10}$ and $u_1(\tau_1) \equiv u_{11}$ etc., we get for $X(\tau_1, \tau_0)$

$$X(\tau_1, \tau_0) =$$

$$\begin{bmatrix} u_{11}u'_{20} - u_{21}u'_{10} & 0 & u_{21}u_{10} - u_{11}u_{20} & V_{10}u_{21} - V_{20}u_{11} + u_{01} \\ V_{11}u'_{20} - V_{21}u'_{10} + u'_{00} & 1 & V_{21}u_{10} - V_{11}u_{20} + u_{00} & -V_{00} + V_{01} + V_{21}V_{10} - V_{11}V_{20} \\ u'_{11}u'_{20} - u'_{21}u'_{10} & 0 & u'_{21}u_{10} - u'_{11}u_{20} & V_{10}u'_{21} - V_{20}u'_{11} + u'_{01} \\ 0 & 0 & 0 & 1 \end{bmatrix} \quad (2.50)$$

For $\tau_0 = 0$ we have the following:

$$X(\tau_1, 0) = \begin{bmatrix} -(1+e)u_{21} & 0 & \frac{u}{1+e} & \frac{(1+e)^2}{e} u_{21} + u_{01} \\ -(1+e)V_{21} & 1 & \frac{V_{11}}{1+e} - \frac{1+e}{e} & \frac{(1+e)^2}{e} V_{21} + u_{01} \\ -(1+e)u'_{21} & 0 & \frac{u'_{11}}{1+e} & \frac{(1+e)^2}{e} u'_{21} + u'_{01} \\ 0 & 0 & 0 & 1 \end{bmatrix} \quad (2.51)$$

and

$$X^{-1}(\tau, 0) = X(0, \tau) = \begin{bmatrix} \frac{u'_1}{1+e} & 0 & -\frac{u_1}{1+e} & -\frac{V_1}{1+e} + \frac{1+e}{e} \\ \frac{(1+e)^2}{e} u'_2 + u'_0 & 1 & -\frac{(1+e)^2}{e} u_2 - u_0 & V_0 + \frac{(1+e)^2}{e} V_2 \\ (1+e)u'_2 & 0 & -(1+e)u_2 & -(1+e)V_2 \\ 0 & 0 & 0 & 1 \end{bmatrix} \quad (2.52)$$

As a check we note that $X(0, 0) = X^{-1}(0, 0) = I$.

As a further check we compute $X(\tau, \tau_0)$ explicitly for $e = 0$ (i.e., circular orbit) which gives

$$X(\tau, \tau_0) = \begin{bmatrix} c(\tau - \tau_0) & 0 & s(\tau - \tau_0) & 2 - 2c(\tau - \tau_0) \\ -2s(\tau - \tau_0) & 1 & 2c(\tau - \tau_0) - 2 & 4s(\tau - \tau_0) - 3(\tau - \tau_0) \\ -s(\tau - \tau_0) & 0 & c(\tau - \tau_0) & -2s(\tau - \tau_0) \\ 0 & 0 & 0 & 1 \end{bmatrix} \quad (2.53)$$

Note $X^{-1}(\tau, \tau_0) = X(\tau_0, \tau) \neq -X(\tau, \tau_0)$.

In the foregoing development the particular arrangement of the columns of P was chosen in a completely arbitrary fashion. It was clear at the outset that in the form chosen P could never be equal to the identity matrix and thus as chosen P need not be symplectic (i. e., C need not equal J). However, one can rearrange the four solutions in a manner which gives the possibility of the new matrizant being symplectic. We try the following

$$\text{Let } R = \begin{bmatrix} u_2 & 0 & u_1 & u_0 \\ V_2 & 1 & V_1 & V_0 \\ u'_2 & 0 & u'_1 & u'_0 \\ 0 & 0 & 0 & 1 \end{bmatrix} = \begin{bmatrix} r_1 & r_2 \\ r_3 & r_4 \end{bmatrix} = P \begin{bmatrix} 0 & -1 & 0 & 0 \\ 0 & 0 & 0 & 1 \\ 0 & 0 & 1 & 0 \\ 1 & 0 & 0 & 0 \end{bmatrix} \quad (2.54)$$

In this $R(\tau) = I$ for some τ is not excluded. We again compute

$$C = R^\dagger J R \equiv \begin{bmatrix} c_1 & c_2 \\ c_3 & c_4 \end{bmatrix} \quad (2.55)$$

$$c_1 = r_1^\dagger r_3 - r_3^\dagger r_1 = 0 \quad (2.56)$$

$$c_2 = r_1^\dagger r_4 - r_3^\dagger r_2 = \begin{bmatrix} u_2 u'_1 - u'_2 u_1 & V_2 + u_2 u'_0 - u_0 u'_2 \\ 0 & 1 \end{bmatrix} \quad (2.57)$$

$$c_3 = -c_2 \quad (2.58)$$

$$c_4 = \begin{bmatrix} 0 & V_1 + u_1 u'_0 - u_0 u'_1 \\ -V_1 + u_1 u'_0 - u_0 u'_1 & 0 \end{bmatrix} \quad (2.59)$$

Again, since these c 's are constant we can evaluate at any argument (τ) . For simplicity take $\tau = 0$. At $\tau = 0$ we have $u_1(0) = u'_2(0) = u_0(0) = 0$. We see here that $C = J$ is certainly possible. For this to be the case we need:

$$u_2 u_1' - u_2' u_1 = 1 \quad (2.60)$$

$$V_2 = 0 \quad (2.61)$$

$$V_1 - u_0 u_1' = 0 \quad (2.62)$$

We see that we can accomplish this again merely by the same choice of the integration constants in V_1 and V_2 and by taking the Wronskian of $u_2 u_1$ (reverse order) equal to 1. To accomplish this we change the sign of u_2 giving

$$\bar{u}_2 = -u_2 = -\frac{1}{\epsilon^4} \left[\frac{3e}{2} - \epsilon^2 c \tau - \frac{e}{2} (1 + 2e^2)(c^2 \tau - s^2 \tau) - \frac{3e^2 E u_1}{\epsilon} \right] \quad (2.63)$$

which is clearly a solution to Eq. (A.69) since any constant times u_1 or u_2 (or linear combination of u_1 and u_2) is a solution. We also had

$$V_1(0) = \frac{(1+e)^2}{e} \quad (2.64)$$

and

$$V_2(0) = 0 \quad (2.65)$$

With the exception of the change in sign of u_2 the solutions are the same as we had previously! However for this arrangement we have $C = J$ and

$$R^\dagger J R = J \quad (2.66)$$

Thus R is symplectic. An interesting facet of this is that $R \neq I$ for an achievable (real) value of τ^* . This points out the interesting fact that although $R(\tau) = I$ for some τ is sufficient for R to be symplectic it is not necessary. Furthermore the τ need not be one which the actual system can take on.

We can of course construct an R that does take on the value I at any selected argument τ_0 . To do this we have only to take a different linear

*Consider the 3rd column of R (in 2.54). For $R = I$ it is necessary to make u_1 and V_1 simultaneously 0 for which we require $(1 + e c \tau) = 0$ (not achievable). Furthermore, with that constraint the 3rd element (r_{33}) becomes $-e s^2 \tau \neq 1$.

combination of the existing solutions. We can write this down formally quite simply. Calling the new solution \bar{R} we simply take

$$\bar{R} = P(\tau) P^{-1}(\tau_0) \quad (2.67)$$

or in particular for $\tau_0 = 0$

$$\bar{R}(\tau) = P(\tau) P^{-1}(0) \quad (2.68)$$

This is simply $X(\tau, 0)$, Eq. (2.51). Clearly $\bar{R}(0) = I$ and the columns of \bar{R} are simple linear combinations of the columns of P (or R). Also it is clear that the fundamental matrix $X(\tau, \tau_0)$ is not affected by the choice of R , i.e.,

$$\begin{aligned} X(\tau, \tau_0) &= \bar{R}(\tau) \bar{R}^{-1}(\tau_0) = P(\tau) P^{-1}(0) \left[P(\tau_0) P^{-1}(0) \right]^{-1} \\ &= P(\tau) P^{-1}(0) P(0) P^{-1}(\tau_0) = P(\tau) P^{-1}(\tau_0) \end{aligned} \quad (2.69)$$

Recall that the above transition matrices are for the state vector

$$x^\dagger = (\xi, \eta, \xi', \eta' + 2\xi) \quad (2.70)$$

In normal usage we will have the initial conditions in terms of $\xi = \Delta r/r = x/r$, $\eta = \Delta \tau = y/r$, \dot{x} , and \dot{y} . ξ and η can be directly obtained from x , y , and r . ξ' and η' , in terms of \dot{x} , \dot{y} , r , and ω are as follows.

$$\begin{aligned} \xi' &= \frac{d\xi}{d\tau} = \frac{d\xi}{dt} \frac{dt}{d\tau} = \frac{1}{\omega} \dot{\xi} = \frac{1}{\omega} \frac{d}{dt} \left(\frac{x}{r} \right) = \frac{1}{\omega} \left(\frac{\dot{x}}{r} - \frac{x}{r} \frac{\dot{r}}{r} \right) \\ &= \frac{1}{r\omega} (\dot{x} - \xi \dot{r}) \\ &= \frac{1}{r\omega} \left(\dot{x} - \frac{e\omega x s \tau}{1 + e c \tau} \right) = \frac{1}{2r\omega^2} (x\dot{\omega} + 2\omega \dot{x}) \end{aligned} \quad (2.71)$$

$$\frac{\dot{r}}{r} = \frac{e\omega s\tau}{1 + ec\tau} \quad (2.72)$$

$$\dot{\omega} = \frac{-2e\omega^2 s\tau}{1 + ec\tau} \quad (2.73)$$

Similarly

$$\eta' = \frac{1}{r\omega} \left(\dot{y} - \frac{e\omega y s\tau}{1 + ec\tau} \right) = \frac{1}{2r\omega^2} (y\dot{\omega} + 2\omega\dot{y}) \quad (2.74)$$

and

$$\eta' + 2\xi = \frac{1}{2r\omega^2} (y\dot{\omega} + 2\omega\dot{y} + 4\omega^2 x) \quad (2.75)$$

With these relations we can interpret both initial and final states in terms of more familiar elements.

With these state transition matrices we can now compute accurate results using Eq. (2.6), i.e.,

$$x(\tau_1) = X(\tau_1, \tau_0) \left[x(\tau_0) + \int_{\tau_0}^{\tau_1} X^{-1}(\theta, \tau_0) D(\theta) f(\theta) d\theta \right] \quad (2.76)$$

for any initial argument τ_0 and any final argument τ_1 and for those (constant or periodic) forces which allow the integration to be carried out in closed form, or in which, because of the periodicity in f , require numerical integration over only one orbit (see Lange and Smith, Ref. 7).

For the example used above it turned out that the choice of P gave a C that was invertible by inspection. A less fortunate choice of P , say φ , might require either that the constant matrix C be inverted by conventional methods or, if at some point τ_0 , $\varphi(\tau_0)$ was more easily invertible, then C^{-1} could be computed directly from the relation

$$C^{-1} = \varphi^{-\dagger}(\tau_0) J^{\dagger} \varphi^{-1}(\tau_0) \quad (2.77)$$

In either event the observation that F has an appropriate K -symmetry allows the inverse to be obtained by at most the inversion of a constant matrix.

2.7 FUNDAMENTAL MATRIX FOR A NON-CANONICAL STATE VECTOR

We may extend these results another step by noting that if we are interested in the transition matrix for some other (non-canonical) state vector, say

$$y = \begin{bmatrix} \xi \\ \eta \\ \xi' \\ \eta' \end{bmatrix} = \begin{bmatrix} 1 & 0 & 0 & 0 \\ 0 & 1 & 0 & 0 \\ 0 & 0 & 1 & 0 \\ -2 & 0 & 0 & 1 \end{bmatrix} \cdot \begin{bmatrix} \xi \\ \eta \\ \xi' \\ \eta' + 2\xi \end{bmatrix} \equiv U_- x \quad (2.78)$$

with

$$x = \begin{bmatrix} 1 & 0 & 0 & 0 \\ 0 & 1 & 0 & 0 \\ 0 & 0 & 1 & 0 \\ 2 & 0 & 0 & 1 \end{bmatrix} \cdot y \equiv U_+ y, \quad U_+ U_- = I \quad (2.79)$$

then having $X(a, b)$, in $x(a) = X(a, b) x(b)$, we can get $Y(a, b)$, in $y(a) = Y(a, b) y(b)$, simply as follows

$$x(a) = U_+ y(a) = X(a, b) x(b) = X(a, b) U_+ y(b) \quad (2.80)$$

$$y(a) = U_- X U_+ y(b) \equiv Y(a, b) y(b) \quad (2.81)$$

From which we have

$$Y(a, b) = U_- X(a, b) U_+ \quad (2.82)$$

and

$$\begin{aligned} Y^{-1}(a, b) &= U_- X^{-1}(a, b) U_+ \\ &= U_- X(b, a) U_+ = Y(b, a) \end{aligned} \quad (2.83)$$

Thus if we can select a state vector, say x where $x' = Fx + Df$, for which the F has some symmetry, then given some matrizant φ (where $\varphi' = F\varphi$) we can always get the transformed fundamental (transition) matrix Y and its inverse Y^{-1} .

Looking at this problem another way, we can write:

$$y = U_- x \quad ; \quad x = U_+ y \quad (2.84)$$

$$y' = U_- x' = U_- F U_+ y + U_- D f \quad (2.85)$$

or

$$y' = F_1 y + D_1 f$$

where

$$D_1 = U_- D \quad (2.86)$$

and

$$F_1 = U_- F U_+ = \begin{bmatrix} 0 & 0 & 1 & 0 \\ 0 & 0 & 0 & 1 \\ 4+q & 0 & 0 & -2 \\ 0 & 0 & 2 & 0 \end{bmatrix} \quad (2.87)$$

This F_1 is essentially that used by Lange and Smith and does not have the readily apparent symmetry of the F of Eq. (2.25) [as seen in Eq. (2.26)]. However, a K can be found namely

$$K_1 = \begin{bmatrix} 0 & -2 & 1 & 0 \\ 2 & 0 & 0 & 1 \\ -1 & 0 & 0 & 0 \\ 0 & -1 & 0 & 0 \end{bmatrix} \quad (2.88)$$

such that

$$K_1 F_1 = \begin{bmatrix} 4+q & 0 & 0 & 0 \\ 0 & 0 & 0 & 0 \\ 0 & 0 & -1 & 0 \\ 0 & 0 & 0 & -1 \end{bmatrix} \quad (2.89)$$

is symmetric, and $K_1 F_1 = (K_1 F_1)^\dagger = F_1^\dagger K_1^\dagger = -F_1^\dagger K_1$. Thus, for any Ψ satisfying $\Psi' = F_1 \Psi$, we have $\Psi^\dagger K_1 \Psi = C_1$, and thus

$$\Psi^{-1} = C_1^{-1} \Psi^\dagger K_1 \quad (2.90)$$

This particular example is somewhat special in that, since F_1 can be obtained from F by a similarity transformation, K_1 can always be obtained from K by the corresponding congruent transformation, i.e.,

for

$$F^\dagger K + K F = 0 \quad (2.91)$$

and

$$F_1 = U_+ F U_- \quad (2.92)$$

Then

$$K_1 = U_-^\dagger K U_- \quad (2.93)$$

gives

$$F_1^\dagger K_1 + K_1 F_1 = 0 \quad (2.94)$$

However, it does illustrate the point that for an F with no "apparent" symmetry an appropriate K -symmetry may exist.

For completeness we write the explicit form of $Y(\tau_1, \tau_2)$ the fundamental matrix for the state vector $y^\dagger = (\xi, \eta, \xi', \eta')$

$$Y(\tau_1, \tau_2) = \begin{bmatrix} u_{21}(2V_{12}-u_{12}')-u_{11}(2V_{22}-u_{22}')-2u_{01} & 0 & u_{21}u_{12}-u_{11}u_{22} & u_{21}V_{12}-u_{11}V_{22}+u_{01} \\ 2(V_{21}V_{12}-V_{11}V_{22}+V_{01}-V_{02}) & 1 & V_{21}u_{12}-V_{11}u_{22}+u_{02} & V_{01}-V_{02}+V_{21}V_{12}-V_{11}V_{22} \\ u_{21}u_{12}-u_{11}u_{22}+2(u_{21}'V_{12}-u_{11}'V_{22}+u_{01}') & 0 & u_{21}'u_{12}-u_{11}'u_{22} & u_{21}'V_{12}-u_{11}'V_{22}+u_{01}' \\ 2+2u_{01}+2u_{11}(2V_{22}-u_{22}')-u_{21}(2V_{12}-u_{12}') & 0 & 2(u_{11}u_{22}-u_{21}u_{12}) & 1+2(u_{11}V_{22}-u_{21}V_{12}-u_{01}') \end{bmatrix} \quad (2.95)$$

and for $e = 0$ we get (letting $\tau_1 = a$ and $\tau_2 = b$)

$$Y(a, b) = \begin{bmatrix} 4-3c(a-b) & 0 & s(a-b) & 2[1-c(a-b)] \\ 6[s(a-b) - a+b] & 1 & 2[c(a-b)-1] & 4s(a-b)-3(a-b) \\ 3s(a-b) & 0 & c(a-b) & 2s(a-b) \\ 6[c(a-b)-1] & 0 & -2s(a-b) & 4c(a-b)-3 \end{bmatrix} \quad (2.96)$$

If we take $b = 0$ in the above and recall

$$[\dot{\cdot}] = \frac{d[\cdot]}{dt} = \frac{d\tau}{dt} \cdot \frac{d[\cdot]}{d\tau} = \omega[\cdot],$$

Eq. (2.96) is identical to the result of Lange (Ref. 1).

2.8 THE FUNDAMENTAL MATRIX OF THE ORIENTATION OF A FREE BODY IN EULER PARAMETERS

In Chapter 3 we deal with a body which is tumbling in an uncontrolled and torque free mode as a result of arbitrary but known initial rates. Although it will not be necessary to know its orientation to effect the proposed translation control it is convenient in the analysis and evaluation of the results to view the relative motion in a locally level (non-tumbling) frame.

By expressing the "state of the body orientation" as a 4-vector in terms of Euler parameters one can then obtain the state at any time in terms of the initial state through the fundamental matrix of the system.

Although expressions for Euler parameters in terms of Euler angles, direction cosines, etc., are available, the fundamental matrix for a free body having two equal moments of inertia is developed for the first time in this section.

This solution affords an interesting insight into the structure of the fundamental matrix and in the process a theorem is presented for the solution of a class of matrix differential equations which includes the rotation of a free body with two equal principal moments of inertia.

The corresponding problem for the general body has not been solved to date. A closed form solution would still be academically interesting, although it would probably include elliptic functions and thus present the problem in digital machine simulation of the relative economics of obtaining the elliptic functions versus solving the differential equations continually.

In terms of Euler angles defined in Fig. 2-1 the four Euler parameters are defined as follows:

$$\begin{aligned}\xi &= s \frac{\theta}{2} c \frac{\varphi - \Psi}{2} \\ \eta &= s \frac{\theta}{2} s \frac{\varphi - \Psi}{2} \\ \zeta &= c \frac{\theta}{2} s \frac{\varphi + \Psi}{2} \\ \chi &= c \frac{\theta}{2} c \frac{\varphi + \Psi}{2}\end{aligned}\tag{2.97}$$

If we define a state (row) matrix $q^\dagger = (\xi, \eta, \zeta, \chi)$ then the dynamic equation of torque free rotation of a rigid body can be written as

$$\frac{dq}{dt} \equiv q' = \frac{1}{2} \Omega q \tag{2.98}$$

where Ω is a 4×4 skew symmetric matrix composed of the angular velocities in body coordinates namely

$$\Omega = \begin{bmatrix} 0 & \omega_3 & -\omega_2 & \omega_1 \\ -\omega_3 & 0 & \omega_1 & \omega_2 \\ \omega_2 & -\omega_1 & 0 & \omega_3 \\ -\omega_1 & -\omega_2 & -\omega_3 & 0 \end{bmatrix} \quad (2.99)$$

Matrices of this form containing only four distinct elements are quite useful in dealing with 4-vectors. They have several interesting properties which follow from direct operations. (See Weiten, Ref. 16.) First note that for 0's on the diagonal as indicated

$$\Omega^2 = -(\omega_1^2 + \omega_2^2 + \omega_3^2)I = -\omega^2 I \quad (2.100)$$

in which the scalar ω^2 is the square of the magnitude (norm) of the total angular velocity.

Note also that

$$\det \Omega = |\Omega| = \omega^4 \neq 0 \quad (2.101)$$

and that

$$\Omega^\dagger \Omega = \omega^2 I \quad (2.102)$$

so that

$$\Omega^{-1} = \frac{1}{\omega^2} \Omega^\dagger = \frac{-1}{\omega^2} \Omega \quad (2.102)$$

Thus $(1/\omega) \Omega$ is an orthonormal matrix.

There is of course considerable symmetry in Ω . This is very evident under the following partitioning: we can write

$$\Omega = \begin{bmatrix} \bar{A} & \bar{B} \\ -\bar{B} & \bar{A} \end{bmatrix} \quad (2.104)$$

where

$$\bar{A} \equiv \begin{bmatrix} 0 & \omega_3 \\ -\omega_3 & 0 \end{bmatrix} \quad (2.105)$$

and

$$\bar{B} \equiv \begin{bmatrix} -\omega_2 & \omega_1 \\ \omega_1 & \omega_2 \end{bmatrix} \quad (2.106)$$

and define

$$A \equiv \begin{bmatrix} \bar{A} & 0 \\ 0 & \bar{A} \end{bmatrix} \quad (2.107)$$

$$B \equiv \begin{bmatrix} 0 & \bar{B} \\ -\bar{B} & 0 \end{bmatrix} \quad (2.108)$$

and note that $\Omega = A + B$.

By direct multiplication we find

$$A^2 = \begin{bmatrix} \bar{A}^2 & 0 \\ 0 & \bar{A}^2 \end{bmatrix} = -\omega_3^2 I \quad (2.109)$$

$$B^2 = -\begin{bmatrix} \bar{B}^2 & 0 \\ 0 & \bar{B}^2 \end{bmatrix} = -(\omega_1^2 + \omega_2^2) I \equiv -b^2 I \quad (2.110)$$

Furthermore since

$$\omega_3^2 + b^2 = \omega^2 \quad (2.111)$$

we have

$$A^2 + B^2 = -\omega^2 I \quad (2.112)$$

and since

$$\Omega^2 = (A + B)^2 = A^2 + B^2 + AB + BA = -\omega^2 I \quad (2.113)$$

we have that

$$AB + BA = 0 \quad (2.114)$$

We will find this useful in what follows.

As a direct consequence of the vector Eq. (2.98) we can write the corresponding matrix equation

$$Q' = \frac{1}{2} \Omega Q \quad (2.115)$$

where

$$q(t) = Q(t) c \quad (2.116)$$

and c is a constant vector and Q is a 4×4 matrix.

If we find a matrizant solution Q such that $\det Q \neq 0$ it is well-known (see also Note 3b) that, since Ω is skew symmetric, Q is orthogonal, i.e.,

$$Q Q^\dagger = I \quad (2.117)$$

It is also well-known from rigid body dynamics that in the case of torque free motion that since ω_x, ω_y , and ω_z can be written in closed form in terms of Jacobian elliptic functions, the angular velocity is periodic, i.e.,

$$\Omega(t) = \Omega(t + T) \quad (2.118)$$

For Ω periodic we know from Floquet theory (Ref. 25) that we can express the matrizant Q in the factored form

$$Q = P e^{Ct} \quad (2.119)$$

where C is a constant 4×4 matrix and $P(t) = P(t + T)$ is a periodic 4×4 matrix with the same period (T) as Ω . Furthermore P and C are related by the equation

$$P' = \frac{1}{2} \Omega P - PC$$

and due to orthogonality of Q we have

$$P^\dagger P = I, \text{ iff, } C + C^\dagger = 0$$

2.8.1 The Form of the Matrizant Solution

For certain Ω it will turn out that P may always be chosen in a particular form namely

$$P = e^{Gt} \quad (2.122)$$

where G is a constant 4×4 matrix. We investigate the implications of this.

For $P = e^{Gt}$ we have

$$P' = Ge^{Gt} = \frac{1}{2} \Omega e^{Gt} - e^{Gt} C \quad (2.123)$$

or

$$\frac{1}{2} \Omega = e^{Gt} (G + C) e^{-Gt} \quad (2.124)$$

since this is true for all t , we have at $t = 0$

$$\frac{1}{2} \Omega(t=0) \equiv \frac{1}{2} \Omega_0 = G + C \quad (2.125)$$

Thus $P = e^{Gt}$ implies that Ω has the form

$$\Omega = e^{Gt} \Omega_0 e^{-Gt} \quad (2.126)$$

and

$$\Omega^2 = e^{Gt} \Omega_0^2 e^{-Gt} \quad (2.127)$$

Recall $\Omega^2 = -\omega^2 I$ for all t

thus

$$\Omega_0^2 = -\omega_0^2 I \quad (2.128)$$

giving

$$\Omega^2 = -e^{Gt} \omega_0^2 I e^{-Gt} = -\omega_0^2 I = \text{constant} \quad (2.129)$$

Thus the implications of choosing $P = e^{Gt}$ are that ω^2 is a constant and Ω has the form

$$\Omega = e^{Gt} \Omega_0 e^{-Gt} \quad (2.130)$$

Now we know from rigid body dynamics that for arbitrary initial rates in order for the square of the total angular velocity to be a constant at least two of the principal moments of inertia must be equal.* Taking ω_3 to be the angular velocity about the axis of unequal inertia, then ω_3 will be constant and $I_1 = I_2$.

Recalling our partitioning we see that in $\Omega = A + B$ that for $\omega_3 = \text{constant}$, since

$$A = \omega_3 \begin{bmatrix} j & 0 \\ 0 & j \end{bmatrix} \quad j = \begin{bmatrix} 0 & 1 \\ -1 & 0 \end{bmatrix} \quad (2.131)$$

we have

$$A' = 0 \quad (2.132)$$

*For $\omega^2 = \text{constant}$, $0 = \omega_1' \omega_1 + \omega_2' \omega_2 + \omega_3' \omega_3 = \omega_1 \omega_2 \omega_3 (k_1 + k_2 + k_3) = k_1 k_2 k_3 \omega_1 \omega_2 \omega_3$ [see Eq. (2.134) for definition of k 's]. Thus for arbitrary $\omega_1, \omega_2, \omega_3 \neq 0$ one of the k 's must be zero. If we take $k_3 = 0$, we have $I_1 = I_2$ and since $\omega_3' = k_3 \omega_1 \omega_2$, $\omega_3 = \text{constant}$.

Furthermore, we have

$$\bar{B}' = \begin{bmatrix} -\omega_2' & \omega_1' \\ \omega_1' & \omega_2' \end{bmatrix} \quad (2.133)$$

which from Eulers equations we know to be

$$\bar{B}' = \begin{bmatrix} -k_2 \omega_1 \omega_3 & k_1 \omega_2 \omega_3 \\ \omega_1' & \omega_2' \end{bmatrix} \quad (2.134)$$

where

$$k_1 \equiv \frac{I_3 - I_2}{I_1}, \quad k_2 \equiv \frac{I_1 - I_3}{I_2}, \quad k_3 \equiv \frac{I_2 - I_1}{I_3}$$

and that for $I_1 = I_2$ we have $k_1 = -k_2$, and $k_3 = 0$ (which led to $\omega_3 = \text{constant}$). Thus

$$\bar{B}' = k_1 \omega_3 \begin{bmatrix} \omega_1 & \omega_2 \\ \omega_2 & -\omega_1 \end{bmatrix} = k_1 \bar{A} \bar{B} \quad (2.135)$$

From this we can easily conclude for the 4x4 matrix B that

$$B' = k_1 AB = \frac{k_1}{2} (AB - BA) \quad (2.136)$$

Since $A' = 0$ we have

$$\Omega' = (A' + B') = B' = \frac{k_1}{2} [A(\Omega - A) - (\Omega - A)A] \quad (2.137)$$

$$\Omega' = \frac{k_1}{2} (A\Omega - \Omega A) \quad (2.138)$$

2.8.2 Theorem on the Form of the Angular Rotation Matrix

We now state the following theorem:

For matrices satisfying the differential equation

$$\Omega' = G\Omega - \Omega G \quad (2.139)$$

where G is a constant matrix then Ω can always be written in the form

$$\Omega = e^{Gt} \Omega_0 e^{-Gt} \quad (2.140)$$

where $\Omega_0 = \Omega(t=0)$.

Proof: we make the substitution

$$\Omega = \Omega^* e^{-Gt}, \quad \Omega_0 = \Omega_0^* \quad (2.141)$$

we find from Eq. (2.139) that

$$\begin{aligned} \Omega' &= (\Omega^{*'} - \Omega^* G) e^{-Gt} = G\Omega^* e^{-Gt} - \Omega^* e^{-Gt} G \\ &= (G\Omega^* - \Omega^* G) e^{-Gt} \end{aligned} \quad (2.142)$$

which gives

$$\Omega^{*'} = G\Omega^* \quad (2.143)$$

which for $G = \text{constant}$ has the unique solution:

$$\Omega^* = e^{Gt} \Omega_0^* \quad (2.144)$$

Hence, since $\Omega_0^* = \Omega_0$, we have

$$\Omega = e^{Gt} \Omega_0 e^{-Gt} \quad (2.140)$$

Thus the condition that two principal moments of inertia are equal in a body moving according to Eulers equations for torque free motion is sufficient for the angular velocity magnitude ω to be constant and for the angular velocity matrix Ω to have the form $\Omega = e^{Gt} \Omega_0 e^{-Gt}$ in which

$$G = \frac{1}{2} k_1 A \quad (2.146)$$

2.8.3 Exponential Form of the Matrizant Q

We previously established [Eq. (2.126)] that $P = e^{Gt}$ was sufficient for Ω to have the form $\Omega = e^{Gt} \Omega_0 e^{-Gt}$. This combined with Eq. (2.146) suggests that we try

$$Q = e^{\frac{1}{2} k_1 A t} e^{Ct} \quad (2.147)$$

as a solution to $Q' = \frac{1}{2} \Omega Q$ [Eq. (2.115)]. Direct verification shows that Eq. (2.147) is a solution to Eq. (2.115). We can now easily evaluate the constant matrix C . We have from Eq. (2.125) that

$$C = \frac{1}{2} \Omega_0 - G \quad (2.148)$$

with $G = \frac{1}{2} k_1 A$ this gives for C

$$C = \frac{1}{2} \Omega_0 - k_1 A \quad (2.149)$$

or in light of our partitioning of Ω [see Eq. (2.108)]

$$C = \frac{1}{2} (1 - k_1) A + B(0) \quad (2.150)$$

giving finally

$$Q = e^{k_1 A t / 2} e^{(\Omega_0 - k_1 A) t / 2} \quad (2.151)$$

We observe now that the matrizant Q can be easily converted into a "Fundamental matrizant" by the simple expedient of writing $t_1 - t_0$ for t .

Thus for

$$\left. \begin{aligned} t &= t_1 - t_0 \\ Q(t_1, t_0) &= e^{k_1 A (t_1 - t_0) / 2} e^{(\Omega_0 - k_1 A) (t_1 - t_0) / 2} \\ Q(t_0, t_0) &= I \\ Q^{-1}(t_1, t_0) &= Q(t_0, t_1) \end{aligned} \right\} \quad (2.152)$$

and

2.8.4 Geometric Interpretation of the Exponents of Q

Before proceeding with further evaluation of Q it will be useful to get a geometric picture of the problem. Figure 2-1 is the familiar Euler angle view of the displacement of a rigid body.

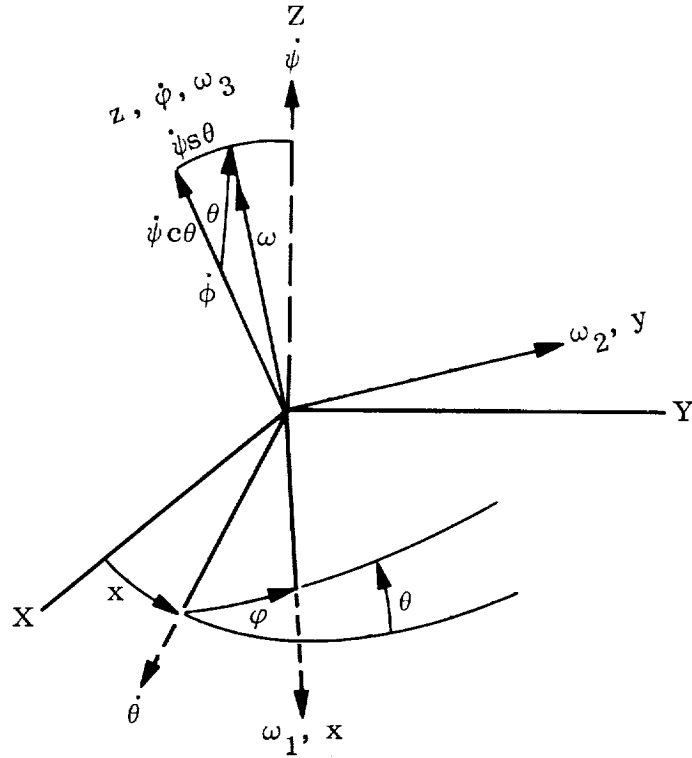


Fig. 2-1 Rotation of a Rigid Body in Terms of Euler Angles

The following geometric relations are valid

$$\left. \begin{aligned}
 \omega^2 &= \omega_1^2 + \omega_2^2 + \omega_3^2 & \omega_1^2 + \omega_2^2 &= (\dot{\psi} s \theta)^2 \\
 \omega_1 &= \dot{\psi} s \theta s \varphi & \omega_3^2 &= (\dot{\varphi} + \dot{\psi} c \theta)^2 \\
 \omega_2 &= \dot{\psi} s \theta c \varphi & \text{for } \omega_z &= \text{constant}, \theta = \text{constant}, \\
 \omega_3 &= \dot{\varphi} + \dot{\psi} c \theta & \dot{\theta} &= 0
 \end{aligned} \right\} (2.153)$$

Now we had

$$\omega_1^2 + \omega_2^2 = b^2 = \text{constant} = (\dot{\psi} s \theta)^2 \quad (2.154)$$

Since θ is a constant we see that $\dot{\psi}$ is a constant. Similarly $\dot{\phi}$ is a constant. From Euler's equation we have

$$\dot{\omega}_1 = k_1 \omega_2 \omega_3, \quad k_1 = \frac{I_2 - I_3}{I_1}, \quad I_1 = I_2 \quad (2.155)$$

Thus

$$\dot{\omega}_1 = \dot{\phi} \dot{\psi} s \theta c \varphi = k_1 \dot{\psi} s \theta c \varphi (\dot{\phi} + \dot{\psi} c \theta) \quad (2.156)$$

which gives

$$\left. \begin{aligned} \dot{\phi} &= k_1 \omega_3 \\ \dot{\phi}(1 - k_1) &= k_1 \dot{\psi} c \theta \\ (1 - k_1) \omega_3 &= \dot{\psi} c \theta \end{aligned} \right\} \quad (2.157)$$

and

We now evaluate Q using these quantities. We have for A

$$A = \begin{bmatrix} 0 & \omega_3 & 0 & 0 \\ -\omega_3 & 0 & 0 & 0 \\ 0 & 0 & 0 & \omega_3 \\ 0 & 0 & -\omega_3 & 0 \end{bmatrix} \equiv \omega_3 K \quad \text{and} \quad K^2 = -I \quad (2.158)$$

Thus (taking $\dot{\varphi}t = \varphi$)

$$\frac{1}{2} k_1 A t = \frac{1}{2} k_1 \omega_3 t K = \frac{1}{2} \dot{\varphi} t K = \frac{1}{2} \varphi K \quad (2.159)$$

(this implies $\varphi = 0$ at $t = 0$). Now since

$$\Omega_0 = A + B_0 \quad (2.160)$$

$$\begin{aligned} \Omega_0 - k_1 A &= (1 - k_1) A + B_0 = (1 - k_1) \omega_3 K + B_0 \\ &= \dot{\psi} c \theta K + B_0 \end{aligned} \quad (2.161)$$

Recall

$$B_0^2 = B^2 = - (\omega_1^2 + \omega_2^2) I \quad (2.162)$$

giving

$$B_0^2 = - (\dot{\psi} s \theta)^2 I \quad (2.163)$$

If we now define the constant 4×4 matrix β_0

$$\beta_0 = \frac{1}{\dot{\psi} s \theta} B_0, \quad \beta_0^2 = - I \quad (2.164)$$

and since at $t = 0$, $\varphi = 0$

$$\bar{\beta}_0 = \begin{bmatrix} -c\varphi & s\varphi \\ s\varphi & c\varphi \end{bmatrix} = \begin{bmatrix} -1 & 0 \\ 0 & 1 \end{bmatrix}, \text{ and } \beta_0 = \begin{bmatrix} 0 & 0 & -1 & 0 \\ 0 & 0 & 0 & 1 \\ 1 & 0 & 0 & 0 \\ 0 & -1 & 0 & 0 \end{bmatrix} \quad (2.165)$$

then

$$\Omega_0 - k_1 A = \dot{\psi} (K c \theta + \beta_0 s \theta) \quad (2.166)$$

which gives for Q (taking $\psi t = \psi$)

$$Q = e^{\varphi K/2} e^{\psi(Kc\theta + \beta_0 s\theta)/2} \quad (2.167)$$

Now

$$e^{\varphi K/2} = I \cos \frac{\varphi}{2} + K \sin \frac{\varphi}{2} \quad (2.168)$$

and since

$$K\beta_0 + \beta_0 K = 0 \quad (2.169)$$

we have

$$(Kc\theta + \beta_0 s\theta)^2 = K^2 c^2 \theta + \beta_0^2 s^2 \theta = -I \quad (2.170)$$

Hence

$$e^{\psi(Kc\theta + \beta_0 s\theta)} = I c \frac{\psi}{2} + (Kc\theta + \beta_0 s\theta) s \frac{\psi}{2} \quad (2.171)$$

Thus

$$Q = \left(I c \frac{\varphi}{2} + K s \frac{\varphi}{2} \right) \left[I c \frac{\psi}{2} + (Kc\theta + \beta_0 s\theta) s \frac{\psi}{2} \right] \quad (2.172)$$

which is the fundamental matrix of the Euler parameter 4-vector for a free body having two principal inertias equal.

2.8.5 Explicit Form of the Fundamental Matrix Q

Carrying out the matrix multiplication gives

$$\begin{aligned} Q = & I \left(c \frac{\varphi}{2} c \frac{\psi}{2} - \frac{s\varphi}{2} s \frac{\psi}{2} c\theta \right) + K \left(s \frac{\varphi}{2} c \frac{\psi}{2} + c \frac{\varphi}{2} s \frac{\psi}{2} c\theta \right) \\ & + \beta_0 \left(c \frac{\varphi}{2} s \frac{\psi}{2} s\theta \right) + K\beta_0 \left(s \frac{\varphi}{2} s \frac{\psi}{2} s\theta \right) \end{aligned} \quad (2.173)$$

where again I is the identity and

$$K = \begin{bmatrix} 0 & 1 & 0 & 0 \\ -1 & 0 & 0 & 0 \\ 0 & 0 & 0 & 1 \\ 0 & 0 & -1 & 0 \end{bmatrix} \quad \beta_0 = \begin{bmatrix} 0 & 0 & -1 & 0 \\ 0 & 0 & 0 & 1 \\ 1 & 0 & 0 & 0 \\ 0 & -1 & 0 & 0 \end{bmatrix} \quad K\beta_0 = \begin{bmatrix} 0 & 0 & 0 & 1 \\ 0 & 0 & 1 & 0 \\ 0 & -1 & 0 & 0 \\ -1 & 0 & 0 & 0 \end{bmatrix}$$

We notice Q has certain symmetry and thus we partition Q as follows:

$$Q = \begin{bmatrix} \bar{Q}_1 & \bar{Q}_2 \\ -\bar{Q}_2 & \bar{Q}_1 \end{bmatrix} \quad (2.174)$$

where

$$\bar{Q}_1 = \begin{bmatrix} c \frac{\varphi}{2} c \frac{\psi}{2} - s \frac{\varphi}{2} s \frac{\psi}{2} c\theta & s \frac{\varphi}{2} c \frac{\psi}{2} + c \frac{\varphi}{2} s \frac{\psi}{2} c\theta \\ -s \frac{\varphi}{2} c \frac{\psi}{2} - c \frac{\varphi}{2} s \frac{\psi}{2} c\theta & c \frac{\varphi}{2} c \frac{\psi}{2} - s \frac{\varphi}{2} s \frac{\psi}{2} c\theta \end{bmatrix} \quad (2.175)$$

and

$$\bar{Q}_2 = \begin{bmatrix} -c \frac{\varphi}{2} s \frac{\psi}{2} s\theta & +s \frac{\varphi}{2} s \frac{\psi}{2} s\theta \\ s \frac{\varphi}{2} s \frac{\psi}{2} s\theta & c \frac{\varphi}{2} s \frac{\psi}{2} s\theta \end{bmatrix} \quad (2.176)$$

making the substitution

$$\left. \begin{aligned} \frac{\beta - \alpha}{2} &= \frac{\varphi}{2} & \alpha &= \frac{\psi + \varphi}{2} \\ \frac{\beta + \alpha}{2} &= \frac{\psi}{2} & \beta &= \frac{\psi - \varphi}{2} \\ \theta &= 2\gamma \end{aligned} \right\} \quad (2.177)$$

gives the following equivalent form

$$\bar{Q}_1 = \begin{bmatrix} c\alpha c^2\gamma + c\beta s^2\gamma & s\alpha c^2\gamma - s\beta s^2\gamma \\ -s\alpha c^2\gamma + s\beta s^2\gamma & c\alpha c^2\gamma + c\beta s^2\gamma \end{bmatrix} \quad (2.178)$$

$$\bar{Q}_2 = \begin{bmatrix} -s\gamma c\gamma(s\beta + s\alpha) & s\gamma c\gamma(c\beta - c\alpha) \\ s\gamma c\gamma(c\beta - c\alpha) & s\gamma c\gamma(s\beta + s\alpha) \end{bmatrix} \quad (2.179)$$

This Q , in any of the forms above, is the solution to the equation $Q' = (1/2)\Omega Q$ with the initial condition $Q(t = 0) = I$.

The point of main interest is that, since $Q(0) = I$, the 4-vector of Euler parameters is given by

$$q(t) = \begin{bmatrix} \xi \\ \eta \\ \zeta \\ \chi \end{bmatrix} = Q(t) q(t = 0) \equiv Q(t) q_0 \quad (2.180)$$

For any initial q_0 (within the constraint that $q_0^\dagger q_0 = 1$).

As a check on the algebra we compute q for $q_0^\dagger = [s(\theta/2), 0, 0, c(\theta/2)]$ (corresponding to $\varphi = \psi = 0$) and get:

$$\left. \begin{aligned} \xi &= s\gamma(c\alpha c^2\gamma + c\beta s^2\gamma) - c^2\gamma s\gamma(c\beta - c\alpha) = s\gamma c\beta = s \frac{\theta}{2} c \frac{\psi - \varphi}{2} \\ \eta &= s\gamma(s^2\gamma s\beta - c^2\gamma s\alpha) + s\gamma c^2\gamma(s\beta + s\alpha) = s\gamma s\beta = s \frac{\theta}{2} s \frac{\psi - \varphi}{2} \\ \zeta &= s^2\gamma c\gamma(s\beta + s\alpha) + c\gamma(s\alpha c^2\gamma - s\beta s^2\gamma) = c\gamma s\alpha = c \frac{\theta}{2} s \frac{\psi + \varphi}{2} \\ \chi &= s^2\gamma c\gamma(c\alpha - c\beta) + c\gamma(c\alpha c^2\gamma + c\beta s^2\gamma) = c\gamma c\alpha = c \frac{\theta}{2} c \frac{\psi + \varphi}{2} \end{aligned} \right\} \quad (2.181)$$

which is the familiar expression relating the Euler parameters to the Euler angles.

Chapter 3

EVALUATION OF THRUST CONTROL SYSTEMS FOR A TUMBLING VEHICLE

In this chapter we address the problem of controlling the relative displacement between a reference body and a second satellite vehicle. Nominally we will think of the reference body being wholly contained in, i.e. surrounded by the vehicle. As such, it can be shielded from air drag and various other perturbing forces, and to the extent it is not perturbed by the surrounding vehicle, the reference body will move in a purely gravitational non-decaying orbit. If the "vehicle" is simultaneously controlled so as to never come in contact with the reference, then it must also follow a purely gravitational trajectory.

In order to accomplish control of the relative translative motion between the reference and the vehicle it has been proposed that only the relative position of the two bodies and the angular rate of main (outer) vehicle need be measured (Ref. 1). The control would be accomplished by six gas expulsion jets mounted at each end of a body fixed (orthogonal) axis system (triad). With this concept it would not be necessary to control the angular motion (i.e. attitude) of the vehicle. Indeed only its angular rate relative to inertial space need even be known.

Such a control system has several features or criteria on which it might be judged. First, it must be strong and fast enough to prevent contact between vehicle and reference during some range of perturbations, second it must have certain capture characteristics both for initial capture and capture in case of a low probability event that perturbs the system beyond its normal region of operation (e.g. the outer vehicle experiencing a non-destructive but major meteorite collision), and third and very important it must be efficient in the use of stored (on board) propellant in order to achieve maximum life. There are other factors which would influence a detailed design but for an initial synthesis the above are deemed adequate.

In Ref. 1, the feasibility of this sort of control was proved for a linear control law and conjectured for on-off control and in the early stages of the present work feasibility of the concept was confirmed.

This chapter describes the results of a comparative study of capture characteristics and fuel consumption during limit cycling for three specific nonlinear control systems.

3.1 PRECISE STATEMENT OF LIMIT CYCLE FUEL CONSUMPTION PROBLEM

The limit cycle fuel consumption problem can be stated precisely as follows*

Given.

- (1) A particular dynamic plant to be controlled: in our case we have a second-order system

$$\left. \begin{aligned} \frac{\ddot{\rho}}{\rho} &= \vec{f}_d + \vec{f}_c \\ \text{or in the body frame} \\ \frac{B\ddot{B}}{\rho} + 2\vec{\omega} \times \frac{B}{\rho} + \frac{B}{\omega} \times \vec{\rho} + \vec{\omega} \times (\vec{\omega} \times \vec{\rho}) &= \vec{f}_d + \vec{f}_c \end{aligned} \right\} \quad (3.1)^{**}$$

in which we wish to control the relative displacement $\vec{\rho}$ (See Fig. A-1) with a control force \vec{f}_c in the presence of a disturbing force \vec{f}_d

- (2) A set of noisy observations: in our case the output of a position sensor

$$\vec{x} = \vec{\rho} + \vec{x}_n \quad (3.2)$$

in which the output \vec{x} consists of $\vec{\rho}$ plus the noise \vec{x}_n which we assume to be white, gaussian, and uncorrelated.

- (3) An error criterion: in our case that

$$E(\rho^2) \leq \rho_0^2 \quad (3.3)$$

that is the expected value (E) of the magnitude of the position difference $\vec{\rho}$ be always less than some specified distance ρ_0 .

*B. O. Lange, private communication, April 25, 1966.

** $\frac{\ddot{\rho}}{\rho} \equiv \hat{i}_I \ddot{\rho}_{IX} + \hat{j}_I \ddot{\rho}_{IY} + \hat{k}_I \ddot{\rho}_{IZ}$, i.e., the superscript implies time derivative expressed in the coordinated frame specified, e.g., I = inertial, B = body.

- (4) A control mechanism: in our case body fixed on-off thrusters $\vec{f}_c = k\vec{u}$ in which the u_i can take on only the values 1, 0, -1, and have a threshold for activation \vec{x}_0 (expressed in terms of the signal \vec{x}), and also have some minimum on time δt which results in a minimum impulse $k|\vec{u}\delta t| \equiv I_{\min}$

Then, if we define the total fuel consumption (total impulse) $I(\tau)$ as

$$I(\tau) = k \int_0^\tau \left(|u_1| + |u_2| + |u_3| \right) dt \quad (3.4)$$

$$= k \int u^2 dt$$

The problem can be stated as:

Determine the $\vec{u}(t)$ based on the constraints 1-4 such that

$$E(I^2) + \lambda [E(I)]^2 \quad (3.5)$$

is a minimum, where λ is a parameter which depends upon the mission.

Unfortunately, there is no known exact analytical solution to the problem as stated.

In order to obtain a partial solution to this problem three different control systems were simulated on the B-5500 and their limit cycle fuel consumption in the presence of noisy position measurement were compared. The systems are (1) pseudo-rate with bang-bang control, (2) lead-lag with bang-bang control, (3) lead-lag with PWPF (pulse width-pulse frequency) control. These systems will subsequently be described in detail.

3.2 THE DYNAMIC CHARACTERISTICS OF THE SYSTEM (PLANT)

The dynamical plant which the system must control is illustrated in Fig. 3-1. The vector equations of motion are simply

$$\frac{\ddot{\Pi}}{\rho} = \vec{f}_d + \vec{f}_c \quad (3.1)$$

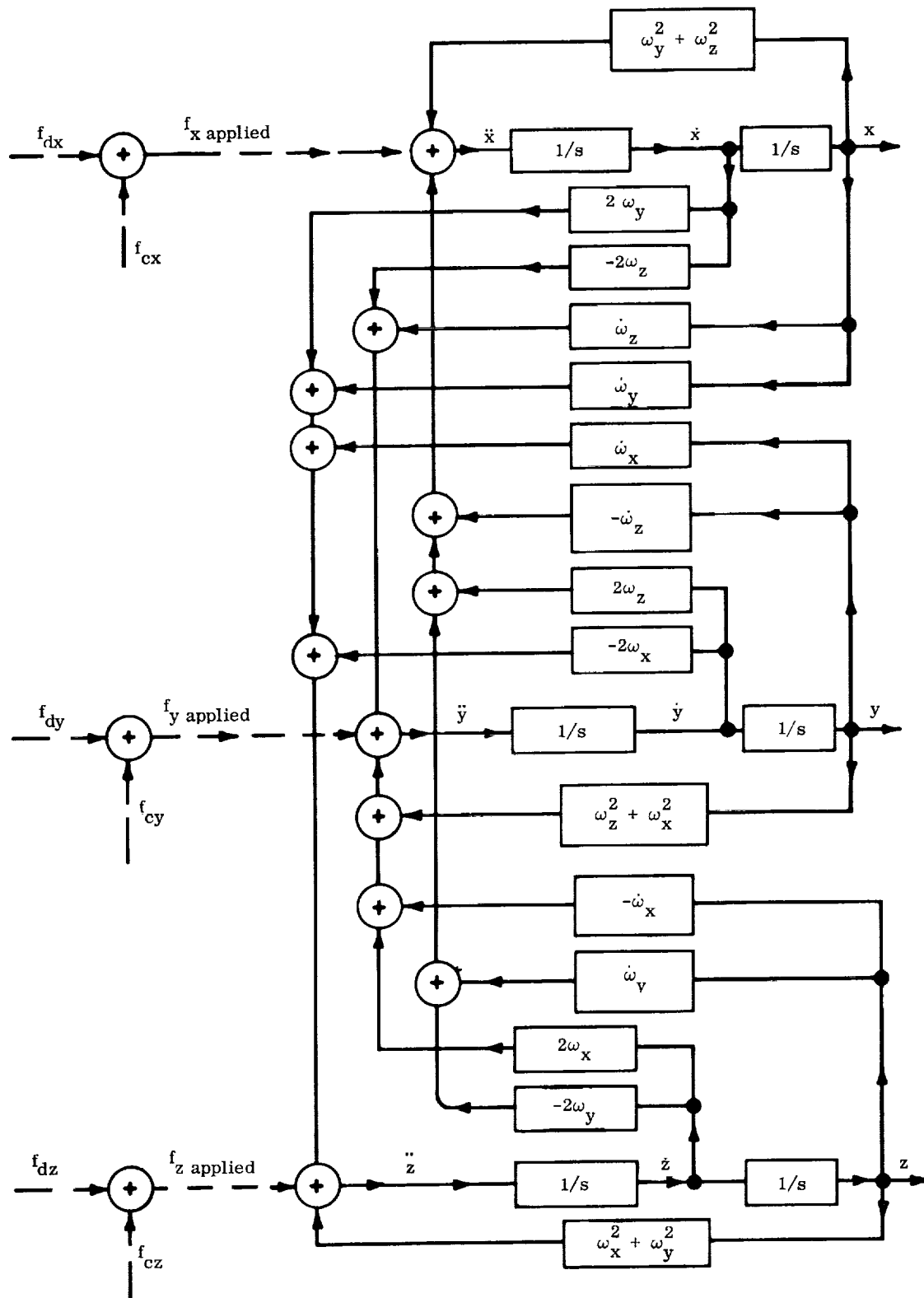


Fig. 3-1 Block Diagram of the Relative Translational Motion Between an Outer Satellite and an Inner Proof Mass. This is the dynamic system to be controlled.

and

$$\frac{\vec{B}}{\vec{I}} \cdot \vec{\omega} + \vec{\omega} \times \vec{I} \cdot \vec{\omega} = M_d^* \quad (3.6)$$

where $\frac{\vec{\Pi}}{\vec{\rho}}$ is the relative acceleration between the reference and the vehicle, where \vec{f}_d is a disturbing specific force and \vec{f}_c the control specific force. Equation (3.1) can be coordinatized in either body or inertial coordinates. As it is written inertial coordinatization is implied. In that reference frame a control law that is known to be capable of controlling a linear version of the system is simply

$$\vec{f}_c = -K_v \frac{\vec{I}}{\vec{\rho}} - K_p \vec{\rho} \quad (3.7)$$

where again $\frac{\vec{I}}{\vec{\rho}}, \vec{\rho}$ are the relative velocity and displacement, and K_v and K_p are positive gain factors. Now the measurements that we can easily and directly make on the state of the system are (1) the position of the proof mass relative to the vehicle in (some) body coordinates and (2) the angular velocity of the (outer) vehicle with respect to inertial space. If we express Eqs. (3.1) and (3.2) coordinatized in the body frame we get

$$\frac{\vec{B}\vec{B}}{\vec{\rho}} + 2\vec{\omega} \times \frac{\vec{B}}{\vec{\rho}} + \frac{\vec{B}}{\vec{\omega}} \times \vec{\rho} + \vec{\omega} \times (\vec{\omega} \times \vec{\rho}) - \vec{f}_d = -K_v \left(\frac{\vec{B}}{\vec{\rho}} + \vec{\omega} \times \vec{\rho} \right) - K_p \vec{\rho} \quad (3.8)$$

in which $\vec{\omega}$ is the angular rate of the body frame (coordinate system) with respect to inertial space. Now the left hand side of Eq. (3.8) contains the terms or elements which are intrinsic to the problem. The right hand side has the terms proposed for control. In order to effect control we must either measure them, derive them or do without them.

In the studies that follow the systems were simulated on the digital computer and the synthesis was developed one step at a time.

* \vec{I} stands for the inertia dyadic.

3.3 ACTUAL RATE SYSTEMS

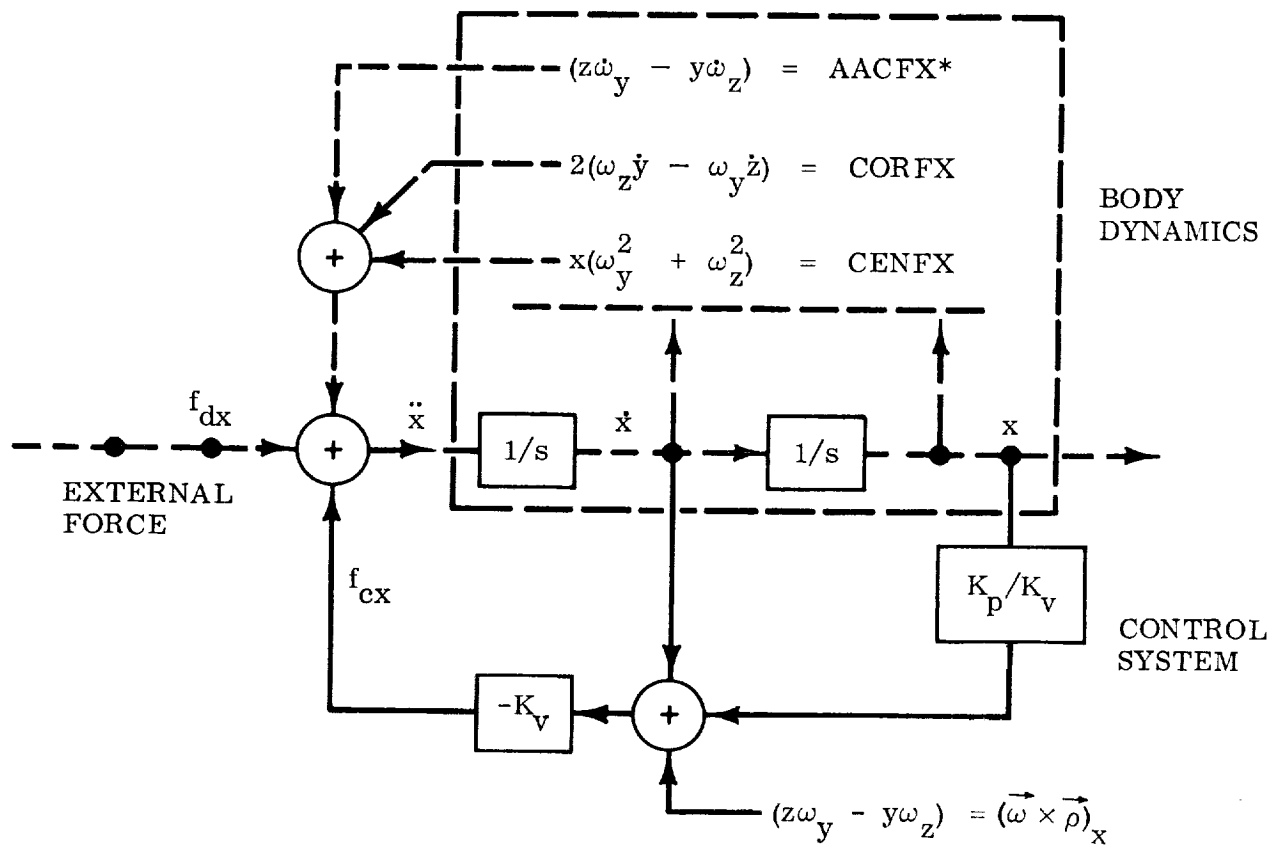
3.3.1 Proportional Control

As a point of departure we first simulated the linear system with proportional control. This provided a check that the program was operating properly and gave a calibration for evaluating the nonlinear system. A block diagram of the system is shown in Fig. 3-2. In all the simulations that follow the condition that the outer vehicle be tumbling in an arbitrary fashion was established by giving the vehicle (having three different principal moments of inertia) an initial angular rate about two of the axes (typically 0.1 rad/sec about z and 0.02 rad/sec about y) and then letting it tumble with no subsequent disturbing moments.

In order to interpret the results, especially the capture characteristics, it was desirable to be able to view the relative displacement between proof mass and vehicle from the non-rotating frame.* Thus, in the simulation the displacement was continuously computed in both the rotating and non-rotating frame. Phase plane plots in both reference frames were made for all systems tested. Because the control law is a familiar one as viewed from the non-rotating frame, the phase plane plots in the non-rotating frame (designated with the subscript I on the plots) are more familiar and thus more readily evaluated.

The plots were all made on the CALCOMP plotter and the presence of straight lines in the phase plots where one would expect parabolas is due to utilizing too few points in the interest of machine time conservation. This phenomenon is especially evident in some of the initial capture excursions.

*This was the reason for the interest in the fundamental matrix of a free body developed in Chapter 2.



*These are ALGOL identifiers standing for specific forces corresponding to angular, Coriolis, and centrifugal accelerations

Fig. 3-2 X Channel (Typical) Actual Rate With Proportional Control

The following system parameters were used throughout:

$$k_1 = \frac{I_3 - I_2}{I_1} = -1 ; k_2 = \frac{I_1 - I_3}{I_2} = 0.3 ; k_3 = \frac{I_2 - I_1}{I_3} = 1 .$$

Drag specific force = 0.0001 ft/sec^2 in y direction at $t = 0$; initial body rate: $\omega_{x0} = 0$; $\omega_{y0} = 0.02$; $\omega_{z0} = 0.1 \text{ rad/sec}$; $\omega_o = 0.001$; $e = 0$; integration step size = 0.1 sec ; control specific force = 0.001 ft/sec^2 .

Figure 3-3 is a phase plane plot of y -axis capture with proportional control,

$$f_{cy} = K_v \left(\dot{y} + (x\omega_z - z\omega_x) + \frac{K_p}{K_v} y \right)^* \equiv K_v P_y \quad (3.9)$$

3.3.2 On-Off Control

The next step consisted of using the same system set-up but replacing the proportional control with a simple on-off (or bang-bang) control [i.e., $f_{cy} = K_v \text{sgn}(P_y)$]. A phase plane plot of the y -axis capture for the above conditions is shown in Fig. 3-4.

A comparison of these two trajectories indicates a nominal (macroscopic) equivalence between the two control laws.

The last step in the preliminary verification of the system was to include hysteresis and dead band in the control law in order to more closely represent a real system.

This was implemented as follows:

Letting

$$P_x = \dot{x} + z\omega_y - y\omega_z + \frac{K_p}{K_v} x$$

*In what follows, the symbol T_2 is also used for the ratio K_v/K_p .

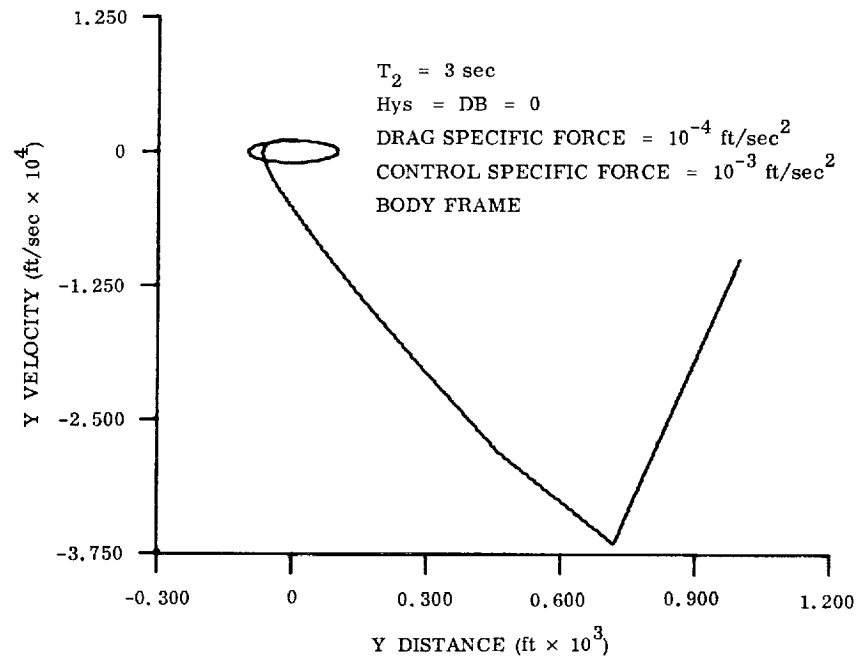


Fig. 3-3 Y-Axis Capture With Actual Rate and Proportional Control

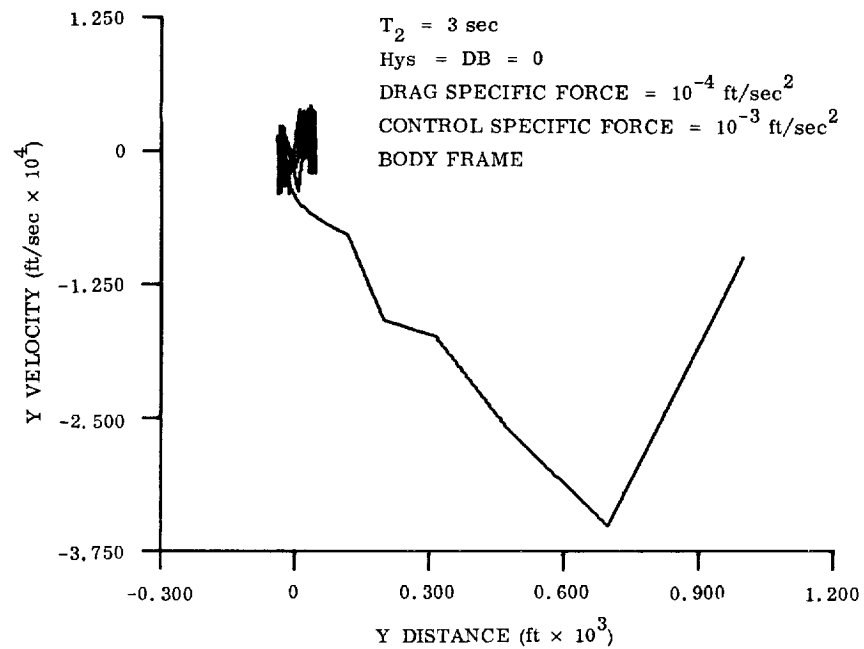


Fig. 3-4 Y-Axis Capture With Actual Rate and Bang-Bang Control

Then

$$f_{cx} \leftarrow \begin{cases} K_v \text{SGN}(P_x) & \text{for } |P_x| > \text{HYS} + \text{DB} \\ 0 & \text{for } |P_x| < \text{DB} \\ f_{cx} & \text{for } \text{DB} < |P_x| < \text{HYS} + \text{DB} \end{cases} \quad (3.11)$$

In Algol language " \leftarrow " means insert the quantity on the right into the storage location identified on the left; HYS is hysteresis and DB is dead band; and where the third condition is understood to apply in a digital system in which we mean the state at some time $(t + \Delta t)$ is the same as it was at time (t) , the previous step. With $\text{HYS} = 0.0005 \text{ ft}$ and $\text{DB} = 0.001 \text{ ft}$ Fig. 3-5 is for proportional control and Fig. 3-6 is for bang-bang control.

3.3.3 Limit Cycle Performance With Bang-Bang Control

In the studies to this point, system performance has been viewed in terms of capture characteristics only, and it is clear from Fig. 3-6 that adequate capture is achieved by this system, i. e., one which uses exact rate plus position to operate an on-off control having deadband and hysteresis.

To establish base line performance for "steady state," during which the system operates in a limit cycle mode, the initial conditions were chosen so that the system started inside the limit cycle states so that no thrust was required for capture. The drag force was sized to correspond to a deceleration of 10^{-4} ft/sec^2 corresponding to the drag at an altitude of about 125 nm. The thrust specific force was set at ten times the drag (i. e., $10 \times 10^{-4} \text{ ft/sec}^2$). For a system in which the thrust just compensates for drag the jets would be on 1/10 of the time. This corresponds to 100% efficiency. One would not expect 100% efficiency in the situation under investigation since the vehicle has an angular velocity about all axes and thus body fixed jets of finite size firing for a finite length of time could not have their entire thrust in a single direction (i. e., opposite the drag force). However, one would hope that the jets would never fire at such a time (position) so as to add to the drag force. In order to investigate

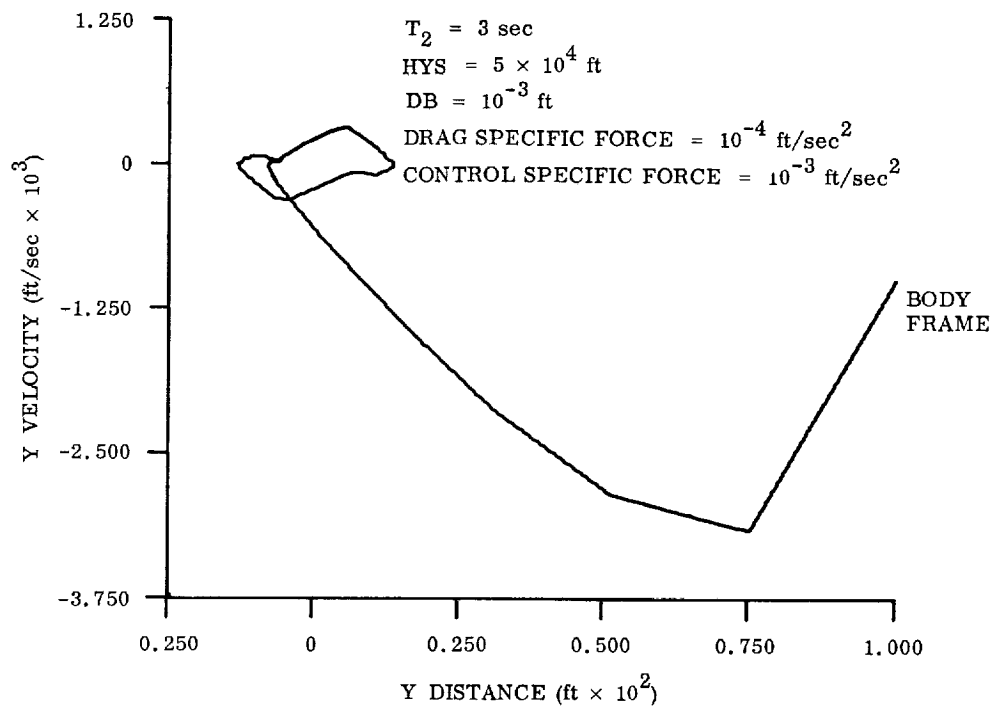
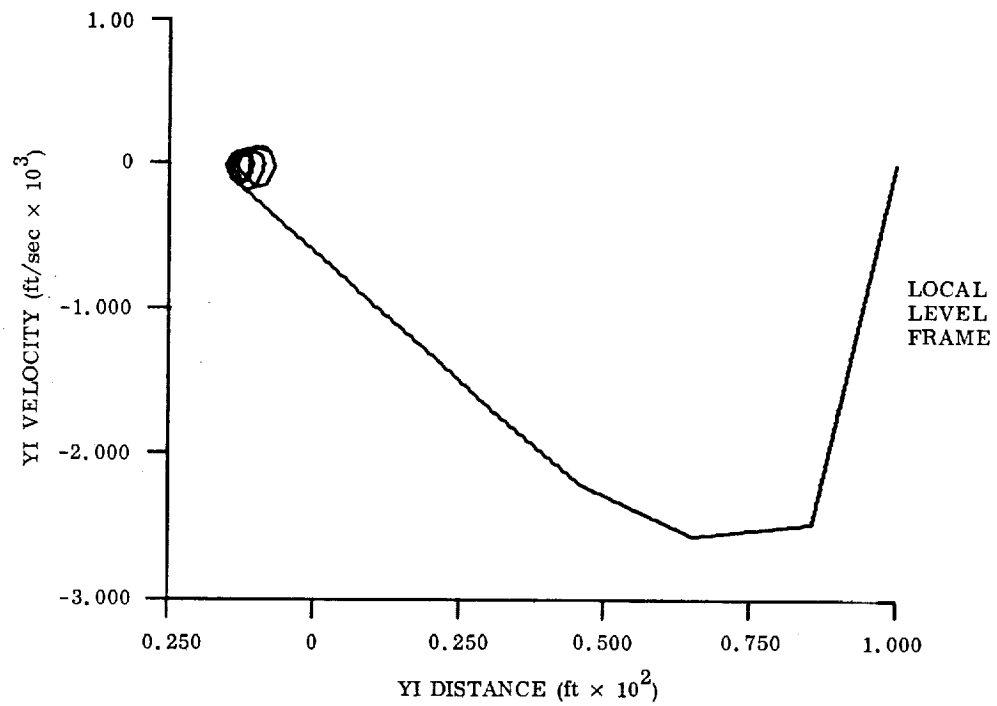


Fig. 3-5 Y-Axis Capture With Actual Rate and Proportional Control With Dead Band and Hysteresis

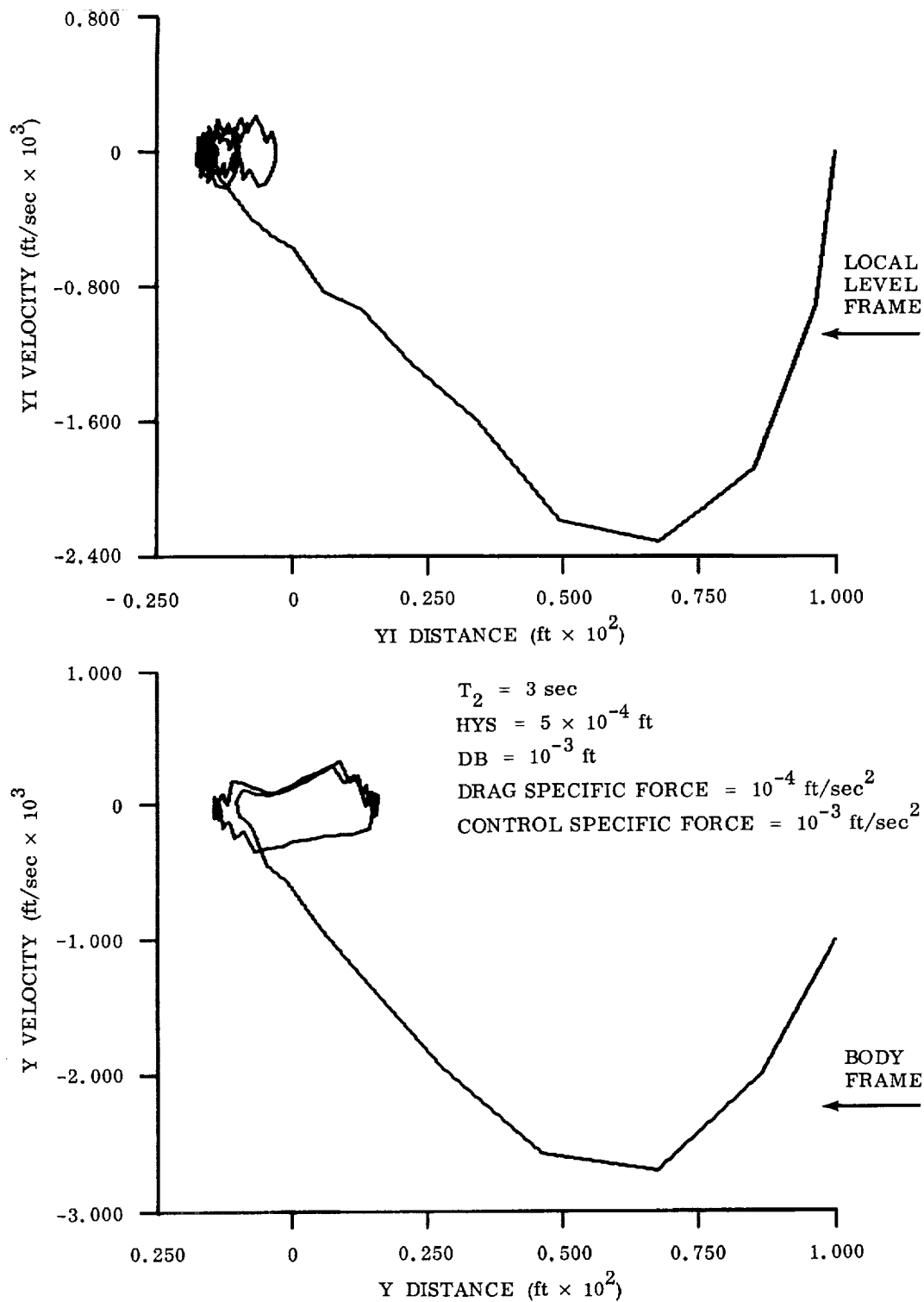


Fig. 3-6 Y-Axis Capture With Actual Rate and Bang-Bang Control With Dead Band and Hysteresis

this, the orientation of the vehicle relative to the drag force was determined explicitly and used to "decommutate" the time-on of the various jets. In a typical run this system was operated for 500 steps. At each step it was noted which jet(s) was on. To operate this system in the limit cycle mode required 75 on-impulses (66% efficiency) compared to an absolute minimum (100% efficiency) of 50 impulses (1/10 of 500). The phasing of the impulses was, however, such that no pulses came on in a direction that aided the drag so that we may interpret the extra fuel as that required for control in the directions transverse to the drag force.

The limit cycle performance of this system is shown in the graphs in Fig. 3-7. Close inspection of the phase plane plots in body and "inertial" coordinates shows the effect of the predominant vehicle rotation, which is about the z body axis, in that the drag causes each axis in turn to operate up against one side of its dead band. One would expect this with the continuous drag force. Figure 3-8 is a "decommutated" display showing the time and direction of x -jet thrust-on relative to the direction of drag. Note that the thrust-on impulses are nominally all in the same direction; i.e., negative for $y > 0$ and positive for $y < 0$. The drag force is in the plus y direction.

With the investigation to this point, then, we have established the "baseline" performance of a system in which an on-off thruster having both hysteresis and dead band is used. In this system the thruster is controlled by actual position and rate of the vehicle relative to the proof mass. The control law used for the switching line is the position plus a constant times the velocity as viewed in a non-rotating coordinate system (i.e., not fixed to the tumbling vehicle). The quantities used, however, are explicitly available and used in terms of body coordinates so that the control law explicitly exhibits the transformation between the rotating and nonrotating coordinates. With the results of this investigation the efficacy of this type control law as proposed by Lange (Ref. 1) is established.

3.4 DERIVED RATE SYSTEMS

From here we proceed with variations of this system in which some form of derived rate (velocity) is used in place of actual rate in the control law.

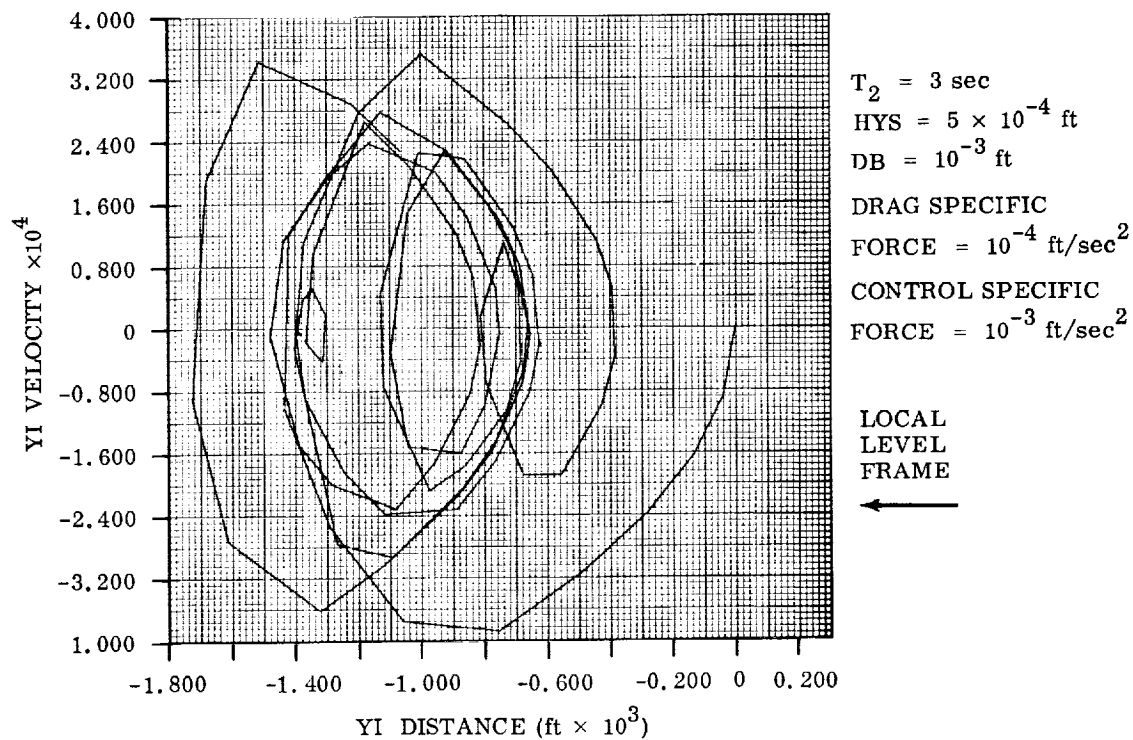
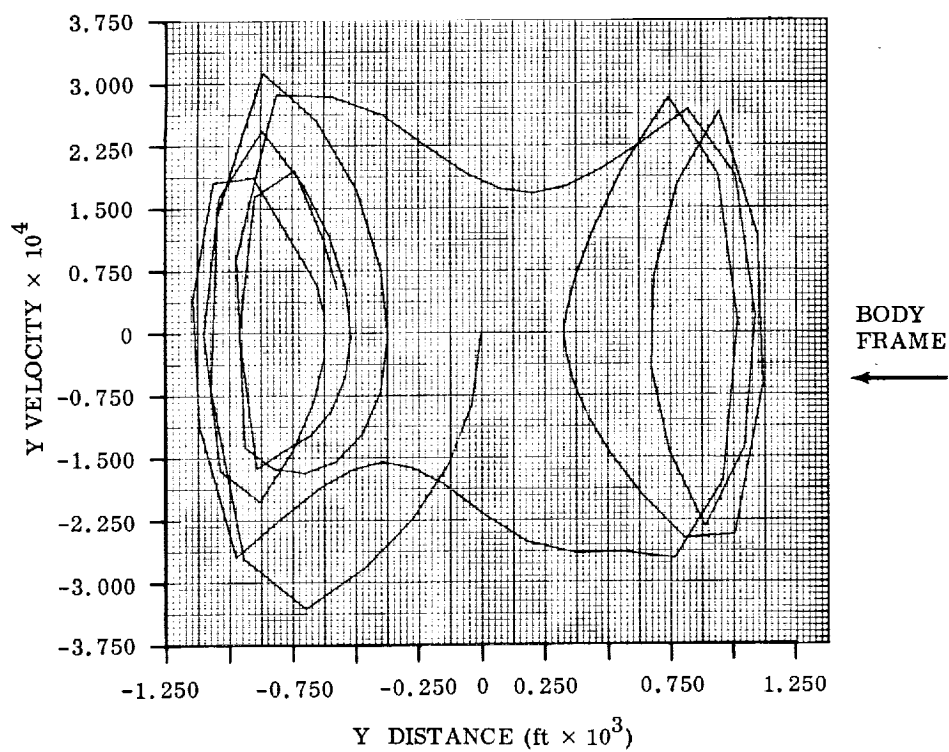


Fig. 3-7 Y-Axis Limit Cycle Performance Actual Rate With Dead Band and Hysteresis

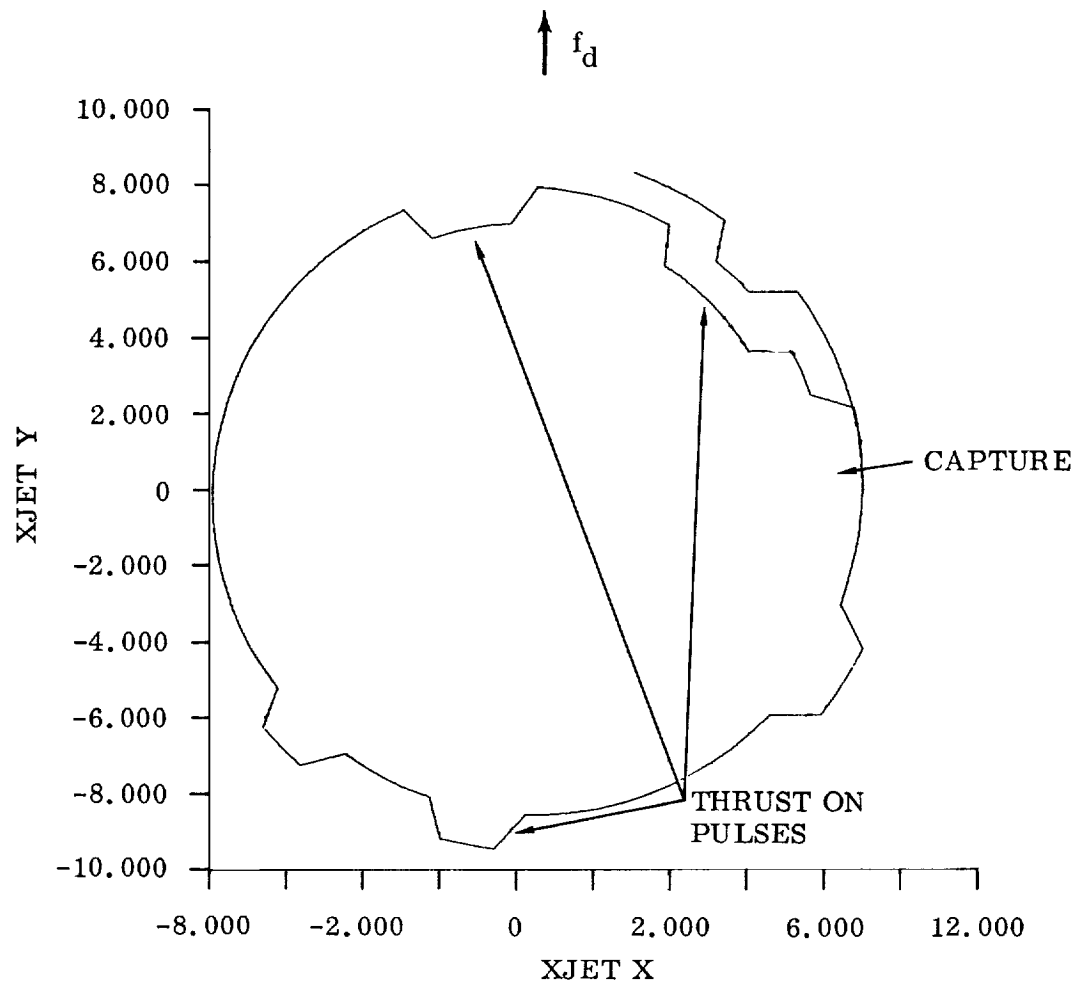


Fig. 3-8 X Jet Thrust in Orbit Frame

This procedure is motivated by the difficulty in making a direct measurement of the velocity. Also, in the hope of simplifying the systems, we investigate the effect of omitting some of the terms in the process of "deriving the rate." The three different control schemes previously mentioned are compared.

For these tests, no specific capture performance criteria were defined since in normal operation capture is expected to occur only once in the system lifetime, although in some missions occasional excursions out of the dead band region might arise and be overcome without compromising the mission. For that type mission capture would be more important. In this study the function of the capture runs was essentially to verify that the systems would capture and were thus operating properly. In initial runs the rate gain $T_2 = K_v/K_p$ was varied from about 0.1 to 10 and T_1 the lag gain from about 0.02 to 1. Comparison between systems was made for similar parameters. Final tests were run with $T_1 = 0.1$ and T_2 between 1 and 3.

3.4.1 Pseudo Rate with Bang-Bang Control

The first scheme for deriving the velocity we give the name "pseudo rate." This scheme consists of integrating the output of the switching amplifier (or relay) that turns on the thrust valves. Since the output of this amplifier results directly in vehicle acceleration, one integration of the amplifier output corresponds nominally to vehicle relative velocity (assuming proper initial conditions). This procedure has the desirable feature that the switching amplifier output is typically very clean (noise free) and thus the derived velocity signal is also clean (as opposed to a system in which rate is derived by taking a derivative). Since this signal is very noise free the system has little tendency to waste fuel due to unwanted jet firings. The scheme has the disadvantage that the effect of the perturbing force (drag) is not directly included in the velocity derivation. (The drag is indirectly included, however, by virtue of its effect on the position which also affects the switching amplifier.) A block diagram of this system is shown in Fig. 3-9. The characteristics of this type system are similar to the

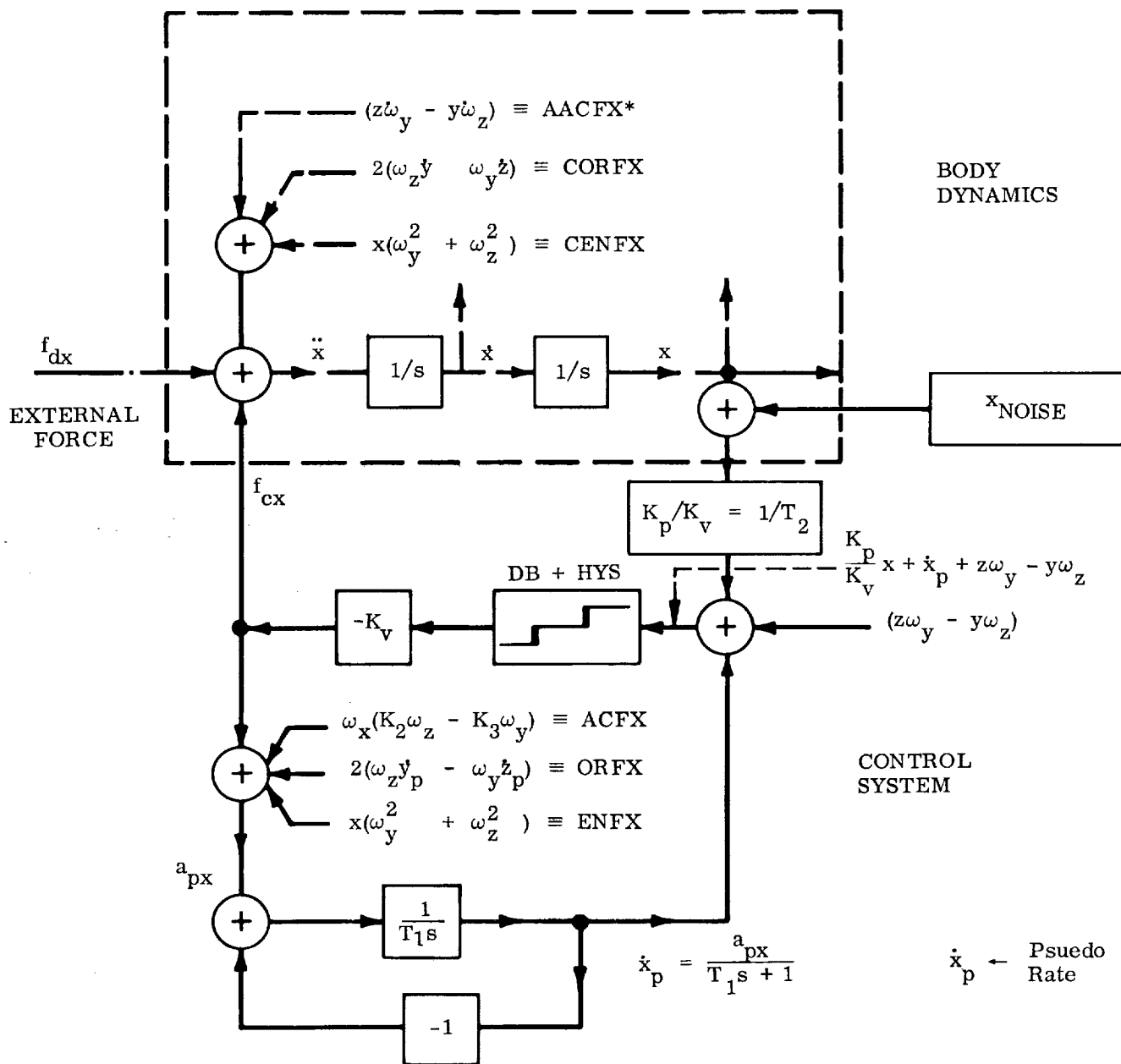


Fig. 3-9 X Channel (Typical) Pseudo-Rate Control System

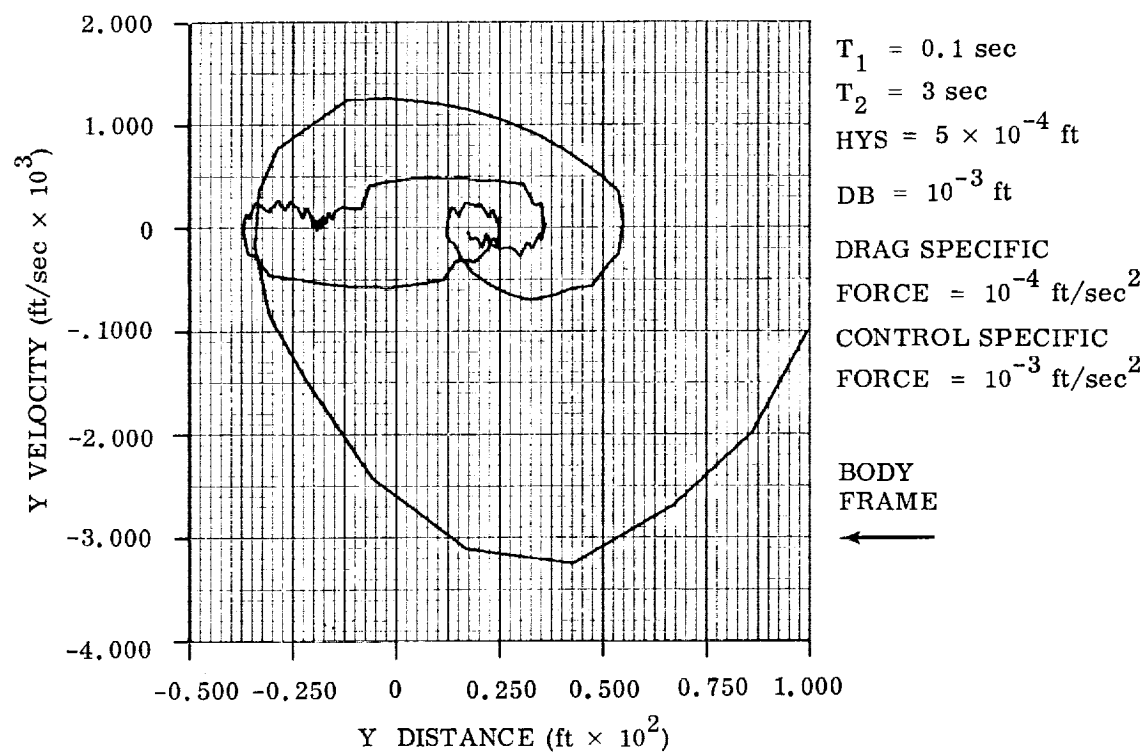
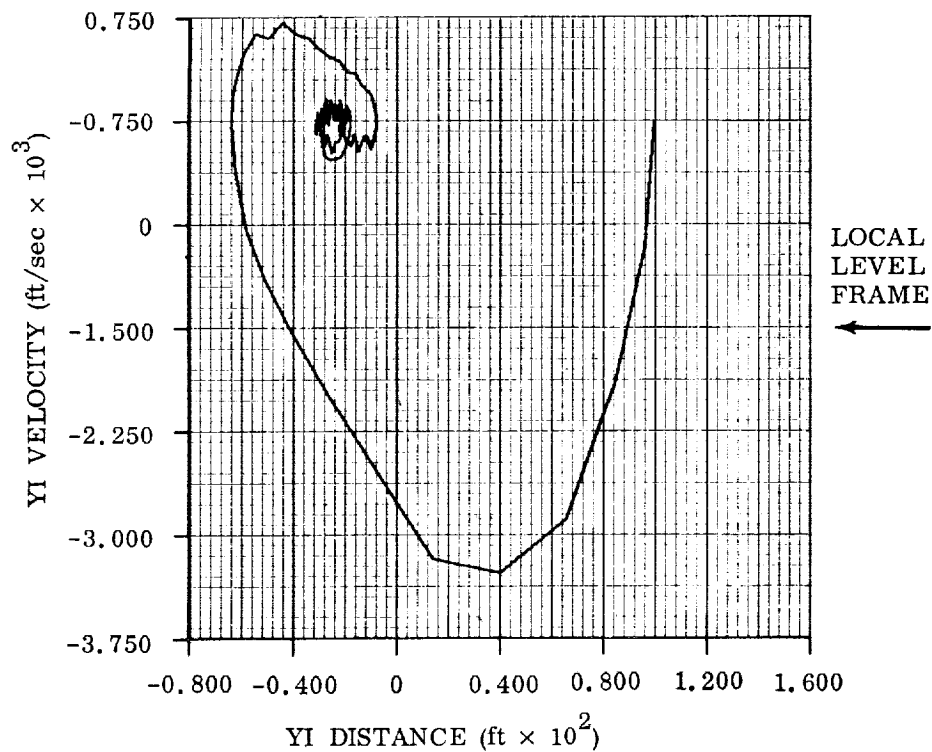


Fig. 3-10 Pseudo-Rate Capture Performance

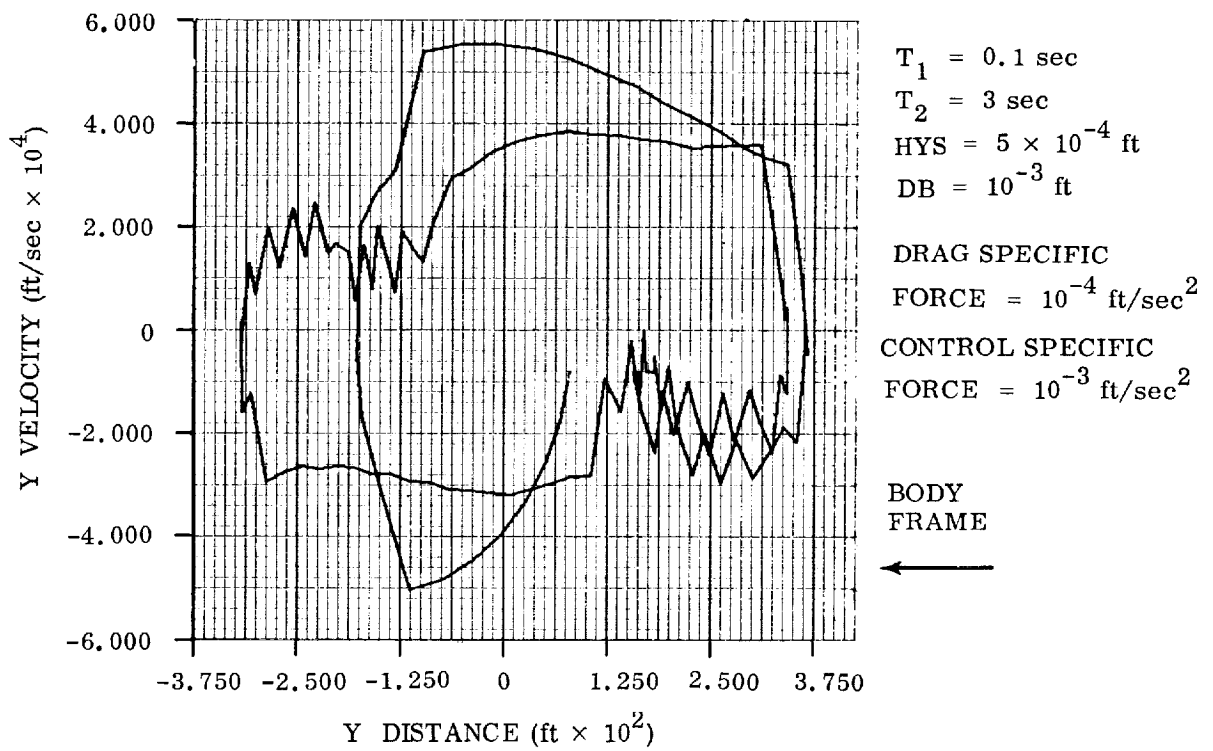
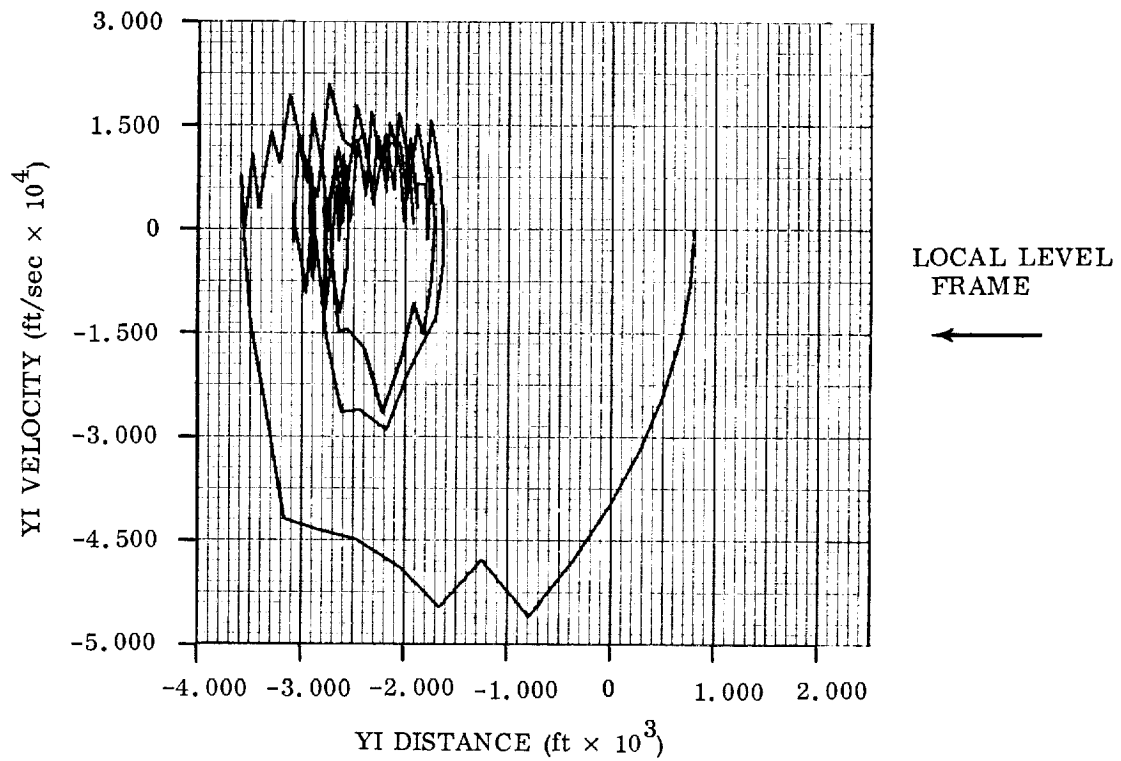


Fig. 3-11 Pseudo-Rate Limit Cycle Performance

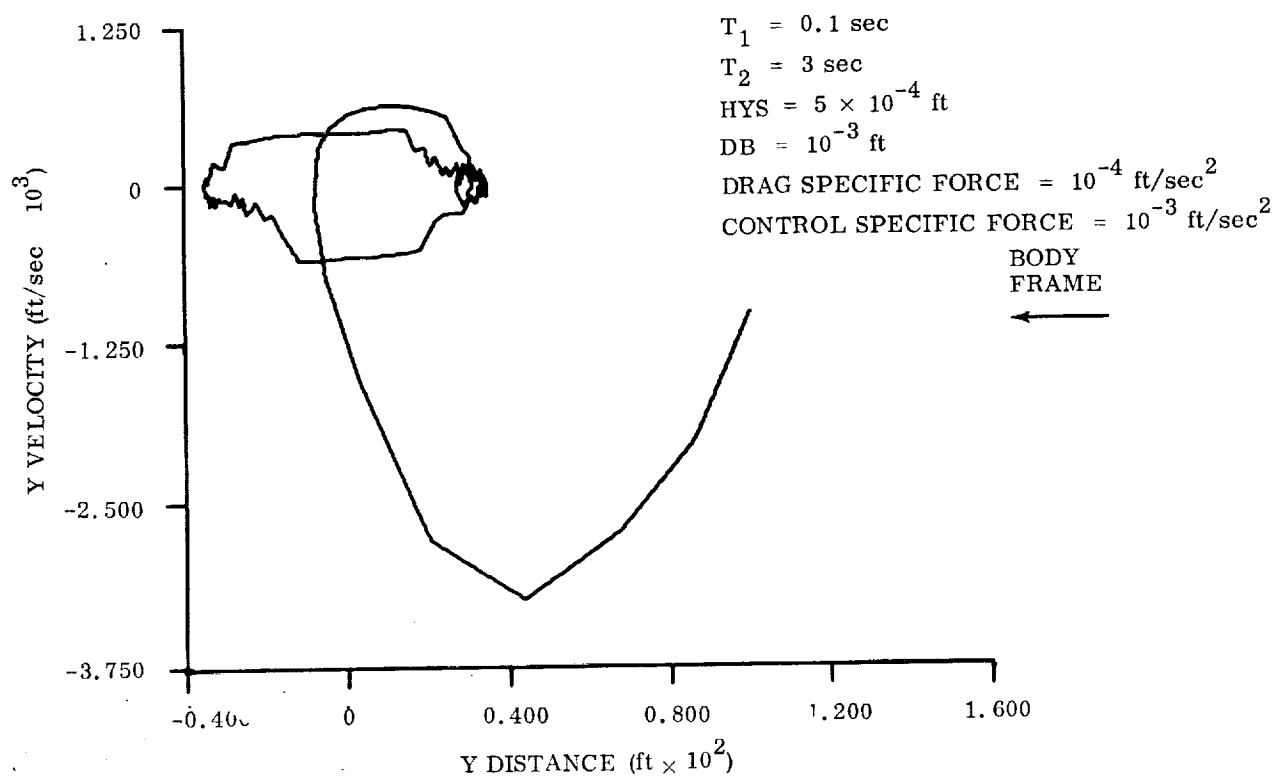
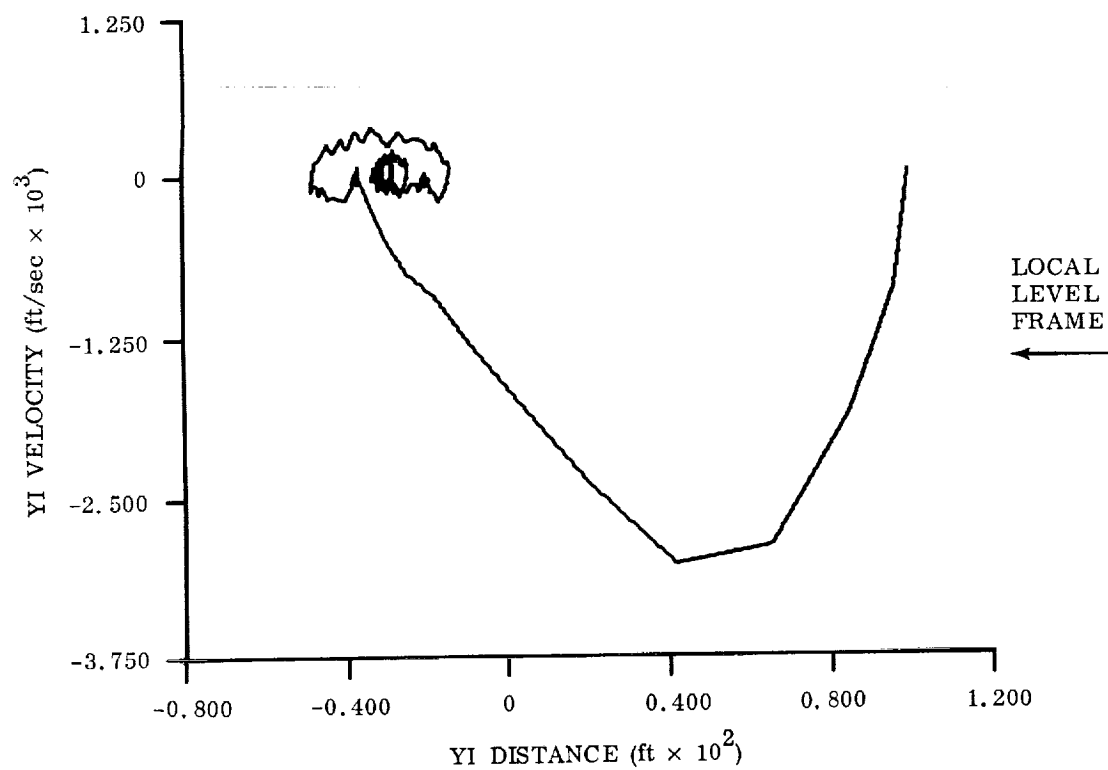


Fig. 3-12 Y-Axis Capture Partial Pseudo-Rate (No ORF, ACF)

exact rate system. Figure 3-10 shows typical capture, and Fig. 3-11 limit cycle performance. The system is not quite as efficient as the exact rate, however for rate gain $T_2 = 1$ in that it requires about 83 impulses in 500 steps (compared to 75 for exact rate and 50 minimum) for an efficiency of about 60%. At rate gain of $T_2 = 3$ the efficiency increases to about 80%.

Dropping two terms (those arising from Coriolis and angular acceleration) in the generation of the pseudo rate yields a system which still captures, Fig. 3-12, and even more interesting shows greater limit cycle efficiency namely about 65% for $T_2 = 1$ and about 80% for $T_2 = 3$.

3.4.2 Lead-Lag With Bang-Bang Control

The second control system studied was the lead-lag system with bang-bang control. It consists of routing the position sensor output through a single lead single lag network and using the combined position-rate signal to switch on the controller. A block diagram of this system is shown in Fig. 3-13. The capture characteristics of this system are somewhat better (more efficient) than for the pseudo rate system but the limit cycle performance is not as good.

Figure 3-14 shows the capture performance of the LL with BB system for $T_2 = 3$ and $T_2 = 1$. Capture for $T_2 = 1$ is somewhat better than for $T_2 = 3$.

3.4.3 Lead-Lag With Pulse-Width, Pulse-Frequency Modulation (PWPF) Control

The third system LL with PWPF control is the most complex to mechanize. Rate is derived in this system by routing the position sensor output through a lead-lag network as above. The control, however, is by means of a modulation scheme identified as PWPF which produces in effect a proportional control for signals up to several times the dead-band level.*

*The theory of operation of the PWPF control is presented in Appendix D.

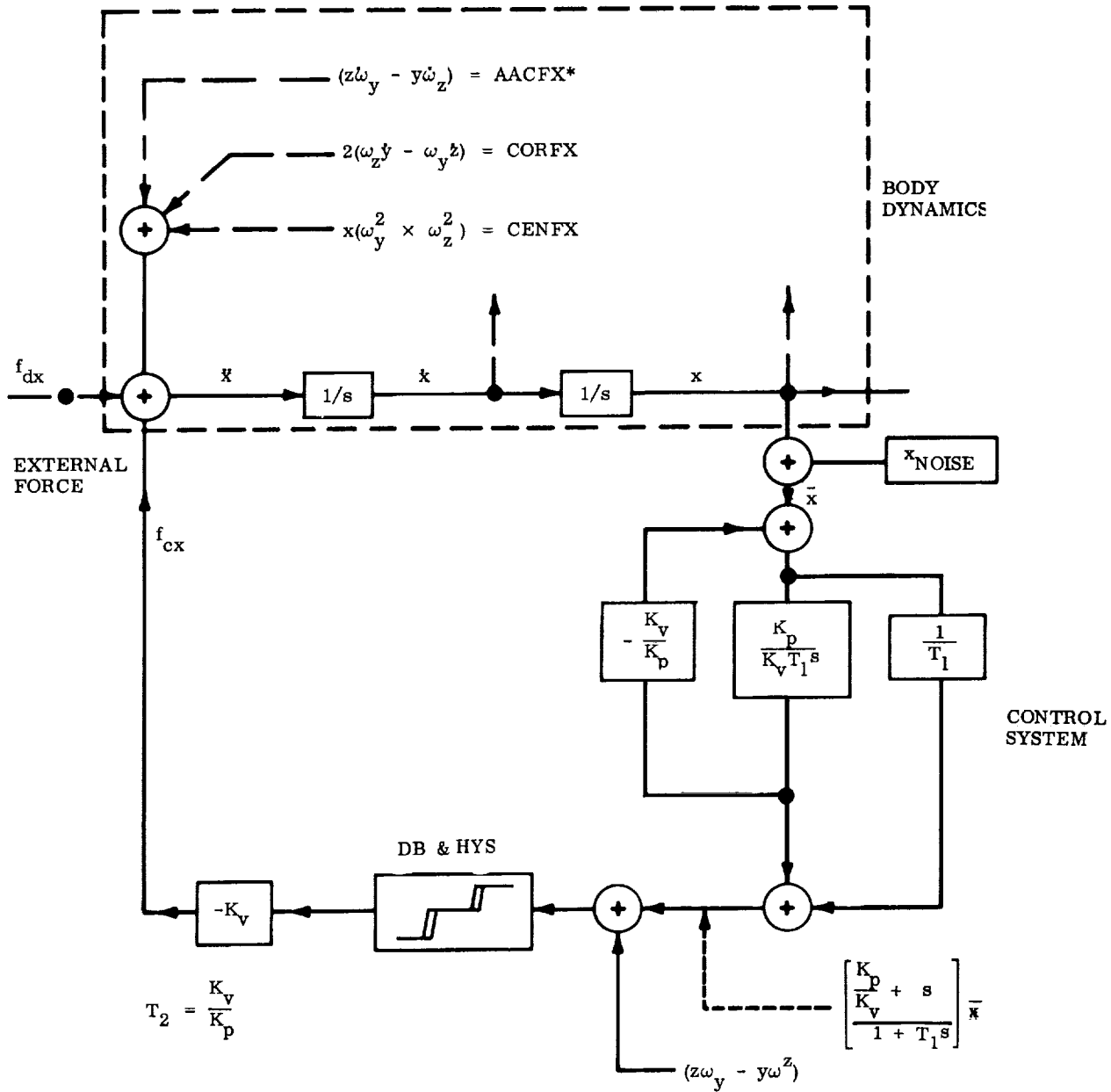


Fig. 3-13 X Channel (Typical) Lead-Lag With Bang-Bang Control

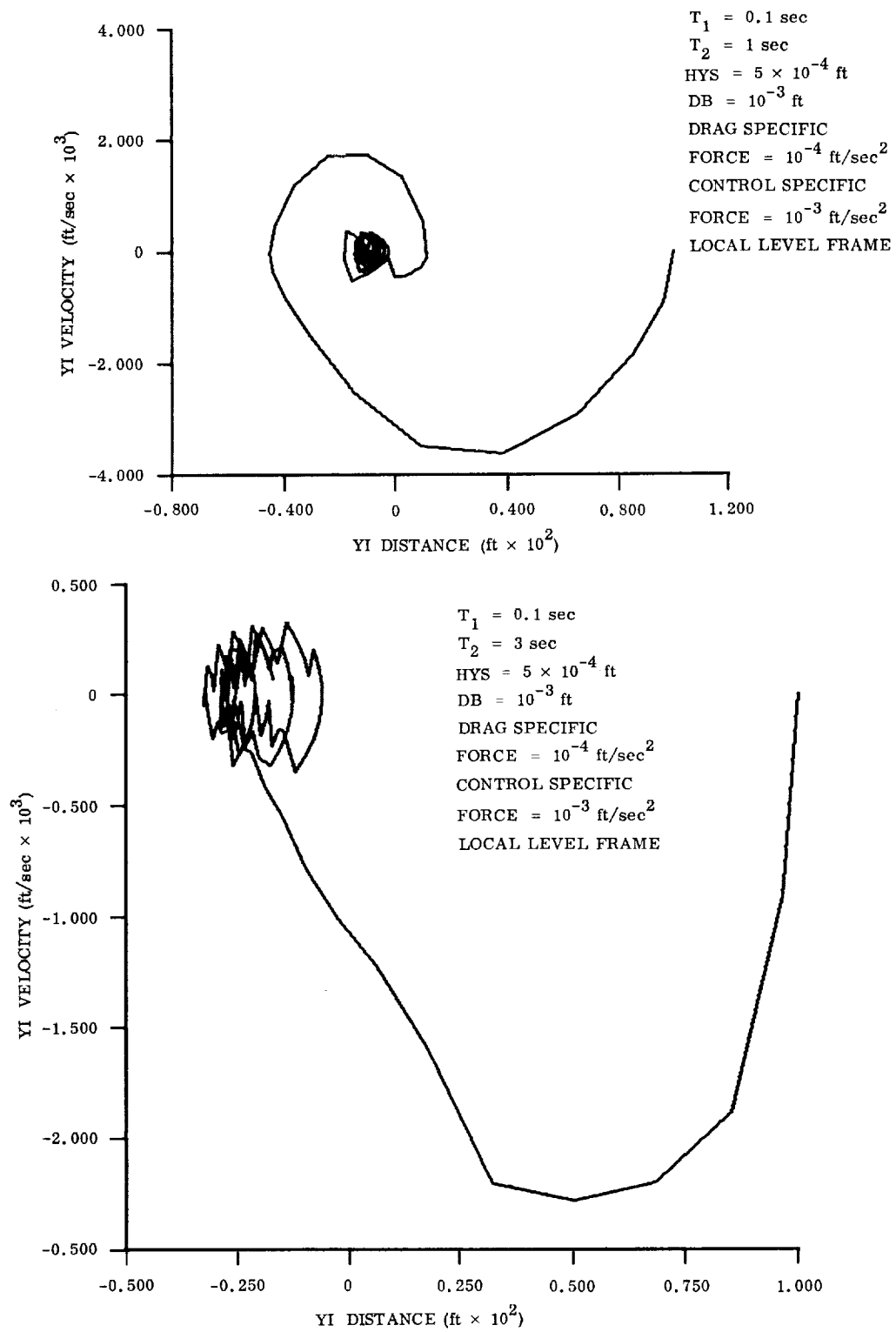


Fig. 3-14 Y-Axis Capture Lead-Lag Bang-Bang Control

A block diagram of the system is shown in Fig. 3-15. The capture characteristics are good as is the limit cycle fuel consumption. Figure 3-16 illustrates the capture and Fig. 3-17 the limit cycle performance of this system. The following PWPF parameters were used in all runs:

$$\begin{aligned} \text{HYS} &= 0.01 & T_1 &= 0.1 \text{ sec} \\ K_A &= 0.06 & T_2 &= K_v/K_p = 3 \text{ sec} \\ \text{DB} &= 0.001 \text{ ft} & T_3 &= 1 \text{ sec} \end{aligned}$$

3.5 SYSTEM PERFORMANCE WITH POSITION MEASUREMENT NOISE

The major goal of the experimental investigation was to compare the limit cycle performance of the systems in the presence of noise in the relative position sensor. The block diagrams in Figs. 3-9, 3-13, and 3-15 show the points at which noise was injected. With a digital subroutine pseudo-random numbers u_1 and u_2 were generated.* From these a set of numbers (sequence) "N", normally distributed with zero mean and standard deviation SF, were generated by the relation (Ref. 26)

$$N = \text{SF} \times (-2\pi \ln u_1)^{1/2} \cos 2\pi u_2$$

N was the noise signal used.

The systems were evaluated by means of a parametric study in which the standard deviation of the noise (SF) was varied for each system. At each value of SF, several different random values of N were used and the total impulse required to operate the system in the limit cycle mode for a given length of time was computed. Specifically noise was simulated by adding a different random signal N to the position signal from the three body-position sensors at

*In this routine the pseudo random numbers N_j are obtained from the following algorithm: $N_j = R_j/d$ where $R_j = 2(kR_{j-1} + c)_{28}$ where $()_{28}$ means that the number $()$ is truncated by taking only the last 28 binary digits, and where the constants are $d=2^{28}$, $k=2^{11}-3$, $c=211527139$. The N_j are uniformly distributed from 0 to 1. The sequence is called pseudo random because it repeats after being called 2^{28} times.

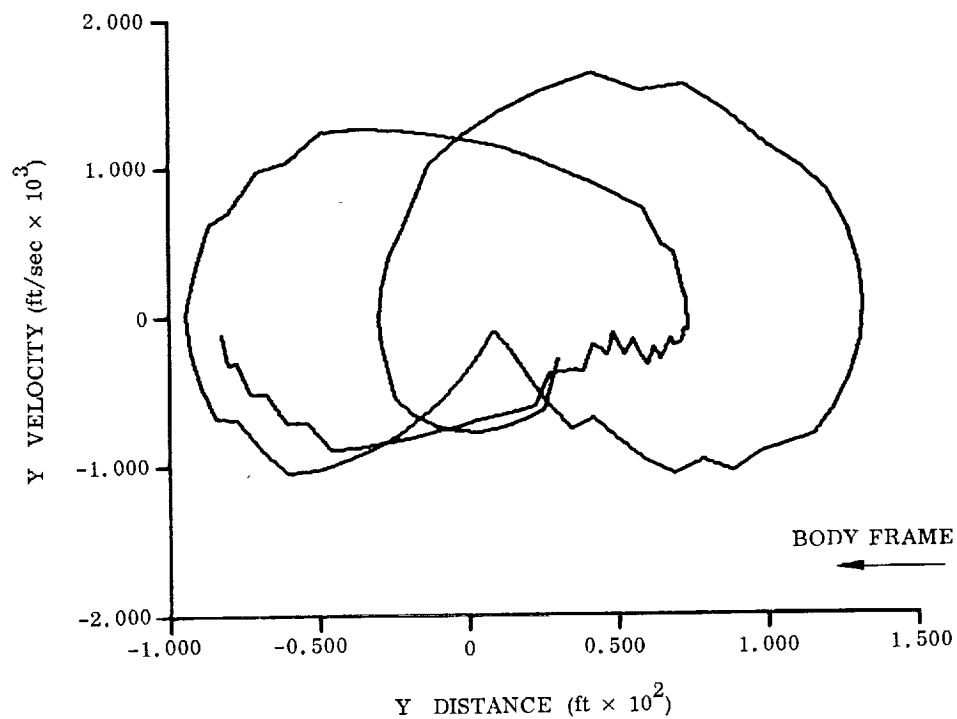
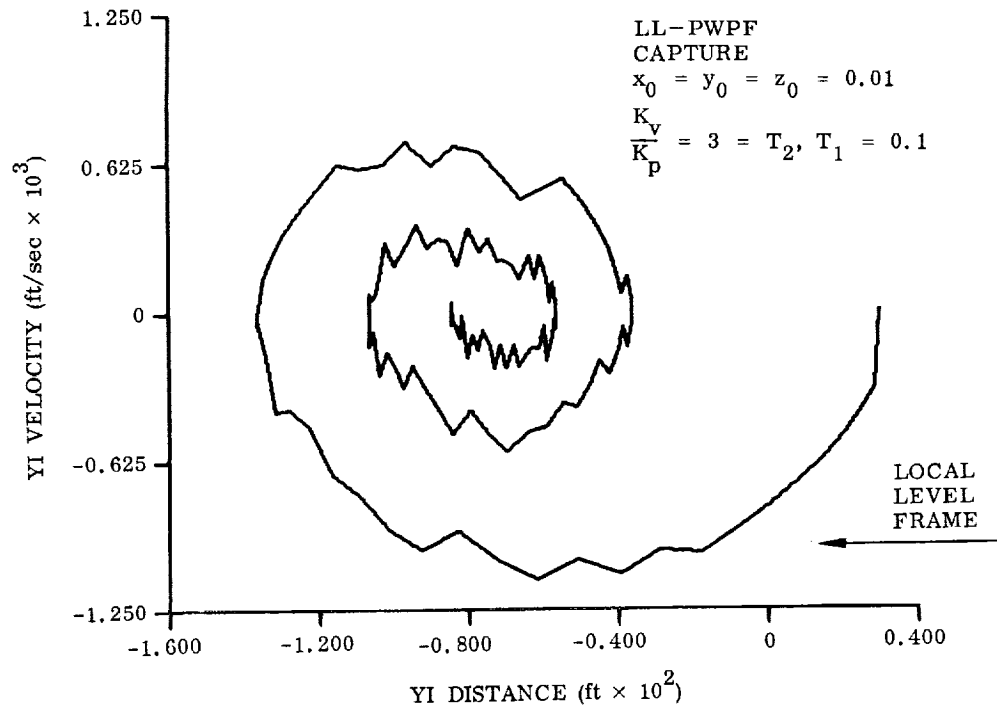


Fig. 3-16 Y-Axis Capture LL-PWPF Control

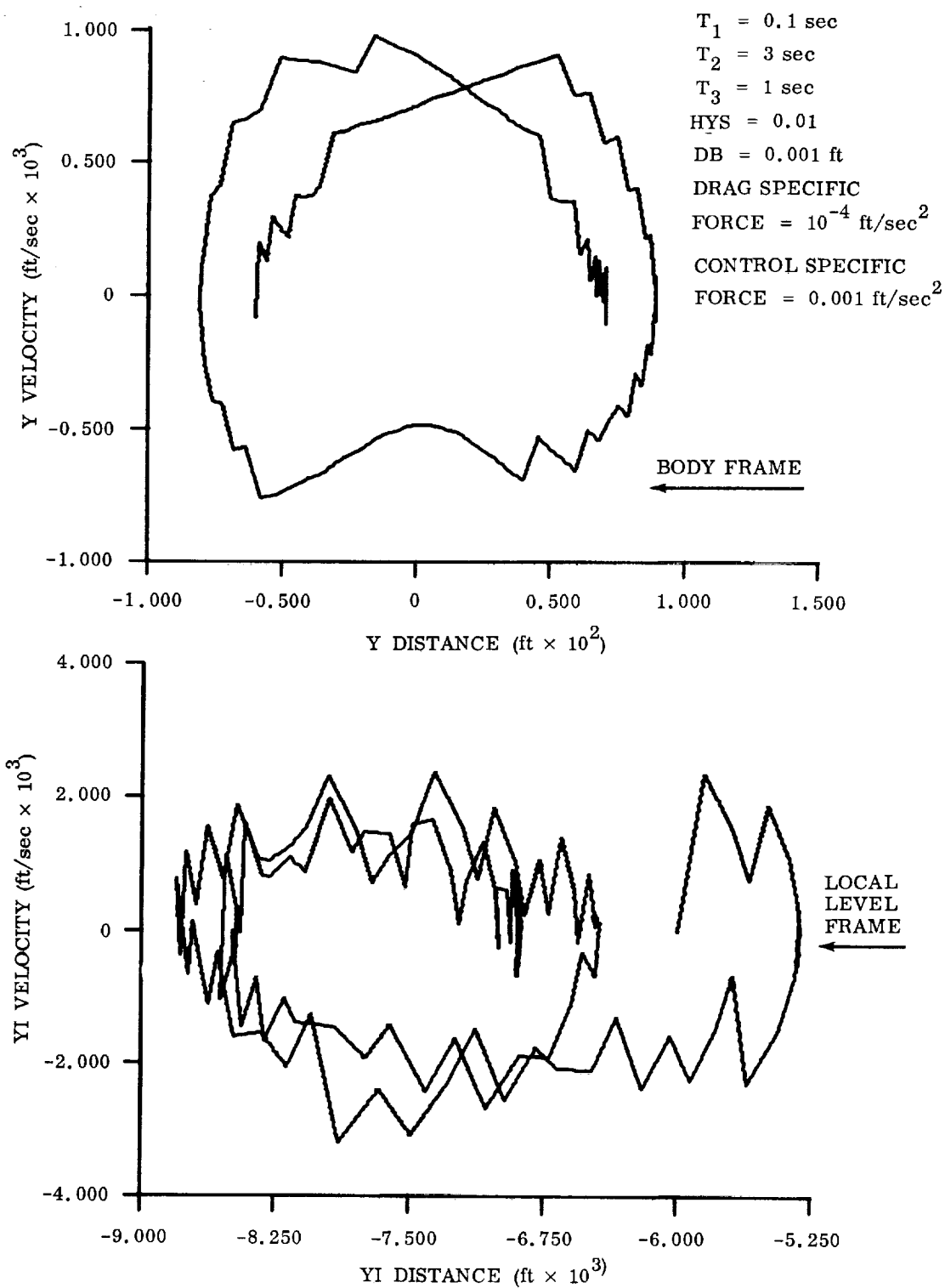


Fig. 3-17 Y-Axis Limit Cycle LL-PWPF Control

each machine integration step. It was assumed that by making the integration step size sufficiently small so that the system state did not change appreciably between steps, that the uncorrelated sequence described above simulated the introduction of "white noise" into the system.

Since the nature of the noise that will actually be encountered is unknown at this time, the above technique seems reasonable for providing some insight into the performance of the different systems in the presence of some random inputs.

Each system was operated at several different values of rms noise level, specifically at values in feet of 1^{-3} , 3^{-4} , 1^{-4} , 3^{-5} , 1^{-5} , 3^{-6} , 1^{-6} , 3^{-7} * or at ratios of rms-noise level (SF) to dead band (0.001 ft) of 3^{-1} , 1^{-1} , 3^{-2} , 1^{-2} , 3^{-3} , 1^{-3} , 3^{-4} . At the small values of SF/DB the performance was identical to that with no noise. Figures 3-18 through 3-27 show the performance of several systems. Note that in all cases both the mean value of total impulse the spread increases with increasing SF/DB ratio. The ordinate of all plots is the ratio of the total impulse used in the run to that required to just compensate for drag. The value 1 would be achieved by a system in which the jets always fired in direct opposition to the drag.

From these charts we see quite clearly that, for the system parameters (time constants) chosen, the limit cycle performance of the lead-lag bang-bang system is significantly poorer than that of the others especially in the presence of noise having scale factor (standard deviation) approaching the size of the dead band. The pseudo rate and PWPF are very close in limit cycle fuel consumption. The greater simplicity in mechanization and the slightly better capture characteristic of the pseudo rate system would thus probably become the deciding factor in system selection. It is very interesting to note that the pseudo rate system with two terms missing from the rate signal is essentially the same as that with all terms included. In fact, for the particular sample at hand both pseudo rate-systems appear slightly better than

* $3^{-7} \equiv 3 \times 10^{-7}$, etc.

the PWPF system for DB to noise ratios between about 2 and 20. The following system conditions applied for all runs:

Initial Conditions

$$\omega_{z0} = 0.1 \text{ rad/sec}$$

$$\omega_{y0} = 0.02 \text{ rad/sec}$$

$$\omega_{x0} = 0$$

$$x_0 = y_0 = z_0 = 0.0008 \text{ ft}$$

$$f_{\text{thrust}}/f_{\text{drag}} = 10$$

The number of integration steps per run varied between 300 and 1000. In all cases this corresponded to a system time of about 100 seconds (i.e., enough for the vehicle to tumble more than once relative to the drag field). Other variations in system parameters are indicated on the charts. The constants referenced can be identified in the block diagram of the appropriate system.

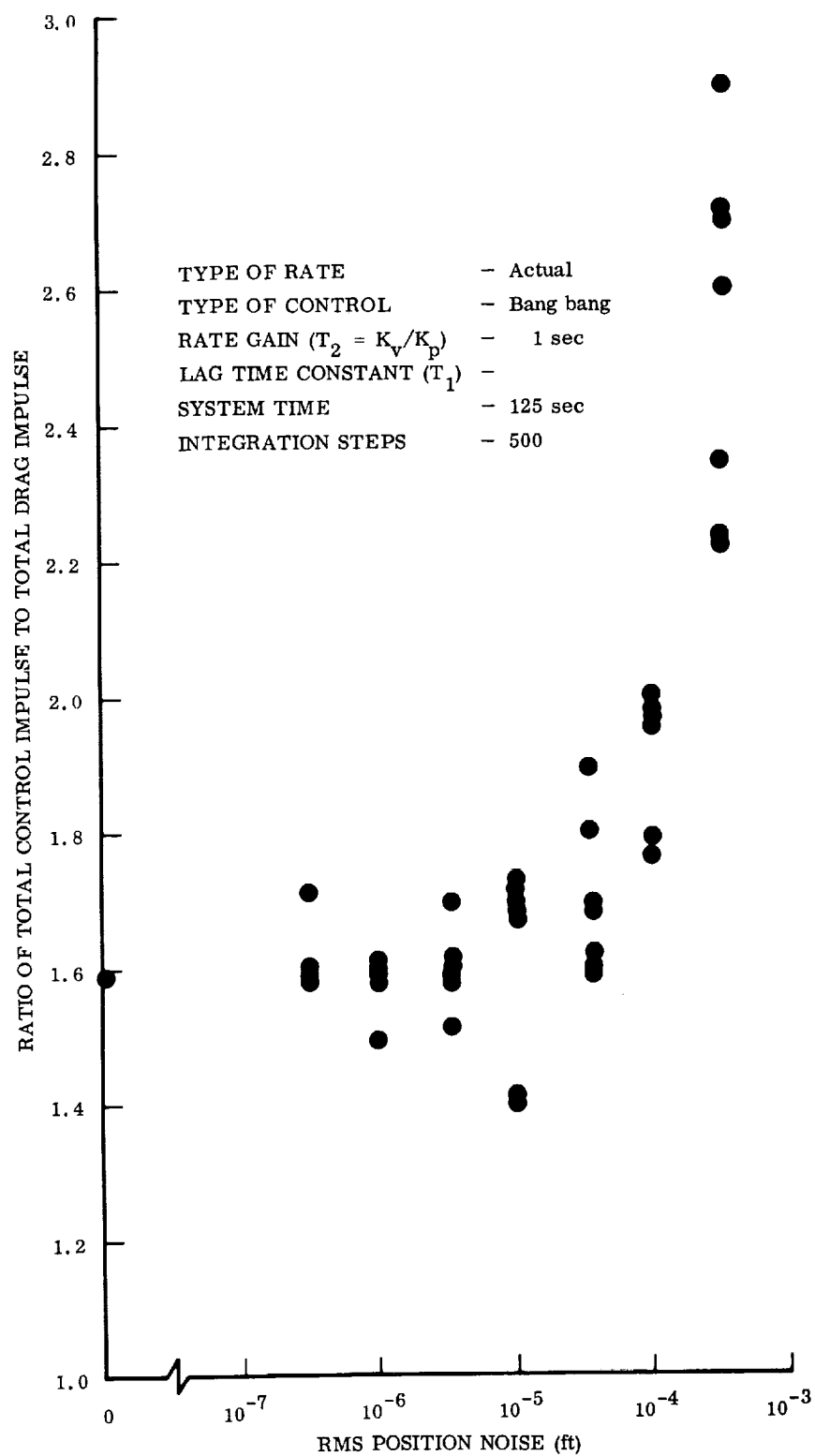


Fig. 3-18 Limit Cycle Fuel Consumption in the Presence of Noise: Actual Rate With Bang-Bang Control

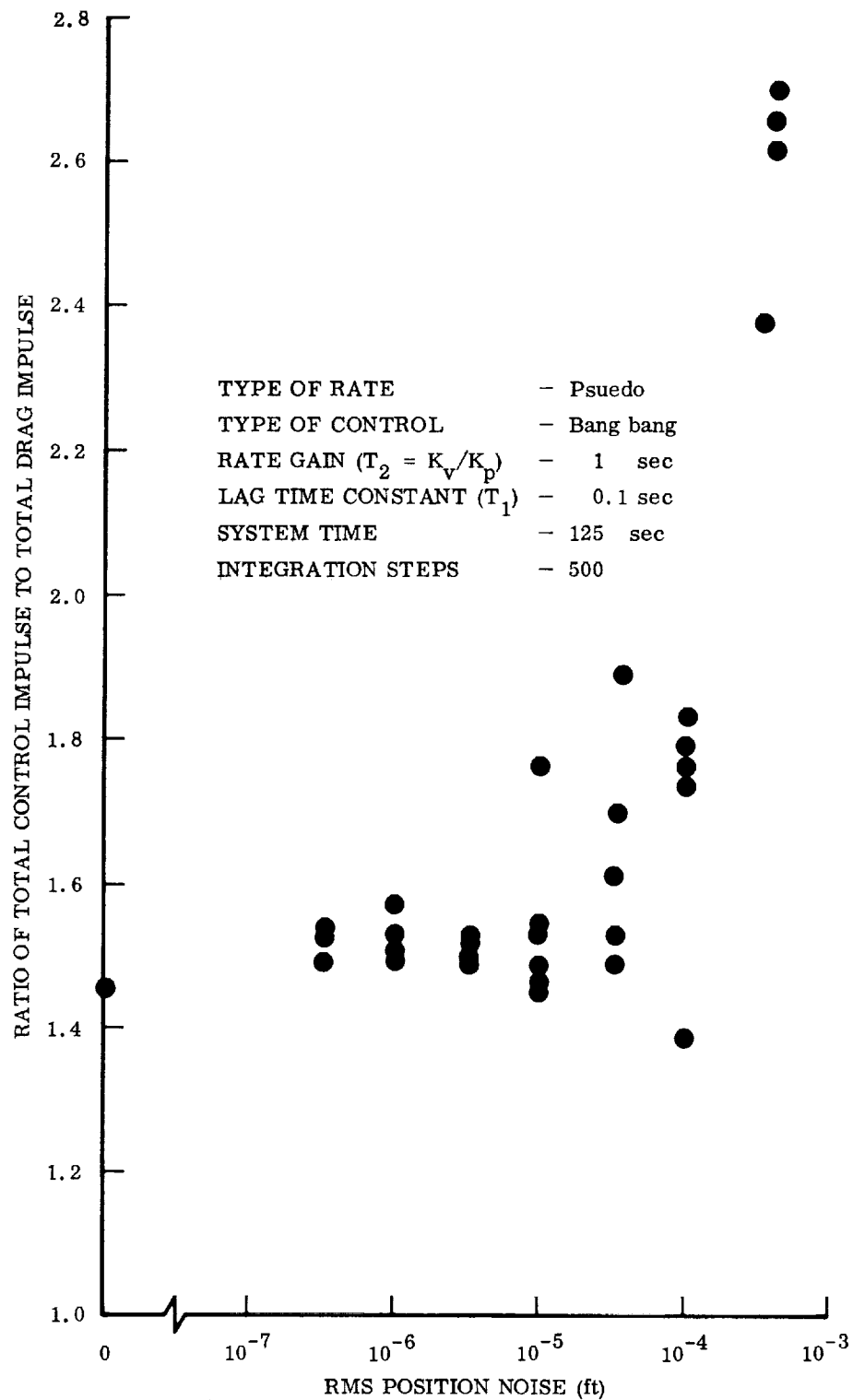


Fig. 3-19 Limit Cycle Fuel Consumption in the Presence of Noise:
 Pseudo-Rate With Bang-Bang Control

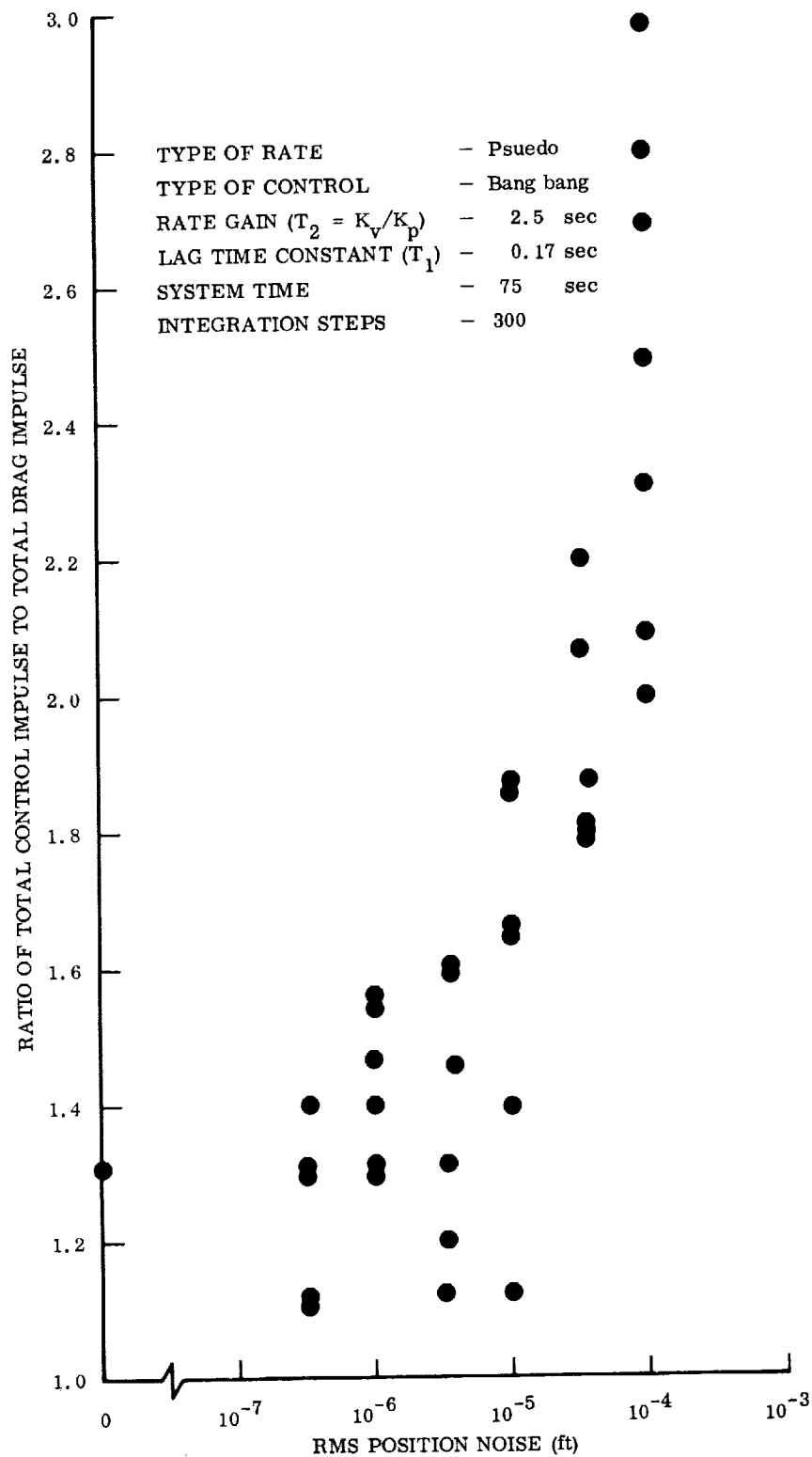


Fig. 3-20 Limit Cycle Fuel Consumption in the Presence of Noise:
 Pseudo-Rate With Bang-Bang Control

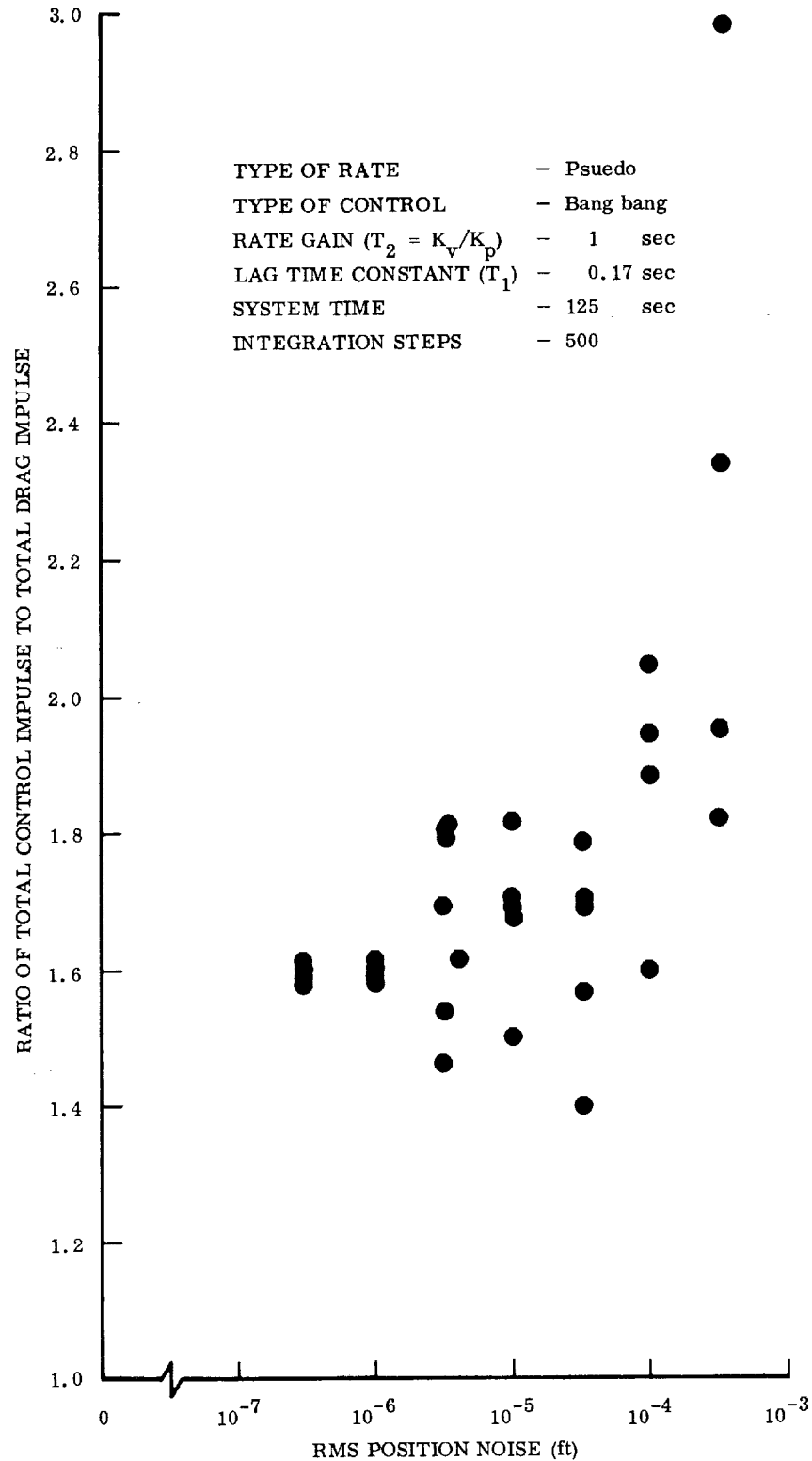


Fig. 3-21 Limit Cycle Fuel Consumption in the Presence of Noise:
 Pseudo-Rate With Bang-Bang Control

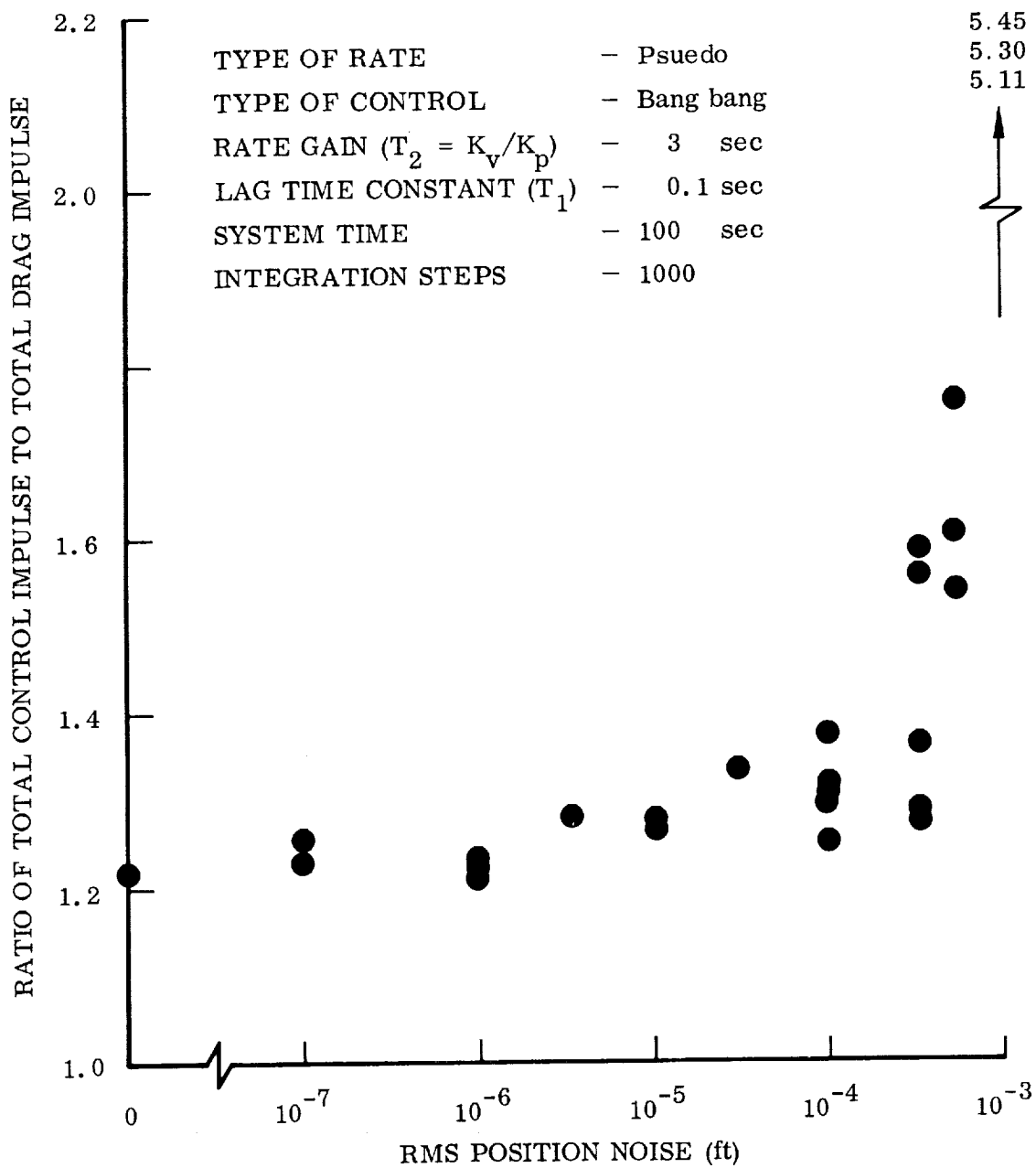


Fig. 3-22 Limit Cycle Fuel Consumption in the Presence of Noise:
 Pseudo-Rate With Bang-Bang Control

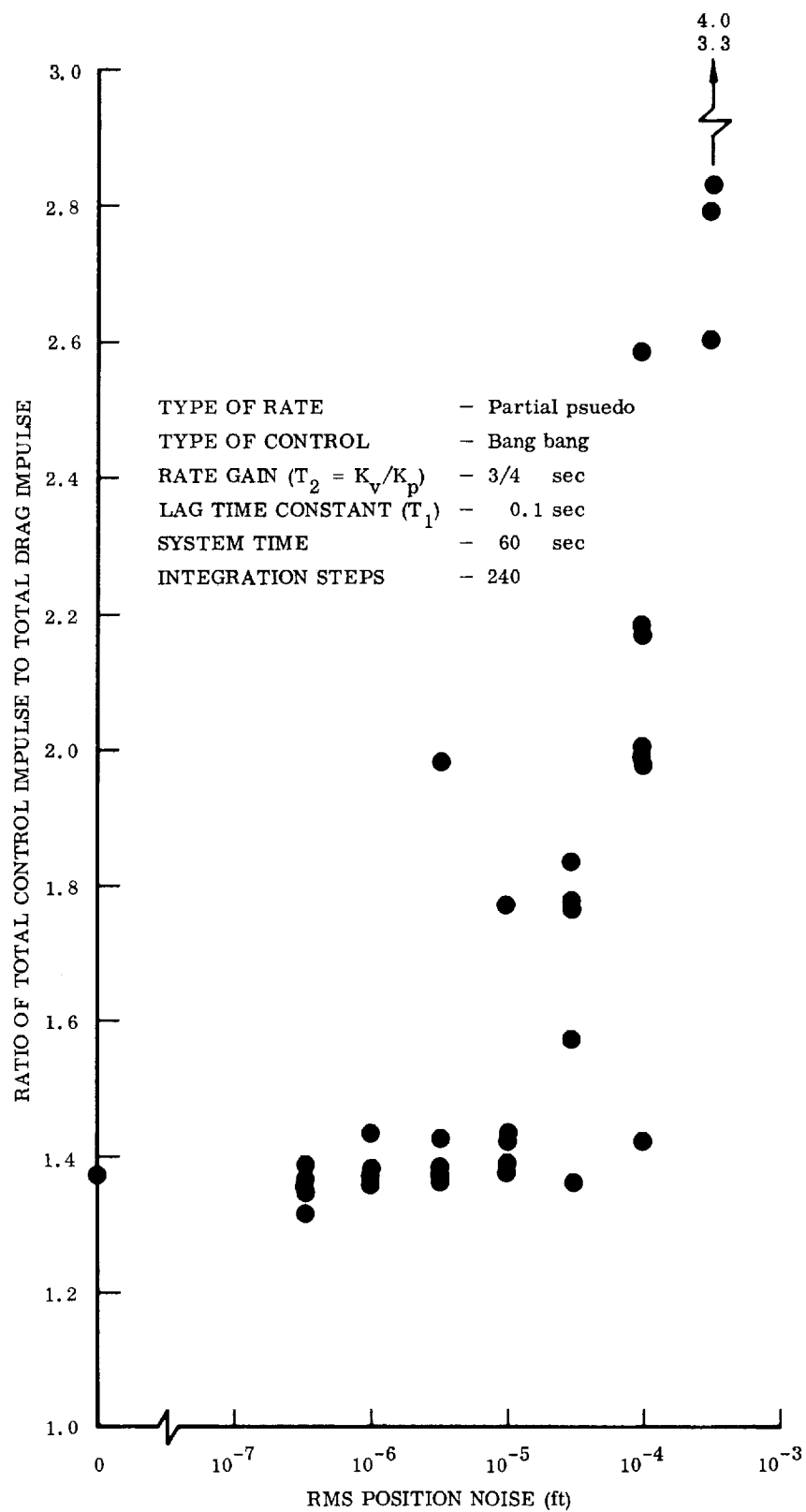


Fig. 3-23 Limit Cycle Fuel Consumption in the Presence of Noise: Partial Pseudo-Rate no CORF, AAF, CENF With Bang-Bang Control

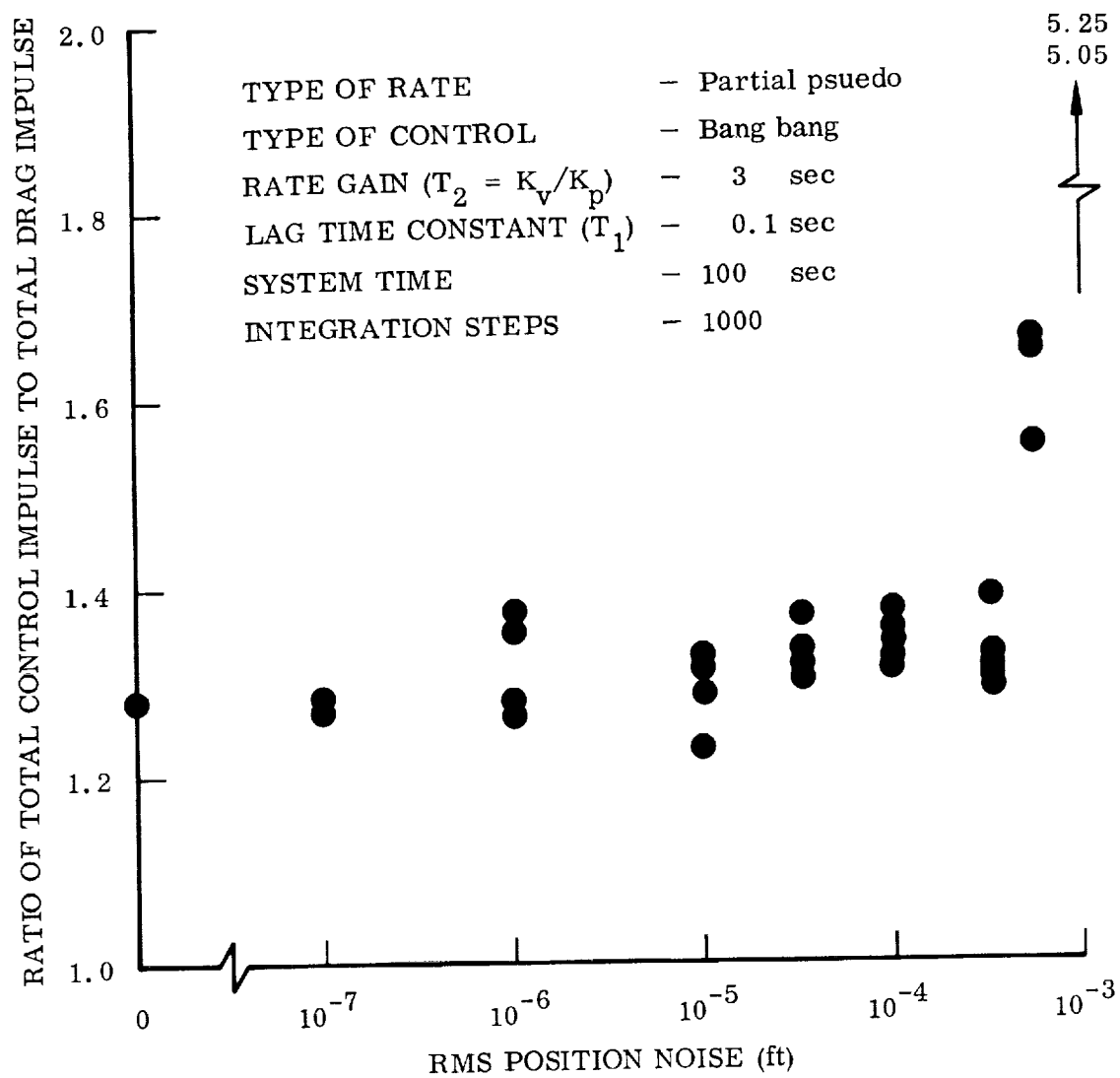


Fig. 3-24 Limit Cycle Fuel Consumption in the Presence of Noise: Partial Pseudo-Rate no AACF or CORF With Bang-Bang Control

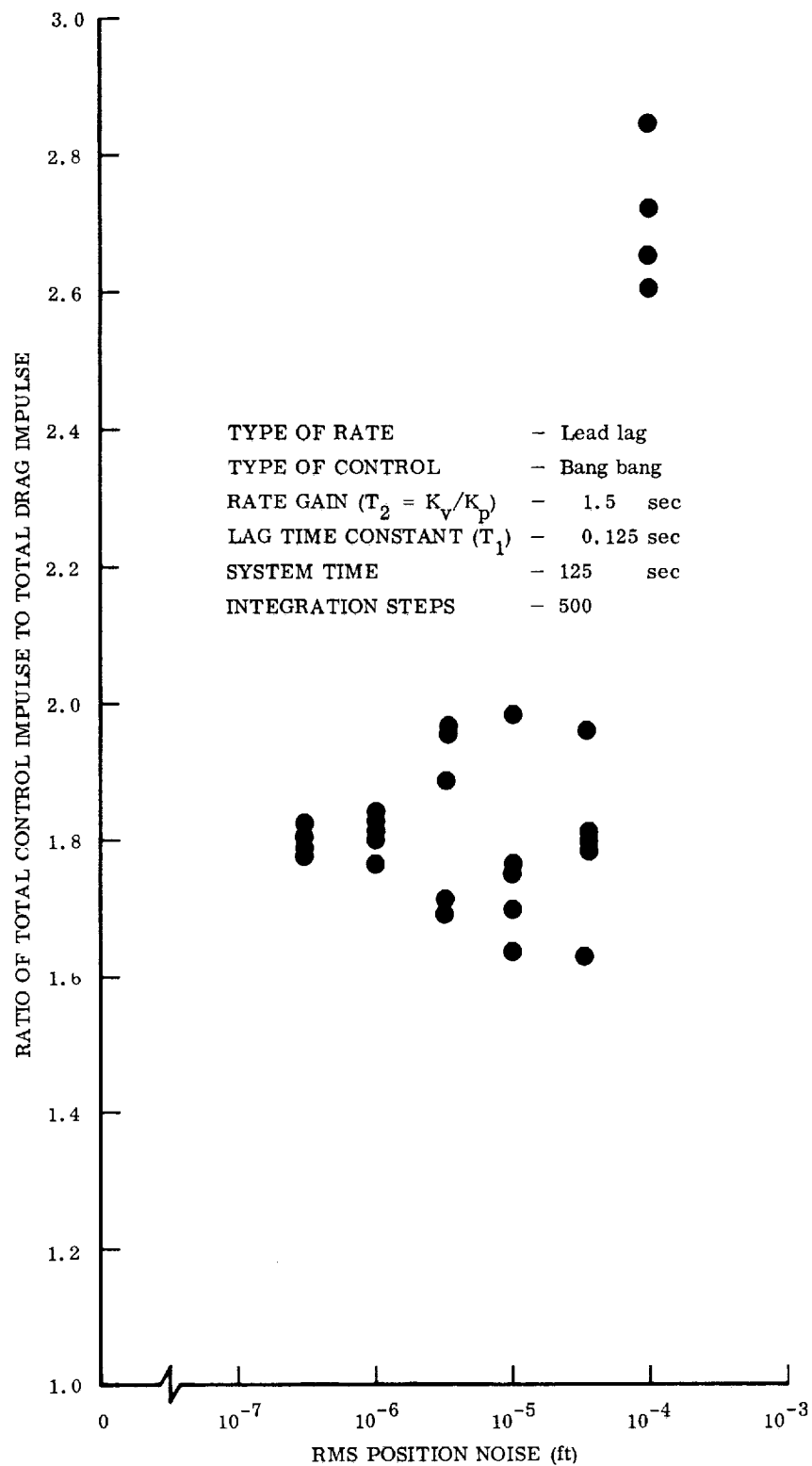


Fig. 3-25 Limit Cycle Fuel Consumption in the Presence of Noise: Lead-Lag With Bang-Bang Control

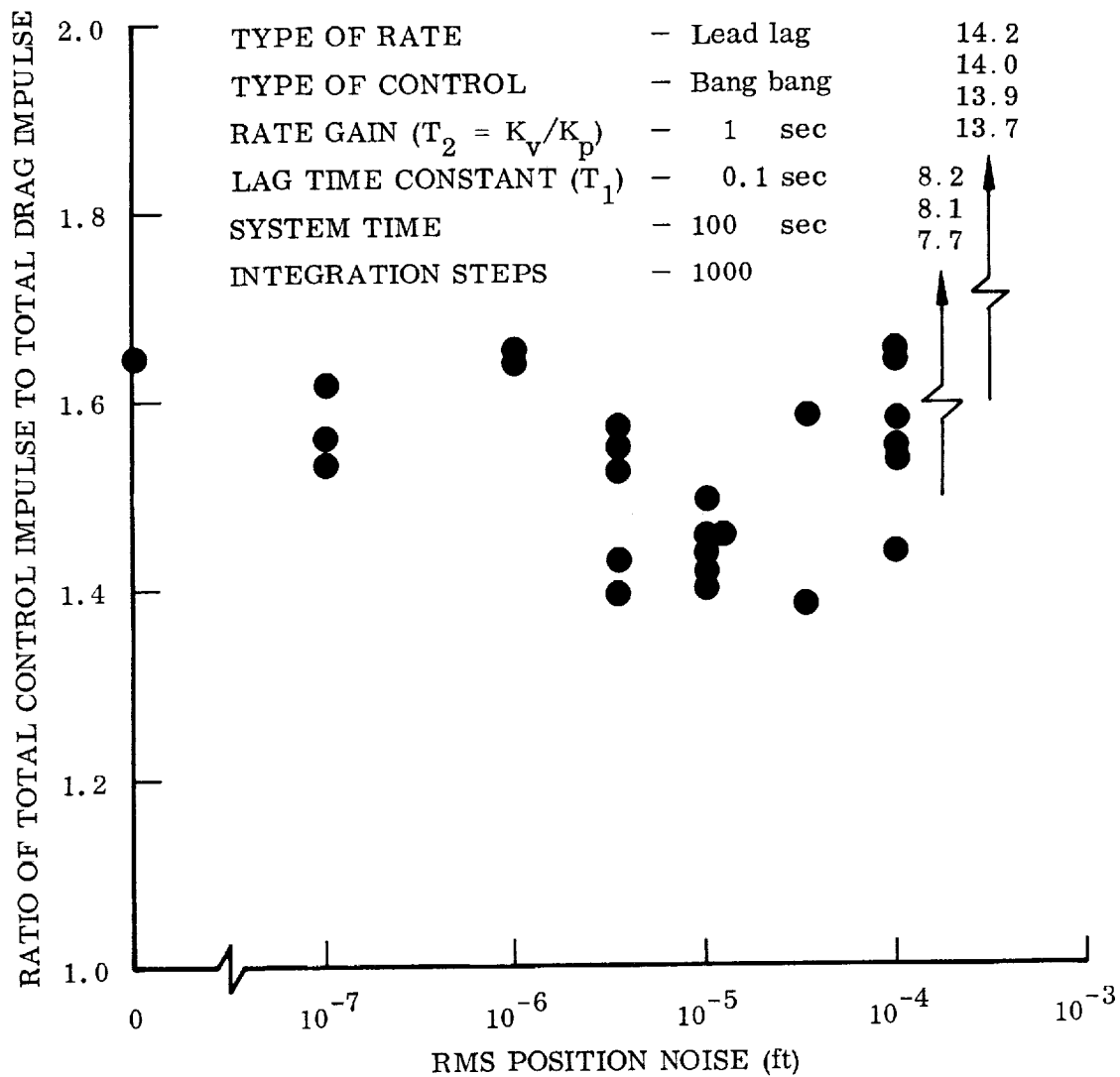


Fig. 3-26 Cycle Fuel Consumption in the Presence of Noise: Lead-Lag With Bang-Bang Control Limit

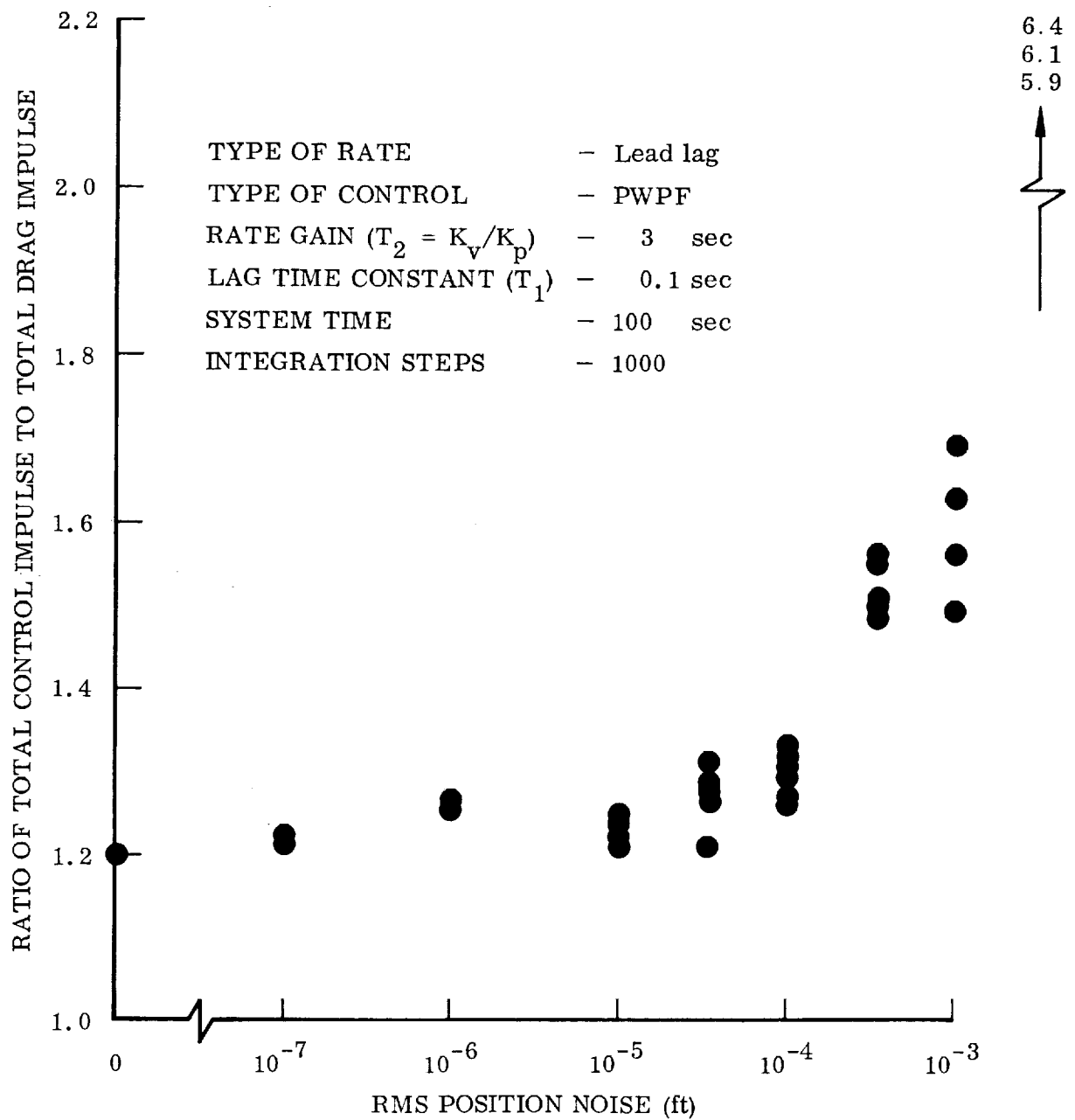


Fig. 3-27 Limit Cycle Fuel Consumption in the Presence of Noise: Lead-Lag With PWWF Control

Chapter 4

THE SINGLE AXIS DRAG MAKE-UP CONTROL SYSTEM

For a vehicle which has an attitude control system to keep one vehicle axis aligned (nominally) along the velocity vector (i. e. , in the direction of the drag force), it is not necessary to require the vehicle to "follow" and not touch the ball (proof mass) in a direction transverse to the direction of the drag force. This realization led to the design of a system in which only the position of a ball along the axis aligned with the drag force is monitored and controlled. In this scheme, the ball is allowed to contact the side walls of a tubular cage, and displacement along the cage axis is measured by a photo-transistor and this information is used to control thrust on the vehicle and prevent the ball from contacting either end of the cage. This chapter will discuss the design and error analysis of such a system. It will be shown that errors due to the proof-mass contacting the lateral constraints are not prohibitive for low altitude missions in which drag make-up to less than 1% of the drag is satisfactory.

The system is of particular interest because it will probably be the first drag compensating system to actually fly. The analysis is important since it gives insight into the possible system accuracy and therein provides a means for evaluating the system performance and also a measure of system capability for realizing new results on the nature and extent of the earth's atmosphere at low satellite altitudes (100 to 200 nm) as well as new geophysical data relating to the earth's exact gravitational potential.

4.1 SYSTEM COMPONENTS

The entire system for drag make-up described in this chapter has been developed and fabricated specifically to fly on and control an Agena satellite. The system consists of a sensor for detecting the effect of the drag and control forces on the vehicle, an electronic control package for processing the sensor output, two on-off valve gas jets controlled by the electronic package for producing thrust on the vehicle, plus necessary stored gas and batteries. Figures 4-1, 4-2, and 4-3 are photographs of the pertinent flight hardware.

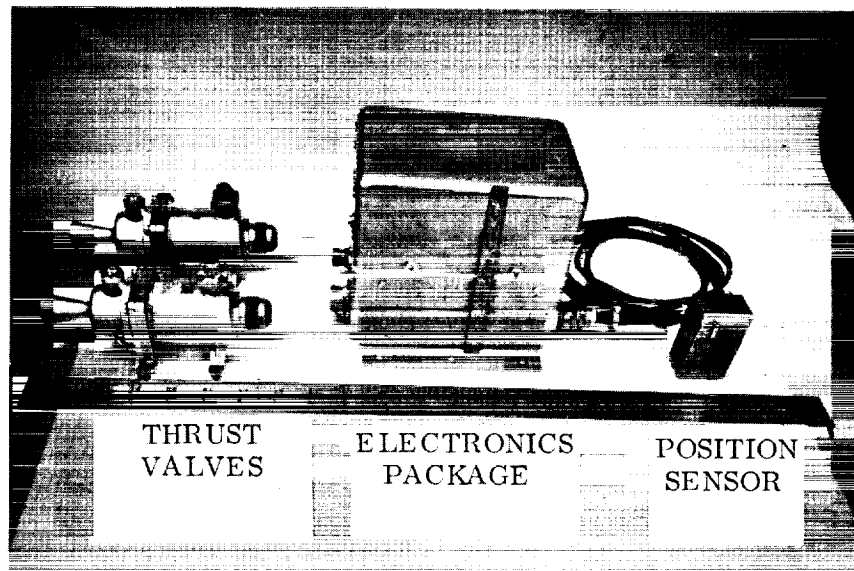


Fig. 4-1 Drag Make-up System

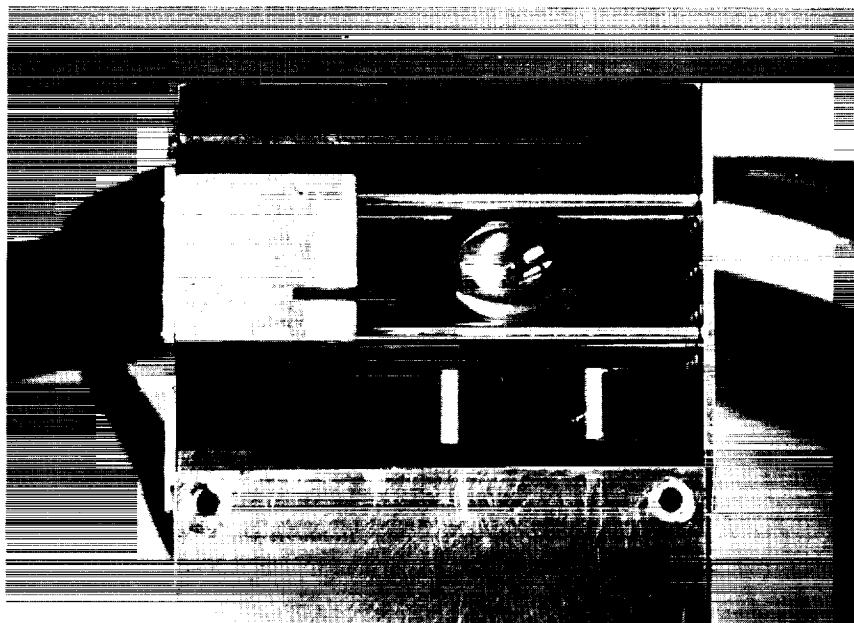


Fig. 4-2 Position Sensor

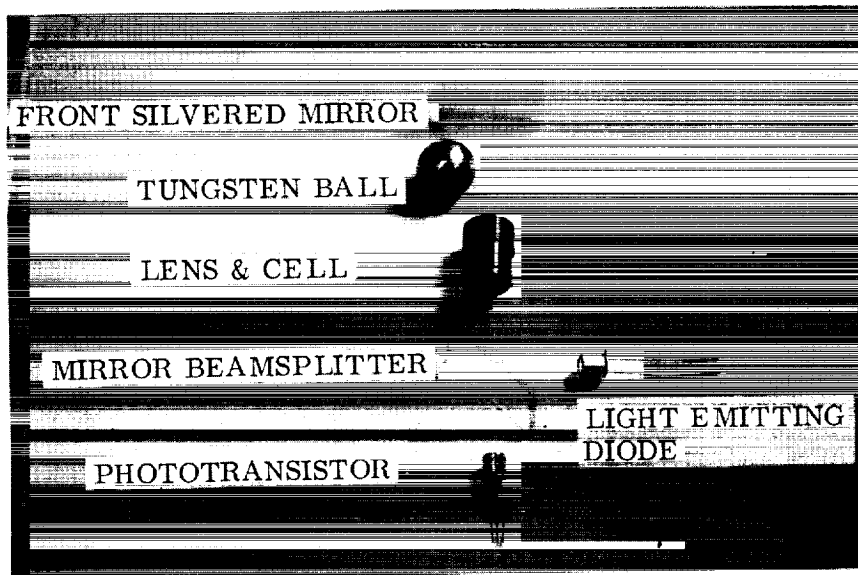


Fig. 4-3 Position Sensor Optical Components

The rationale used in arriving at this configuration was briefly as follows. Since it was desired to perturb the ball as little as possible in sensing its position, a light beam seemed the most logical choice, especially since it could be readily and easily mechanized. Figure 4-4 shows a functional sketch of the sensor concept.

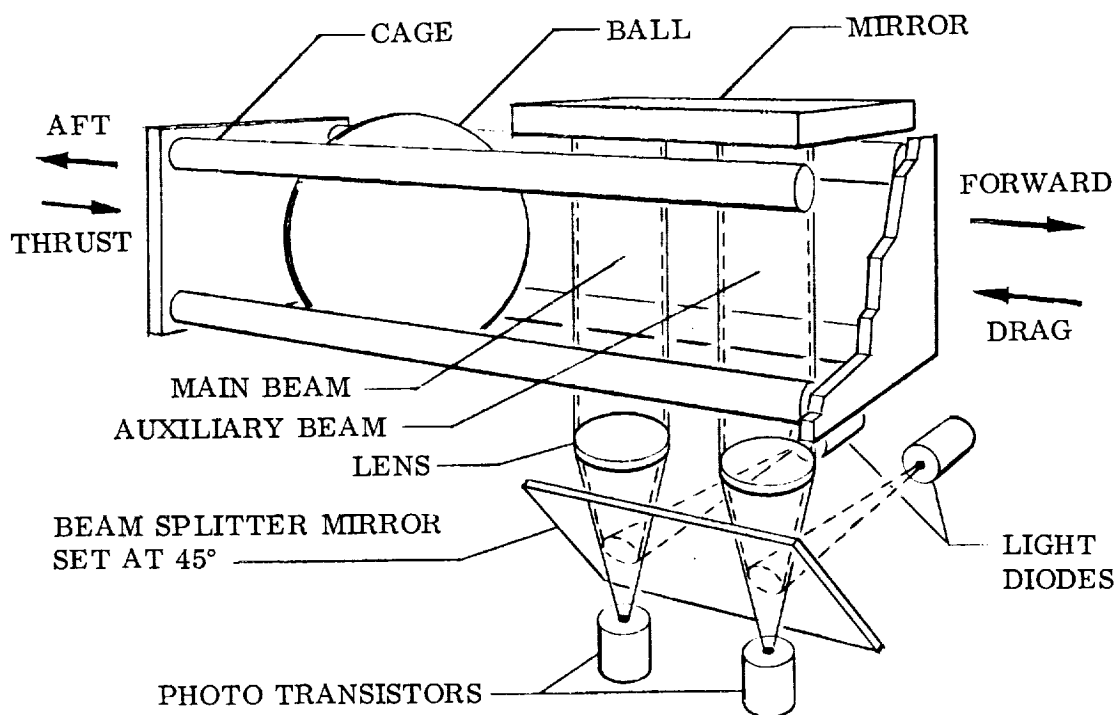


Fig. 4-4 Ball-in-Cage Mechanization

Since only position of the ball can be easily measured, a system was synthesized in which the rate (ball-cage relative velocity) was derived electronically.

The use of derived states in control systems is a standard technique. Recent work of Luenberger (Ref. 22) condenses and presents quite general results and applications in a very elegant and concise form. The particular method of deriving rate in this system was suggested by the work of Leonard (Ref. 23) on long-life control systems and is commonly called "pseudo-rate."

The electronics employed used standard solid state components (Fig. 4-5). These include in addition to the photo-transistors, a pair of light emitting diodes, about two dozen transistors and associated resistors and capacitors. For thrust the system uses standard Agena attitude control jets modified to operate at a low thrust of about 0.1 lb.

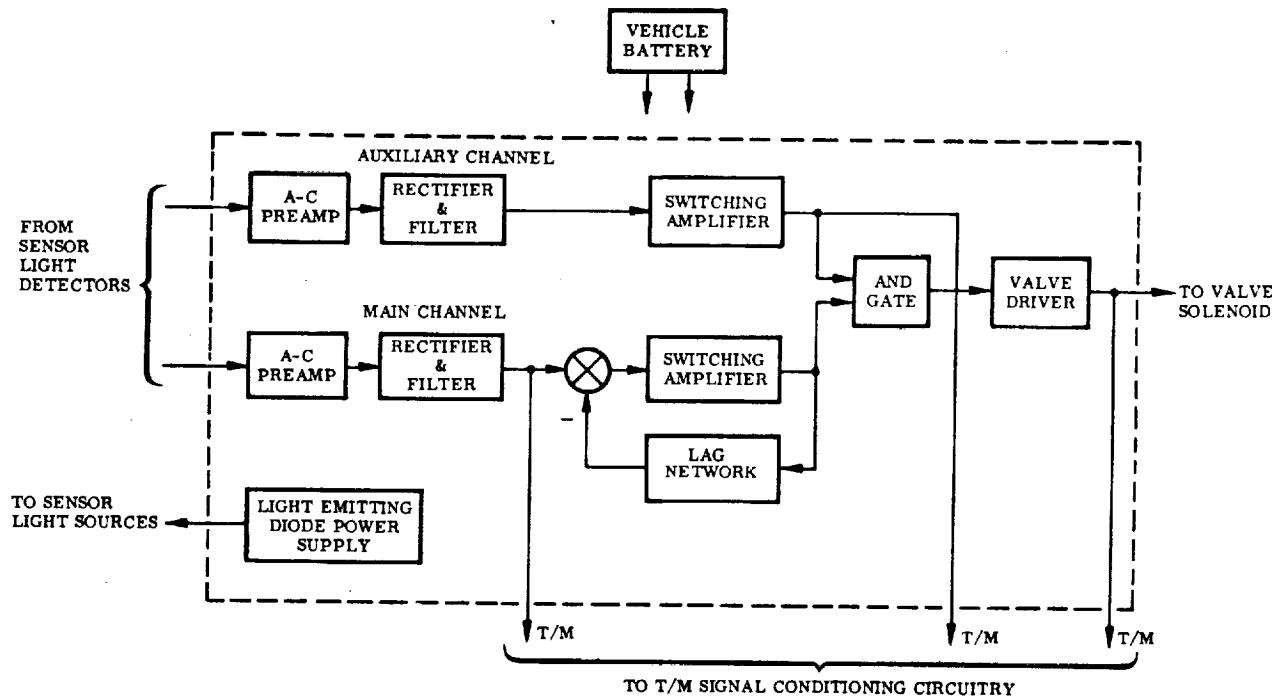


Fig. 4-5 Block Diagram of Electronic Package

4.2 SENSOR THEORY OF OPERATION

The operation of the system is quite simple and straightforward. The overall control scheme utilizes the fact that active thrust need only be provided in one direction – in opposition to the drag. Thus, in the absence of control thrust the ball tends to accelerate toward the front of the cage. The light from two light-emitting diodes is collimated and caused to cross the cage in a transverse direction and fall upon photo-transistors. The two beams are identified as main and auxiliary.

The system is designed such that, for zero rate, the thruster is turned on when the ball is forward of the main beam. It is turned off when the main beam is interrupted by the ball (as it moves relatively aft under the forward thrust on the vehicle). The forward rate of the vehicle relative to the ball at thrust cut-off can carry the ball on through the beam and cause it to uncover the beam from the front (of the beam).

In a more conventional force balance system, the procedure at this point would be to call for thrust in the opposite direction. However, in the interest of conserving fuel and because the drag force is ever present (although perhaps small) to provide a restoring force, no counter thrust (in aid to drag) is provided in this system.

To guarantee adequate control with this concept, two additional provisions are made. First, an auxiliary beam is used to inhibit the thruster when the ball is aft of a particular set point. In the present system, this is set so that when less than 15% of the auxiliary beam is covered by the ball the thruster is inhibited. The effect of this is that the main beam does not have to sense the direction but only the amount of ball displacement and thus can be quite simple.

The second provision is the allowance of a large travel for the ball aft of the beams to accommodate the low restoring force obtainable from low drag at apogee. For operation in more eccentric orbits the distance to the rear end wall can be increased. This helps provide the increased dynamic range necessary due to the greater ratio of perigee to apogee drag force.

4.3 CONTROL SYSTEM DYNAMICS

The foregoing discussion was confined to ball position only (zero rate) in order to make clear the role of the two beams. In actual operation, of course, the switching amplifier which controls the thruster is driven by a combination of position plus "pseudo rate." Figure 4-6 is a block diagram of the control system dynamics.

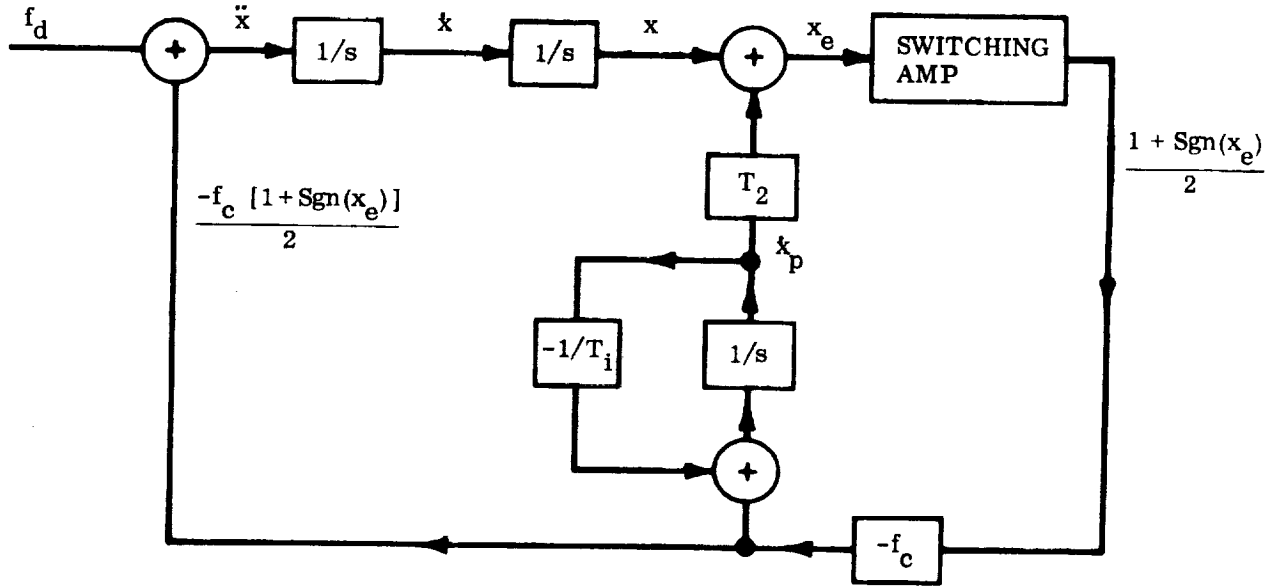


Fig. 4-6 Single Axis Control System Block Diagram

The plant is a simple $1/s^2$ system and control is accomplished by a constant magnitude thruster which is either full on or all off. The modulation accomplished by the combination of position and pseudo rate can best be described as duty cycle modulation, that is, the duty cycle increases proportional to the average forward displacement of the ball in the main beam. This displacement is in turn proportional to the drag. The system clearly has a position offset proportional to the external force.

In the diagram \dot{x}_p represents the derived "pseudo rate." It differs from the true rate \dot{x} in that it does not depend directly on the disturbing force f_d , i.e., the true rate is obtained by integrating:

$$\ddot{x} = f_d - \frac{f_c}{2} [1 + \text{sgn}(x_e)] \quad (4.1)$$

whereas the pseudo rate is obtained from integrating

$$\ddot{x}_p = -\frac{\dot{x}_p}{T_1} - \frac{f_c}{2} [1 + \text{sgn}(x_e)] \quad (4.2)$$

where

$$\text{sgn}(x_e) \equiv \begin{cases} 1 & \text{for } x_e > 0 \\ 0 & \text{for } x_e = 0 \\ -1 & \text{for } x_e < 0 \end{cases}$$

The error signal x_e which controls the force f_c is given by:

$$\left. \begin{aligned} x_e &= x + T_2 \dot{x}_p - (DB + \text{Hys}) & \text{ON} \\ x_e &= x + T_2 \dot{x}_p - DB & \text{OFF} \end{aligned} \right\} \quad (4.3)$$

The average steady state position offset in x (x_{ss}) is given by

$$x_{ss} - \left(DB + \frac{\text{Hys}}{2} \right) = T_1 T_2 f_d \quad (4.4)$$

which can be seen by noting that in steady state the average value of $x_e = 0$ and the average value of $-\dot{x}_p/T_1 = f_d$. A more detailed analysis of this problem is presented in Appendix C.

4.4 LABORATORY SIMULATION OF THE CONTROL SYSTEM

The ideal procedure for any design synthesis would be to operate the actual system in its actual environment and adjust parameters to achieve the best performance. This is not always possible. It is particularly difficult in the present problem because the solution utilizes the near zero-g environment of the satellite. However, the fact that the control is along one axis only allowed a very good simulation to be performed in the laboratory.

By suspending a ball on a bifilar torsion pendulum (Fig. 4-7) time-constants and effective forces corresponding to those expected in orbit were generated. In this simulation torque on the pendulum corresponds to force on the vehicle. The torque was produced by two mechanisms, namely torsion in the bifilar suspension and magnetic torque on a magnet due to both the earth's magnetic field and two Helmholtz coils. By sending an appropriate "bias" current through the coils the

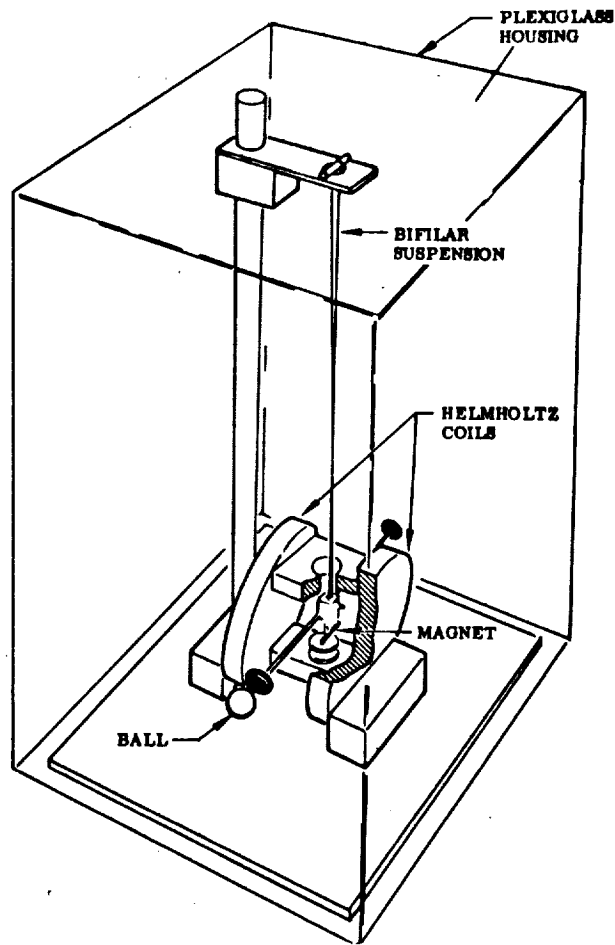


Fig. 4-7 Laboratory Test Fixture

"non-control" torque on the pendulum was matched to the air drag force. To simulate the varying air drag of an eccentric orbit the "bias" current was slowly varied in a pre-programmed fashion.

Control torque was produced by sending a "control" current through the coils. This current was produced by the sensor which was placed in the path of the suspended ball. Thus circumferential motion of the ball in the simulation corresponds to axial motion of the ball relative to the case in orbit.

With this scheme it was possible to incorporate actual system time constants and components in a real time closed loop simulation. Only the gas jets were not used.

Acquisition and damping were evaluated for various system parameters such as integration time constant, cage dimension, switching amplifier hysteresis and

minimum on-time, ball size, and light beam aperture under various external environments especially the extremes in drag force from apogee to perigee. Figure 4-8 shows a series of acquisition runs at various drag levels for various apertures. Typically the system acquires from an extreme ball displacement in less than 1 min. Although it can operate up to 100% duty cycle it is set typically so that a 30% duty cycle will counter the perigee drag force.

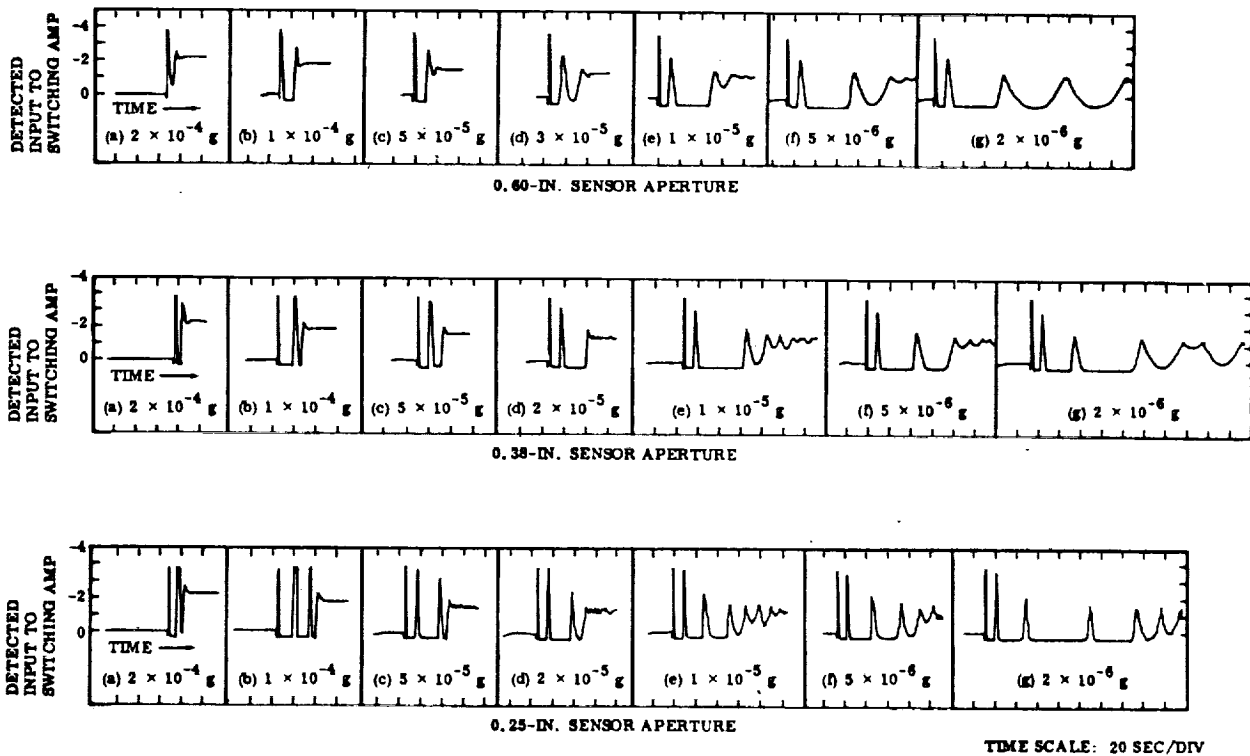


Fig. 4-8 Acquisition Behavior

Performance optimization through the simulation has resulted in the following parameter selection:

Ball size	0.5 in.	Thrust level (2 jets at 0.1 lb ea)	0.2 lb
Cage length	1.55 in.	Minimum impulse	0.012 lb-sec
Light beam aperture	0.28 in.	Switching line to back of cage	0.8 in.
Lag network time constant	0.55 sec	Dynamic range	300:1
Switching amplifier hysteresis	10%		
Switching amplifier minimum on-time	0.06 sec		

4.5 SYSTEM ERROR ANALYSIS

The preceding description related to the details of the scheme for keeping the cage ends from hitting the ball, which was the main criterion in the total design synthesis. To assess the device as an accelerometer for controlling drag make-up it is necessary to look at the total system performance.

Since in this scheme the ball is allowed to contact the side walls of the cage, the thrust control system working against the drag on the vehicle is used only to keep the ball from hitting the cage ends. (More correctly one should perhaps say the system prevents the cage ends from hitting the ball.) To the extent that the system prevents the ball being given an impulse along the direction of the vehicle roll axis, which is nominally along the vehicle velocity vector, the ball proceeds in essentially a drag free orbit. The various irregularities and spurious forces which do act on the ball and perturb it from a drag free trajectory are the subject of the ensuing error analysis.

Since a major objective of this type of system is the compensation for air drag which appears as a nominally constant decelerating force (for a circular orbit), the various errors will be analyzed and their effect computed in terms of an equivalent drag force. Assuming all the errors, then, to be uncorrelated one can combine their effects on a root sum square basis and thus compute the total uncertainty that would exist in a drag determination made by observing the vehicle trajectory.

The following sources of error, i. e., mechanisms which produce forces on the ball and thus perturb it from a purely gravitational trajectory, are considered to be the significant errors for this system:

- Single end wall hit
- Side wall contact – thrust misalignment; vehicle angle of attack; vehicle attitude oscillation; vehicle translational plus attitude oscillations
- Vehicle gravity
- Vehicle stray electromagnetic fields

For each of these sources a number is computed which corresponds to that constant force over one orbit which would produce the same average effect on the ephemeris (e. g., period decrement). A summary of the results is given in Table 4-1.

Table 4-1
SINGLE AXIS SYSTEM ERRORS

Error Source	Error*		Comment
	Direction		
	Along	Transverse	
- DRAG	3×10^{-6}	0	125 nm
0 END WALL HIT	0	6×10^{-7}	System malfunction
1 Thrust Misalignment	9×10^{-10}	6×10^{-8}	Friction coefficient = 1/4 Misalignment = 0.02 rad
2 Angle of Attack	6×10^{-10}	6×10^{-8}	Friction coefficient = 1/4 Angle of attack = 0.02 rad
3 Vehicle Attitude Oscillation	3×10^{-9}	0	1° peak amplitude 600-sec period
4 Attitude Plus Translation Oscillations	3×10^{-9}	0	Oscillations uncorrelated Random wall-ball speeds
5 Vehicle Gravity	1.7×10^{-9}		Assumed simple vehicle model
6 Vehicle Stray Field (magnetic)		10^{-14}	Paramagnetic ball
7 Root Sum Square (RSS) (1-6)	4.6×10^{-9}	8.4×10^{-8}	Assumes 1-6 uncorrelated

*The magnitudes are estimated 1- σ values in g's and represent the constant specific force which over one orbit would produce an average effect on the ephemeris equal to that of the error source.

The effects of the RSS of the perturbing forces (Item 7) are plotted for several orbits. Figure 4-9 shows the effect of a steady specific force on the ball along the trajectory of 4.6×10^{-9} g. Figure 4-10 shows the effect of 8.4×10^{-8} g transverse to the trajectory.

The inclusion of an end wall hit in the list is mainly for the purpose of a comparison with the other sources. In this sense it should not properly be on the "error list" because the event of an end wall hit would constitute a system malfunction or failure whereas all the other listed error sources are viewed as being present in a properly operating system.

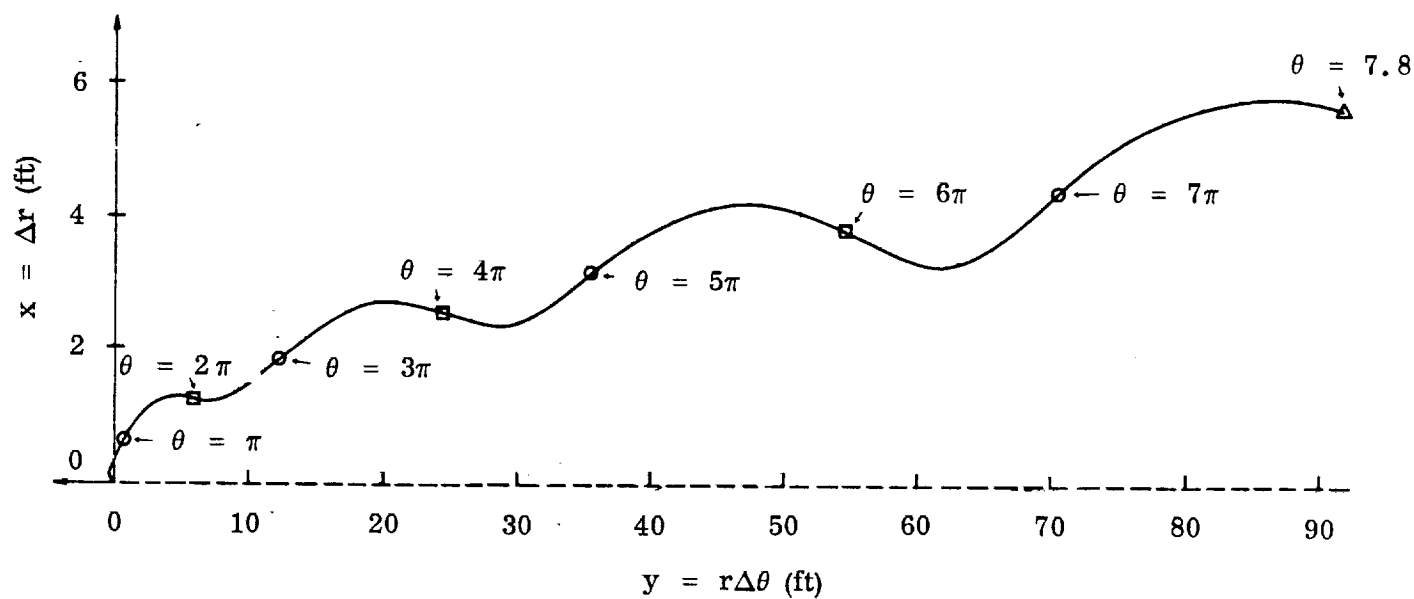


Fig. 4-9 Trajectory Perturbation Due to In-Track Force

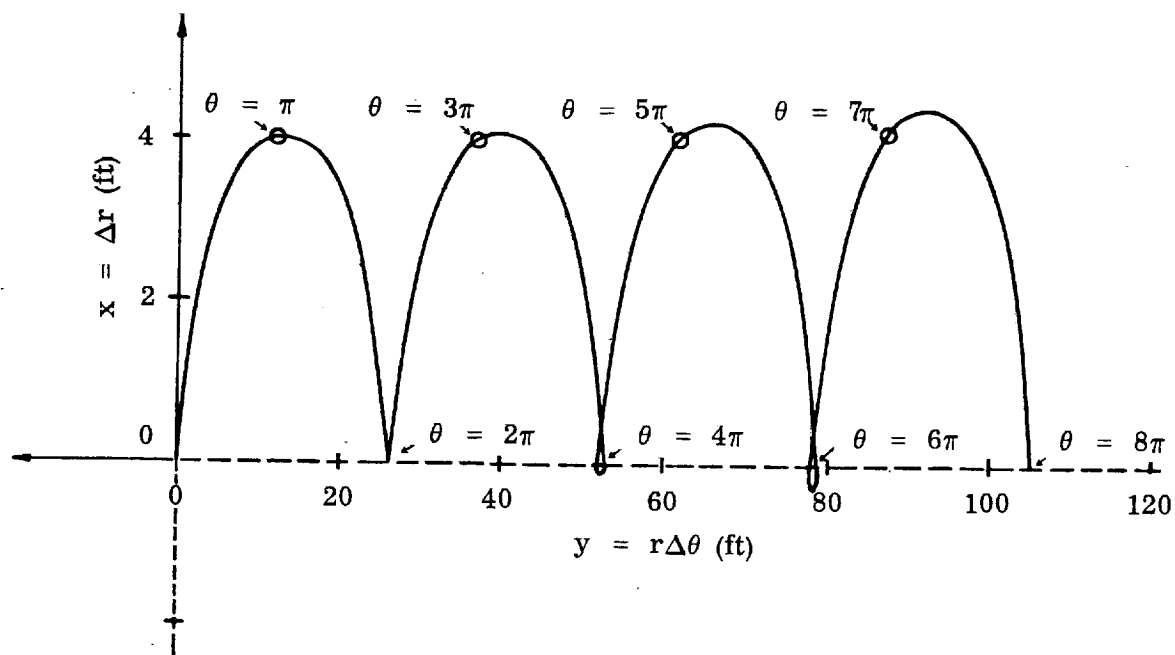


Fig. 4-10 Trajectory Perturbation Due to Cross-Track Force

From Table 4-1, we see that the angle of attack and thrust misalignment produce the significant transverse forces whereas the vehicle attitude oscillations produce the significant longitudinal forces. We further note from Figs. 4-9 and 4-10 that although the transverse forces are about 20 times larger than the longitudinal forces, their effects result in ephemeris perturbations of the same order of magnitude. This is quite interesting and indicates that from an error sensitivity standpoint the system is quite well-balanced.

The absolute magnitude of the RSS in-track force is about 0.15% of the drag force. This means that in operation we should get drag cancellation to about this accuracy. Although it is not evident from the table, the detailed analysis shows that the values for Sources 1-4 are all proportional to drag, thus for these items the cancellation to 0.15% is independent of altitude.

This leads to the observation that for the system as postulated (and designed) Item 5 could, for slightly higher altitudes, become the significant error source. However, as is pointed out in the detailed analysis this force can be manipulated and reduced by appropriate location of the ball within the vehicle.

At the outset it was hoped that a single axis system could be designed which would allow drag compensation to better than 1%. This objective appears quite possible in light of these results.

4.5.1 End Wall Hit

An equivalence between an end wall hit and a constant disturbing force can be established approximately from the circular orbit dispersion equation [see Eq. (2.96)]. Since an end wall hit produces an impulse of velocity along the track (i. e., an increment in $\dot{\eta}_0$), we can establish the $\dot{\eta}$ corresponding to a given hit. We note from Eq. (2.96) that the effect of $\dot{\eta}_0$ on the subsequent state of the system appears always in combination with a constant vertical force, i. e., four terms have the coefficient $(f_\xi + n\omega\dot{\eta}_0)$. Since $n = 1.5$ for the secular term, we will view an end wall hit which produces a velocity impulse of $\dot{\eta}_0$ to be nominally equivalent to a constant vertical force of magnitude,

$$-f_\xi = 1.5 \omega \dot{\eta}_0 \quad (4.5)$$

The most likely worst case of the ball hitting the end wall is for the thrust system to stay on due to a system malfunction while the vehicle is near apogee. For this particular system the distance from the mean position of the ball to the end wall is 0.8 in. Typically the full on thrust is capable of accelerating the vehicle at about 3×10^{-4} ft/sec² (about 3 times the perigee drag deceleration). On this basis the ΔV imparted to the ball in the event of an end wall hit assuming elastic impact is

$$\dot{\eta}_0 = 2 \sqrt{2as} = 12.7 \times 10^{-3} \text{ ft/sec} \quad (4.6)$$

which is in the above sense equivalent to a constant acceleration on the ball of

$$f_\xi = 1.5 \omega \dot{\eta}_0 = 19 \times 10^{-6} \text{ ft/sec}^2 = 0.6 \times 10^{-6} g \quad (4.7)$$

This is about one-fifth the assumed perigee drag deceleration of 10^{-4} ft/sec². It is clear from this result that, if the system experienced an end wall hit very often, the performance would be significantly degraded, although it should be noted that in the sense taken, an end wall hit is equivalent to a vertical force whereas drag is of course a horizontal force.

4.5.2 Side Wall Contact

Constraining the ball in the transverse directions simplifies and minimizes the control hardware, but the side wall constraints can perturb the ball away from a strictly unforced trajectory. Several mechanisms may contribute to this perturbation. We envision types of interaction between the ball and the side wall corresponding to (1) the wall being continually accelerated in one direction against the ball, i.e., constant forces, and (2) the wall hitting the ball back and forth transverse to the cage axis, i.e., oscillating forces.

4.5.2.1 Coefficient of Friction Under Very Low Normal Forces

To compute perturbations due to side wall contacts, it was necessary to know the coefficient of friction, between wall and ball. Because little or no information

is available in the literature on friction between various materials under the very low normal forces expected here, a laboratory investigation was undertaken.

Since minimum friction was desired, several surface conditions and coatings known to give low friction under more normal conditions were tried. The lowest friction was obtained between a steel ball and steel wall-rods both burnished with MoS_2 (moly-kote) powder. (A second choice was a polished ball and Teflon coated rods.) The test procedure consisted of accelerating the ball at a very low rate (about 10^{-4} ft/sec^2) in one direction and opposing this by a force, derived from pushing against the ball transverse to its direction of motion, equal to the coefficient of friction times the normal (transverse) force. The plot in Fig. 4-11 shows the comparison between the time to traverse (at constant acceleration) a given distance under zero normal force and a normal force of $3.3 \times 10^{-6} \text{ lb}$.

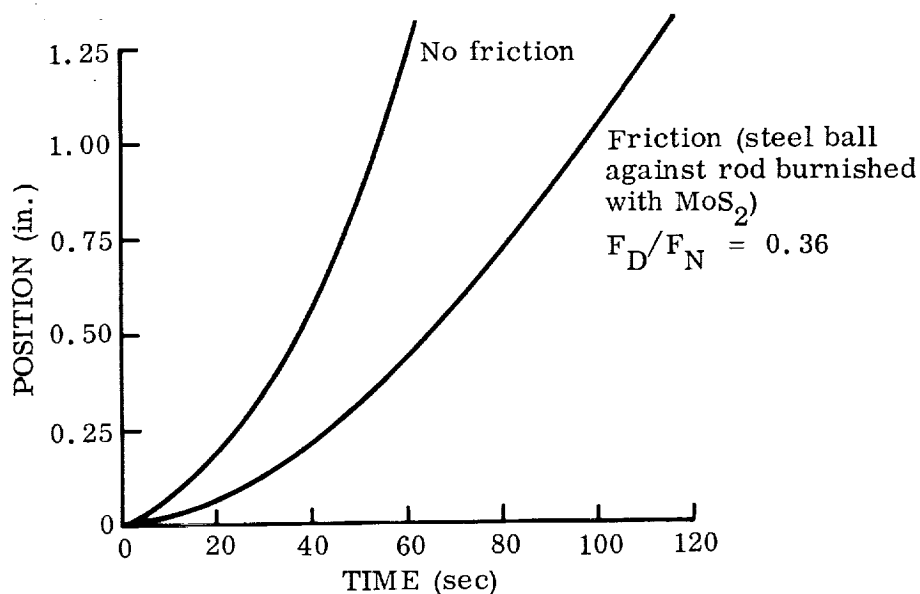


Fig. 4-11 Position Vs. Time Under Constant Drive Force

In this experiment the coefficient of friction is given by the relation

$$\mu = \frac{m}{F_N} (a_1 - a_2) \quad (4.8)$$

where

- a_0 = acceleration with no friction (second derivative of Curve 1)
- a_1 = acceleration under friction (second derivative of Curve 2)
- F_N = normal force = 3.3×10^{-6} lb
- m = equivalent (apparent) ball mass = 0.02 slugs

From this experiment a value of $1/4$ was obtained for μ .

4.5.2.2 Perturbations Due to "Constant" Transverse Forces

If the cage side wall is continually accelerated against the ball it will produce a continual transverse force on the ball. If the ball is simultaneously sliding along the wall it (the wall or transverse force) will also exert a longitudinal force on the ball through the coefficient of sliding friction.

The wall will exert a (nominally) constant, normal (i. e. , transverse) force on the ball whenever the net force on the vehicle is not aligned with the longitudinal axis of the cage. Misalignment of the net force may arise in two ways, namely thruster misalignment and vehicle (cage) angle of attack. Note that in both cases it is the angle that the force makes with the cage axis that is important.

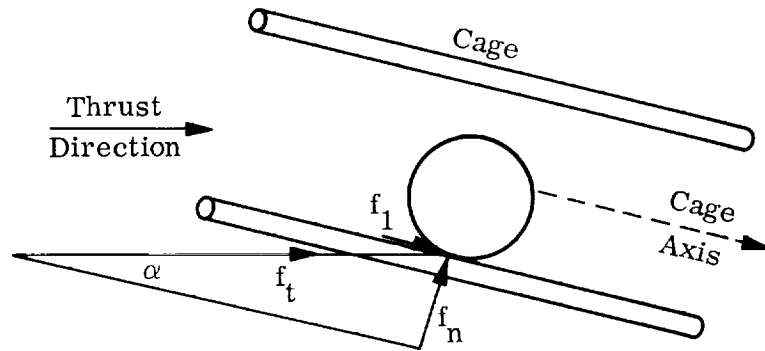
Thrust Misalignment. The geometry for the case of thrust misalignment is shown in Fig. 4-12. Note first that the normal force,

$$f_n = f_t \sin \alpha \cong \alpha f_t \quad (4.9)$$

(for typical misalignments of about 0.02 rad) is only present when the thruster is on. Since the thruster is time modulated to give an average thrust that just compensates for the drag it is clear that $f_{t \text{ average}} \equiv \bar{f}_t = f_d$ and \bar{f}_n is simply

$$\bar{f}_n = \alpha f_d \cong 0.02 f_d \quad (\text{typically}) \quad (4.10)$$

The effect of this transverse force, if it were continually present for several orbits, is shown in Fig. 4-10. Note that the average altitude (period) is increased during the first orbit. Subsequent increase of this average is very slow.



- α = angle of thrust misalignment
 f_t = thrust force
 $f_n = f_t \sin \alpha \cong \alpha f_t$ = normal (transverse) force

Fig. 4-12 Thrust Misalignment

Whenever the ball is in contact with the wall and sliding along the wall this normal force will produce a longitudinal force on the ball which opposes the relative motion. The first question is whether the ball slides or rolls along the wall. Referring to Fig. 4-12, we see that the force tending to accelerate the wall relative to the ball CM is $f_t \cos \alpha \cong f_t$. The moment tending to rotate the ball around its CM is

$$Rf_1 = \mu Rf_n = \mu Rf_t \sin \alpha \quad (4.11)$$

where R is the ball radius. After time t (starting with the ball at rest on the wall) we have

$$V_{B-W} = \int_0^t \frac{F_t}{M} \cos \alpha \, dt \quad (4.12)$$

and

$$- R\omega = \frac{R^2}{I} \int_0^t F_1 dt = \frac{R^2 \mu}{k^2} \int_0^t \frac{F_t dt \sin \alpha}{M} \quad (4.13)$$

$$- R\omega = \mu \tan \alpha \frac{R^2}{k^2} V_{B-W} \quad (4.14)$$

$$R\omega = -\frac{5}{2} \mu \tan \alpha V_{B-W} \quad \text{for a solid sphere} \quad (4.15)$$

where V_{B-W} is the wall-ball relative longitudinal velocity, $R\omega$ is the ball rim velocity, k^2 is the radius of gyration squared ($2R^2/5$ for a sphere), M is the ball mass, and I is the ball inertia. For $\mu = 1/4$, $\alpha = 0.02$ and this gives

$$R\omega = -\frac{1}{80} V_{B-W} \quad (4.16)$$

which indicates that the ball will always slide along the wall since we can never get

$$R\omega + V_{B-W} = 0 \quad (4.17)$$

the condition necessary for rolling. (Note for rolling in any force field one needs

$$\mu \tan \alpha \geq \frac{k^2}{R^2} \quad (4.18)$$

where α is the angle between the force and the velocity. For the case of a sphere with $\mu = 1/4$, this means

$$\tan \alpha \geq \frac{k^2}{R^2 \mu} = 1.6 \quad (4.19)$$

or $\alpha \geq 55^\circ$.)

Since the longitudinal force always opposes the relative velocity, we need to know the relative velocity profile to determine the net force. The steady-state case in which the ball does not contact the wall is illustrated in Fig. 4-13.

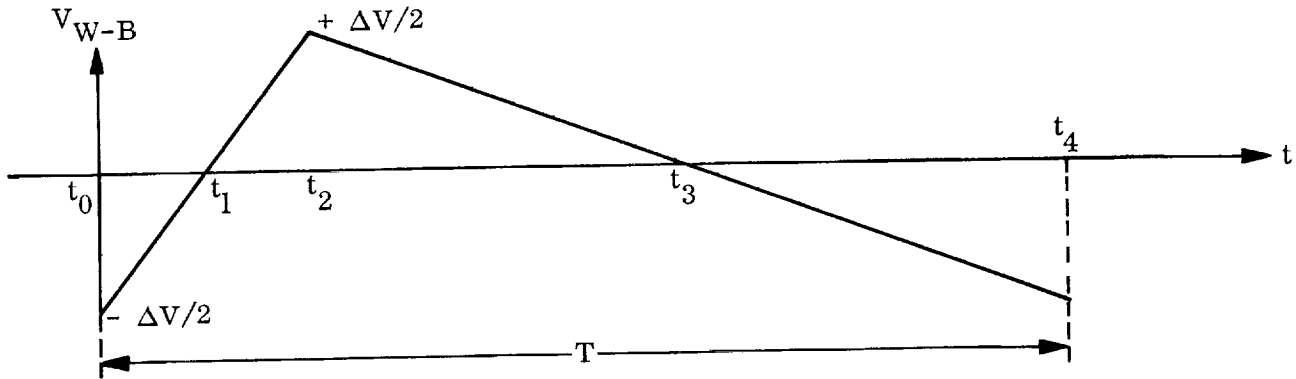


Fig. 4-13 Wall-Ball Relative Velocity

The slope of V_{W-B} vs. t from t_0 to t_2 is $f_t - f_d$. The slope from t_2 to t_4 is $-f_d$. Clearly $t_3 - t_1 = t_4 - t_3 + t_1 - t_0$, that is the ball spends as much time going forward relative to the wall as it does going aft.

Now, if the ball is in constant contact with the wall and slides back and forth due to the relative motion, the picture is altered as shown in Fig. 4-14. One may see this easily by recalling that the tangent force μf_n always tends to drive V_{W-B} to zero.

We can now compute the net (or average) longitudinal force due to thrust misalignment. Referring to Fig. 4-14, we have $f_n = \mu \alpha f_t$ in the region t_0 to t_2 and $f_n = 0$ from t_2 to t_4 . From this we can compute the following relations (taking $\rho \equiv f_t/f_d$)

$$t_a + t_f = \frac{T}{\rho} \quad (4.20)$$

$$T_a + T_f = \frac{\rho - 1}{\rho} T \quad (4.21)$$

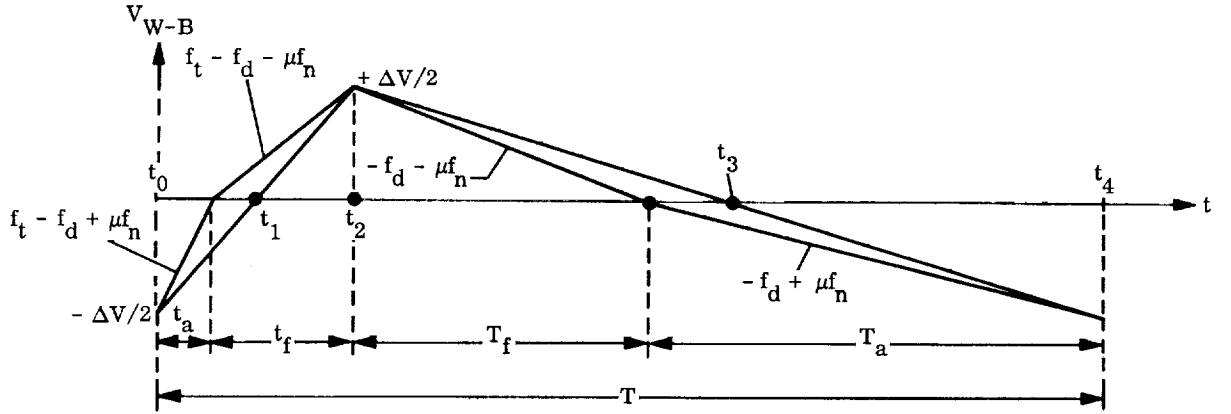


Fig. 4-14 Wall-Ball Relative Velocity With Contact

$$\frac{t_f - t_a}{t_f + t_a} = \frac{\mu\alpha\rho}{\rho - 1} \quad (4.22)$$

$$\frac{t_f - t_a}{T} = \frac{\mu\alpha}{\rho - 1} \quad (4.23)$$

We see that over the interval T there is a net forward force equal to $\mu\alpha f_d$ with a "duty cycle" of $\mu\alpha/(\rho - 1)$. This we assume to be equivalent to an average forward force on the ball over the interval T of

$$\bar{f}_{1\text{net}} = \frac{\mu\alpha}{\rho - 1} f_n \quad (4.24)$$

$$= \frac{\rho}{\rho - 1} (\mu\alpha)^2 f_d \quad (4.25)$$

For $\mu\alpha = 1/200$ and $\rho = 10$, this gives

$$\bar{f}_{1\text{net}} \cong 2.8 \times 10^{-4} f_d \quad (4.26)$$

This effect is therefore quite small!

Angle of Attack. The geometry for this case is shown in Fig. 4-15 and is quite similar to that of the thrust misalignment.

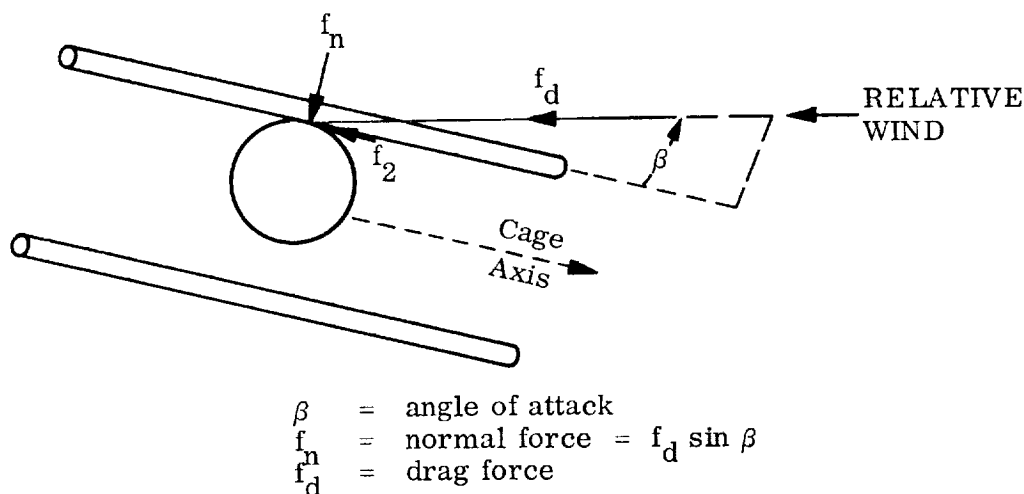


Fig. 4-15 Angle of Attack

The case of the normal force is essentially the same as for thrust misalignment. For low-altitude orbits with $e \leq 0.01$ a reasonable value for β is about 0.02 rad. The result is the same as for thrust misalignment:

$$f_n = f_d \sin \beta \cong \beta f_d \quad (4.27)$$

$$\cong 0.02 f_d \quad (\text{typically}) . \quad (4.28)$$

The effect on the orbit is essentially the same as that in Fig. 4-10. The major difference would be in the case in which angle of attack varied around the orbit due to the eccentricity.

To compute the effect of the friction force we proceed as previously. Referring to Fig. 4-14 and noting that in this case

$$f_n = \beta f_d \quad (4.29)$$

We again take $\rho \equiv f_t/f_d$.

We can compute the following relations:

$$\frac{t_f - t_a}{T} = \frac{\mu\beta}{\rho(\rho - 1)} \quad (4.30)$$

and

$$\frac{T_a - T_f}{T} = \frac{\mu\beta(\rho - 1)}{\rho} \quad (4.31)$$

$$\frac{T_a + t_a - (T_f + t_f)}{T} = \mu\beta \frac{\rho - 2}{\rho - 1} \quad (4.32)$$

Thus over the interval T there is a "net" average rearward force equal to

$$\bar{f}_{2net} = \mu\beta \frac{\rho - 2}{\rho - 1} f_n \quad (4.33)$$

$$\bar{f}_{2net} = (\mu\beta)^2 \frac{\rho - 2}{\rho - 1} f_d \quad (\text{rearward}) \quad (4.34)$$

For $\rho = 10$ and $\mu\beta = 1/200$, we get

$$\bar{f}_{2net} \cong 2.2 \times 10^{-4} f_d \quad (4.35)$$

4.5.2.3 Perturbation Due to Oscillatory Transverse Forces (Vehicle Motions)

The effect of an oscillatory transverse force is to give the ball a velocity impulse as it rebounds from the wall. One tends to get these impulses in pairs since after it leaves one wall it will proceed to the opposite wall and bounce off it. Typically this situation would prevail whenever the vehicle was in an attitude oscillation about any axis transverse to the roll axis. For the vehicle system under consideration typical attitude limit cycle performance yields attitude deviation of about 1° peak at a period of about 600 sec or angular rates of about 10^{-4} rad/sec. The net affect on the ball is proportional to the distance of the ball from the center of rotation (CM) of the vehicle. In particular, one gets a net specific force on the ball in the fore or aft direction, depending on whether

the ball is fore or aft of the vehicle CM, approximately equal to $R\omega^2$ where R is the distance fore or aft of the CM and ω is the angular rate of the vehicle due to the attitude limit cycle. Assuming an R of 5 ft and $\omega = 10^{-4}$ rad/sec, one computes an effect of 5×10^{-8} ft/sec² or about 1.6×10^{-9} g. For a system in which the ball was aft of the CM, the effect would be equivalent to a drag deceleration of 1.6×10^{-9} g. This is about .05% of the assumed nominal drag and is the largest longitudinal perturbing force so far.

4.5.2.4 Perturbation Due to Simultaneous Longitudinal and Transverse Vehicle Motions (Statistical Analysis)

There is an additional way in which wall-ball friction may perturb the ball. It arises from the cross-coupled action of two vehicle motions.* We noted above that the attitude limit cycle oscillation of the vehicle may cause the ball to bounce transversely from wall to wall. Simultaneously the drag and compensating thrust impulses will cause the vehicle, and thus the cage walls, to oscillate continuously in the longitudinal direction relative to the ball. Thus the side walls have a component of velocity relative to the ball which is along the trajectory. Since the ball spends most of its time between walls in this situation, the steady-state relative velocity profile is a sawtooth as shown in Fig. 4-13, where ΔV is the peak to peak velocity excursion and T is the total period between thrust initiations. For proper system operation in which the ball does not contact the cage end walls, the mean value of V_{W-B} is assumed to be zero as implied by the sketch (i.e., we assume the hits do not significantly alter Fig. 4-13).

Now if the attitude limit cycle period is uncorrelated to the longitudinal limit cycle period, then we can assume that when the ball hits the wall, V_{W-B} may have any value between $+\Delta V/2$ and $-\Delta V/2$ with equal probability. That is to say the value of V_{W-B} at a given hit is said to be a random number uniformly distributed between $+\Delta V/2$ and $-\Delta V/2$ with zero mean. Now only a portion of this velocity V_{W-B} will be imparted to the ball. The analysis in Appendix B indicates that the longitudinal velocity imparted to the ball due to a single hit is (for $V_o = 0$) [Eq. (B-9)]

$$V_B \leq \frac{I}{I + mR^2} (R\omega_o + V_{W-B}) = \frac{k^2}{k^2 + R^2} (R\omega_o + V_{W-B}) \quad (4.36)$$

*This effect was called to the author's attention by R. L. McKenzie.

where R is the ball radius, k is the radius of gyration, V_{W-B} is the wall-ball relative velocity and $R\omega_0$ is the peripheral velocity just before impact of the ball relative to its center of mass.

To investigate the effect of this we assume a series of wall-ball hits and thus a series of longitudinal velocity impulses, V_B , imparted to the ball by the wall. By assuming the above statistics for V_{W-B} and by assuming a series of hits spaced equally in time, we can compute the statistics of the state vector. The most useful information about the state vector is the expected value of the square. We will get this in terms of the expected value of the square of V_{W-B} .

We recall [see Eq. (2.81)] that the state of the system at anomaly τ after an impulse of velocity at τ_0 can be expressed as

$$y(\tau) = Y(\tau, \tau_0) [x(\tau_0) + y(\tau_0)] \quad (4.37)$$

where

$$x^\dagger(\tau_0) = (0, 0, 0, \eta'_0) \quad (\text{the impulse at } \tau_0)$$

and

$$y^\dagger(\tau) = (\xi, \eta, \xi', \eta') \quad (\text{the state at } \tau)$$

$$y^\dagger(\tau_0) \equiv 0 \quad (\text{the state at } \tau = \tau_0)$$

If we then postulate a string of N impulses equally spaced (by an amount $\Delta\tau$) then we see that $y(\tau)$ is determined by a sum of impulses:

$$y_1(\tau) \equiv y(\tau_0 + \Delta\tau) = Y(\tau_0 + \Delta\tau, \tau_0) x(\tau_0) \quad (4.38)$$

$$y_2(\tau) \equiv y(\tau_0 + 2\Delta\tau) = Y(\tau_0 + 2\Delta\tau, \tau_0 + \Delta\tau) [y_1 + x(\tau_0 + \Delta\tau)] \quad (4.39)$$

$$y_2(\tau) = Y(\tau_0 + 2\Delta\tau, \tau_0) x(\tau_0) + Y(\tau_0 + 2\Delta\tau, \tau_0 + \Delta\tau) x(\tau_0 + \Delta\tau) \quad (4.40)$$

and

$$\begin{aligned} y_N(\tau) &= Y(\tau, \tau_0) x(\tau_0) + Y(\tau, \tau_0 + \Delta\tau) x(\tau_0 + \Delta\tau) + \\ &\dots Y[\tau, \tau_0 + (N-1)\Delta\tau] x[\tau_0 + (N-1)\Delta\tau] \end{aligned} \quad (4.41)$$

$$y_N(\tau) = \sum_{k=0}^{N-1} Y(\tau, \tau_0 + k\Delta\tau) x(\tau_0 + k\Delta\tau) \quad (4.42)$$

in which we have used the property of fundamental matrices that

$$Y(a, c) = Y(a, b) Y(b, c) \quad (4.43)$$

or for the case above

$$Y(\tau_0 + 2\Delta\tau, \tau_0 + \Delta\tau) Y(\tau_0 + \Delta\tau, \tau_0) = Y(\tau_0 + 2\Delta\tau, \tau_0) \quad (4.44)$$

Employing this same property again we can write y_N as

$$y_N(\tau) = Y(\tau, \tau_0) \sum_{k=0}^{N-1} Y(\tau_0, \tau_0 + k\Delta\tau) x(\tau_0 + k\Delta\tau) \quad (4.45)$$

for convenience we abbreviate the symbol arguments giving for this equation:

$$y_N \equiv Y(\tau, 0) \sum_k Y(0, k) x_k \quad (4.46)$$

We can evaluate the expected value of the square of the state $y_N(\tau)$ as

$$E(y_N y_N^\dagger) = E \left(Y(\tau, 0) \sum_k Y(0, k) x_k \sum_j x_j^\dagger Y^\dagger(0, j) Y^\dagger(\tau, 0) \right) \quad (4.47)$$

If we assume that successive impulses are uncorrelated, which follows from the assumption that the vehicle attitude limit cycle is uncoupled from the drag make-up limit cycle, then product terms for $j \neq k$ will vanish and $E(y_N y_N^\dagger)$ becomes:

$$E(y_N y_N^\dagger) = E \left(Y(\tau, 0) \sum_k Y(0, k) x_k x_k^\dagger Y^\dagger(0, k) Y^\dagger(\tau, 0) \right) \quad (4.48)$$

Since only the impulses are of a random nature we can take the expected value operator, E inside. Thus,

$$E(y_N y_N^\dagger) = Y(\tau, 0) \sum_k Y(0, k) E(x_k x_k^\dagger) Y^\dagger(0, k) Y^\dagger(\tau, 0) \quad (4.49)$$

Since $x_k^\dagger = (0, 0, 0, \eta_k')$, we have

$$E(x_k x_k^\dagger) = \begin{bmatrix} 0 & 0 & 0 & 0 \\ 0 & 0 & 0 & 0 \\ 0 & 0 & 0 & 0 \\ 0 & 0 & 0 & E(\eta_k'^2) \end{bmatrix} \quad (4.50)$$

Now since all the η_k' are assumed to have the same statistics

$$E(\eta_k'^2) = E(\eta_j'^2) = E(\eta_o'^2) \quad (\text{a scalar}) \quad (4.51)$$

Thus

$$E(x_k x_k^\dagger) = E(\eta_o'^2) \begin{bmatrix} 0 & 0 & 0 & 0 \\ 0 & 0 & 0 & 0 \\ 0 & 0 & 0 & 0 \\ 0 & 0 & 0 & 1 \end{bmatrix} \quad (4.52)$$

This matrix will extract the 4th column of $Y(0, k)$ so that in terms of the elements (y_{i4}) of $Y(0, k)$ we get for the triple matrix product the symmetrix covariance matrix:

$$\psi(0, k) \equiv Y(0, \tau) \begin{bmatrix} 0 & 0 & 0 & 0 \\ 0 & 0 & 0 & 0 \\ 0 & 0 & 0 & 0 \\ 0 & 0 & 0 & 1 \end{bmatrix} Y^\dagger(0, \tau) \quad (4.53)$$

$$\psi(0, k) = \begin{bmatrix} y_{14}^2 & y_{14}y_{24} & y_{14}y_{34} & y_{14}y_{44} \\ y_{14}y_{24} & y_{24}^2 & y_{24}y_{34} & y_{24}y_{44} \\ y_{14}y_{34} & y_{24}y_{34} & y_{34}^2 & y_{34}y_{44} \\ y_{14}y_{44} & y_{24}y_{44} & y_{34}y_{44} & y_{44}^2 \end{bmatrix} \quad (4.54)$$

i. e. ,

$$\psi_{ij} = \psi_{ji} = y_{i4}y_{j4} \quad (4.55)$$

Thus we have

$$E(y_N y_N^\dagger) = E(\eta_o'^2) Y(\tau, 0) \sum_k \psi(0, k) Y^\dagger(\tau, 0) \quad (4.56)$$

Now for N equally spaced impulses over an interval $\tau - \tau_o$, the sum of the matrix elements in $\psi(0, k)$ is approximately given by*

$$\sum_k \psi(0, k) = \frac{N}{\tau - \tau_o} \int_{\tau_o}^{\tau} \psi(\tau_o, \theta) d\theta \equiv N\Psi \quad (4.57)$$

thus

$$\Psi_{ij} = \frac{1}{\tau - \tau_o} \int_{\tau_o}^{\tau} \psi_{ij}(\tau_o, \theta) d\theta \quad (4.58)$$

*The ratio of the sum to the integral [i. e. , the R. H. S. to the L. H. S. of Eq. (4.57)] approaches 1 for N large. The two are said to be asymptotically equal. Since we are interested in $N = 1000$, the sum $(\pi/2) \sum_{i=0}^N \sin(\pi i/N)$ was computed for $N = 500$ and was found to be 500.0016 (i. e. , within 0.005% of N). This sum of sines is typical of the sums in what follows.

This gives for the expected value of y_N^2 the following:

$$E(y_N y_N^\dagger) = NE(\eta_o'^2) Y(\tau, 0) \Psi Y^\dagger(\tau, 0) \quad (4.59)$$

To get an idea of the magnitude of the effect we look at the elements of $E(y_N y_N^\dagger)$ corresponding to $E(\xi^2)$ and $E(\eta^2)$ (i.e., elements 11 and 22) for a circular orbit over the interval $0 - 2\pi$. Over this interval $Y(\tau, 0)$ (for $e = 0$) becomes [see Eq. (2.96)]

$$Y(\tau, 0) = \begin{bmatrix} 1 & 0 & 0 & 0 \\ -12\pi & 1 & 0 & -6\pi \\ 0 & 0 & 1 & 0 \\ 0 & 0 & 0 & 1 \end{bmatrix} \quad (4.60)$$

$E(\eta_o'^2)$ is the expected value of the square of the velocity imparted to the ball in a single hit. From Eq. (4.36) we had

$$V_B \leq \frac{k^2}{R^2 + k^2} (R\omega_o + V_{W-B}) \quad (4.61)$$

$$V_B \leq \frac{2}{7} (R\omega_o + V_{W-B}) \quad \text{for a sphere} \quad (4.62)$$

Now in steady state $R\omega_o$, the rim speed of the ball just prior to a hit, is equal to (or less than) V_{W-B} of the previous hit.* Thus we can write for V_B after the k^{th} hit

$$[V_B]_k \leq \frac{2}{7} [(V_{W-B})_{k-1} + (V_{W-B})_k] \quad (4.63)$$

With the assumption that $(V_{W-B})_{k-1}$ is uncorrelated to $(V_{W-B})_k$ we have that

$$E[(V_B^2)_k] \leq \frac{4}{49} E[(V_{W-B})_{k-1}^2 + (V_{W-B})_k^2] \quad (4.64)$$

*See Appendix B.

and since

$$E \left[(V_{W-B})_k^2 \right] = E \left[(V_{W-B})_{k-1}^2 \right] = E \left[(V_{W-B})_0^2 \right] \quad (4.65)$$

We have

$$E \left[(V_B)_k^2 \right] \leq \frac{8}{49} E \left[(V_{W-B})_0^2 \right] \quad (4.66)$$

Hence, since

$$\eta'_0 = (V_B)_0 \quad (4.67)$$

we have

$$E \left(\eta'^2_0 \right) \leq \frac{8}{49} E \left(V_{W-B}^2 \right) \quad (4.68)$$

Now since V_{W-B} is uniformly distributed between

$$+ \frac{\Delta V}{2} \quad \text{and} \quad - \frac{\Delta V}{2} \quad (\text{see Fig. 4-13}) \quad (4.69)$$

we have

$$E(V_{W-B}^2) = \frac{1}{\Delta V} \int_{-\Delta V/2}^{\Delta V/2} x^2 dx = \frac{\Delta V^2}{12} \quad (4.70)$$

Hence

$$E \left(\eta'^2_0 \right) \leq \frac{2}{147} \Delta V^2 \quad (4.71)$$

Finally for $E(\xi^2)$ we have

$$E(\xi^2) = \left[E(Y_N Y_N^\dagger) \right]_{11} \leq \frac{2N\Delta V^2}{147} \Psi_{11} \quad (4.72)$$

$$\leq \frac{2N\Delta V^2}{147} \cdot \frac{1}{2\pi} \int_{\theta}^{2\pi} y_{14}^2 d\theta \quad (4.73)$$

$$\leq \frac{4N}{49} \Delta V^2 \quad (4.74)$$

Now for a vehicle drag deceleration of 10^{-4} ft/sec² drag ΔV in 1 sec is 10^{-4} ft/sec which is 0.09 ft/rad (for $\omega = 0.0011$) or about $\Delta V = 1$ in./rad. Thus for 1000 hits in one orbit we would have (recalling the normalization $\xi = \Delta r/r$)

$$E(\Delta r^2) = 80 \text{ in.}^2 \quad (4.75)$$

or a 1σ value of Δr after 1 orbit of

$$\sigma_{\Delta r} = \sqrt{80} = 8.9 \text{ in.} \cong 3/4 \text{ ft} \quad (4.76)$$

The effect of drag on ξ over one orbit is

$$y(2\pi) = Y(2\pi, 0) \int_0^{2\pi} Y(0, \theta) d\theta f_D \quad (4.77)$$

$$f_D^\dagger = \left(0, 0, 0, \frac{10^{-4}}{r\omega^2} \right) \quad (4.78)$$

$$r\xi(2\pi) = 100 \int_0^{2\pi} 2(1 - c\theta) d\theta = 400\pi \quad (4.79)$$

$$= 1256 \text{ ft} \quad (4.80)$$

Thus the effect on Δr of a $1-\sigma$ deviation due to pulses is about 0.06% of the drag force per orbit. The effect over 36 orbits (the approximate flight length) would be one-sixth this or 0.01% of the drag.

The effect along the track $E(\eta^2)$ is more tedious to compute since it involves several of the matrix elements of Ψ . We persevere, however, getting

$$E(\eta^2) = \left[E(y_N y_N^\dagger) \right]_{22} = \frac{2N}{147} \Delta V^2 \left[-12\pi [-12\pi \Psi_{11} + \Psi_{12} - 6\pi \Psi_{14}] \right. \\ \left. - 6\pi [-6\pi \Psi_{34} - 12\pi \Psi_{13} + \Psi_{23}] - 12\pi \Psi_{21} + \Psi_{22} - 6\pi \Psi_{24} \right] \quad (4.81)$$

$$E(\eta^2) = \frac{2N}{147} \Delta V^2 \left[144\pi^2 \Psi_{11} + 72\pi^2 (\Psi_{14} + \Psi_{13}) + 36\pi^2 \Psi_{34} + \Psi_{22} \right. \\ \left. - 24\pi \Psi_{12} - 6\pi (\Psi_{23} + \Psi_{24}) \right] \quad (4.82)$$

$$\Psi_{11} = 6 \quad (4.83)$$

$$\Psi_{12} = \frac{1}{2\pi} \int_0^{2\pi} y_{14} y_{24} d\theta = \frac{1}{2\pi} \int_0^{2\pi} 2(1 - c\theta)(3\theta - 43\theta) d\theta = 6\pi \quad (4.84)$$

$$\Psi_{14} = \frac{1}{2\pi} \int_0^{2\pi} y_{14} y_{44} d\theta = \frac{1}{2\pi} \int_0^{2\pi} 2(1 - c\theta)(4c\theta - 3) d\theta = -10 \quad (4.85)$$

$$\Psi_{13} = \frac{1}{2\pi} \int_0^{2\pi} y_{14} y_{34} d\theta = 0 \quad (4.86)$$

$$\Psi_{22} = \frac{1}{2\pi} \int_0^{2\pi} y_{24} y_{24} d\theta = \frac{1}{2\pi} \int_0^{2\pi} (9\theta^2 + 16s^2\theta - 24\theta s\theta) d\theta = 51 \quad (4.87)$$

$$\Psi_{23} = \frac{1}{2\pi} \int_0^{2\pi} (8s^2\theta - 6\theta s\theta) d\theta = 10 \quad (4.88)$$

$$\Psi_{24} = \frac{1}{2\pi} \int_0^{2\pi} (-16s\theta c\theta + 12\theta c\theta - 9\theta - 125\theta) d\theta = -9\pi \quad (4.89)$$

$$\Psi_{34} = 0 \quad (4.90)$$

$$E(\eta^2) = \frac{2N}{147} \Delta V^2 [864\pi^2 - 720\pi^2 + 51 - 144\pi^2 + 54\pi^2 - 60\pi] \cong 5.5 N \Delta V^2 \quad (4.91)$$

For $N = 1000$ and $\Delta V = 1$ in./rad. This gives (in light of the normalization $\eta = \Delta\tau$)

$$E[(r\eta)^2] = 5.5 \times 10^3 \text{ in.}^2 \cong 35 \text{ ft}^2 = \sigma_{r\eta}^2 \quad (4.92)$$

giving a 1σ value of $r\eta$ after one orbit of

$$\sigma_{r\eta} \cong 6 \text{ ft} \quad (4.93)$$

The in-track displacement due to drag in the course of one orbit is

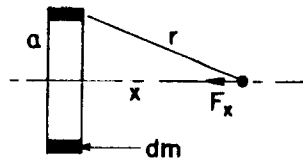
$$r\eta = f_\theta \int_0^{2\pi} (3\theta - 45\theta) d\theta = \frac{fd}{\omega^2} \left| \frac{\theta^2}{2} \right|_0^{2\pi} \cong 600 \pi^2 \text{ ft} \cong 6000 \text{ ft} \quad (4.94)$$

Thus the 1σ effect in-track due to a series of 1000 pulses is 0.1% of the drag force in one orbit. In thirty-six orbits the 1σ effect would be 0.017% of the drag force. This is about the same as the effect due to the oscillatory transverse force obtained in the previous section.

4.5.3 Vehicle Gravity Force

The presence of vehicle mass asymmetrically located and close to the ball can exert a continuous perturbing force on the ball.

The gravitational potential at a point on the axis of a ring distribution of mass dm is

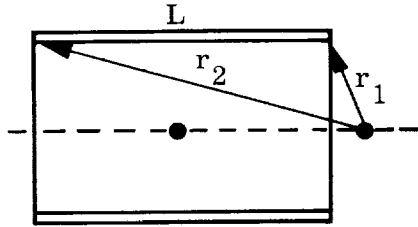


$$V = \frac{Gdm}{r} \quad (4.95)$$

The gravitational specific force at this point is

$$f_x = - \text{grad } V = \frac{G \times dm}{r^3} \quad (4.96)$$

The gravitational specific force at a point on the axis of a cylindrical distribution of mass M is



$$f = \frac{GM}{L} \left(\frac{1}{r_1} - \frac{1}{r_2} \right) \quad (4.97)$$

and is directed toward the CM of the ring. This applies both inside and outside the cylinder.

For the purposes of this analysis we model the satellite vehicle as composed of three homogeneous cylinders of mass as indicated in Fig. 4-16.

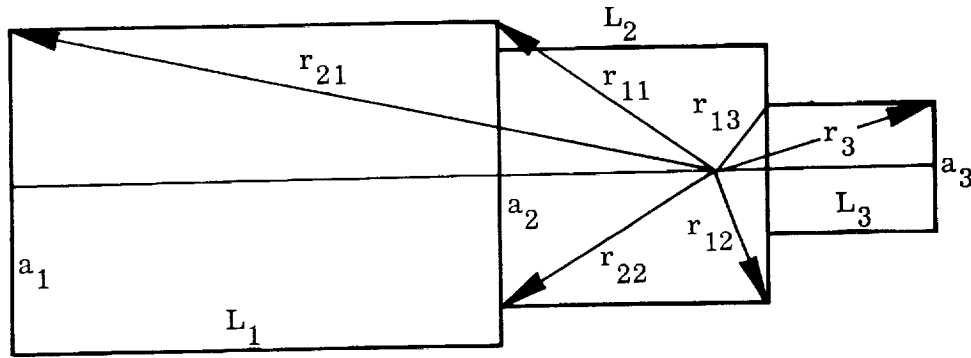


Fig. 4-16 Vehicle Mass Distribution

We assume the sensor to be on the axis as indicated. The net specific force on the ball due to the vehicle mass is then

$$f = G \left[\frac{M_1}{L_1} \left(\frac{1}{r_{11}} - \frac{1}{r_{21}} \right) + \frac{M_2}{L_2} \left(\frac{1}{r_{12}} - \frac{1}{r_{22}} \right) - \frac{M_3}{L_3} \left(\frac{1}{r_{13}} - \frac{1}{r_{23}} \right) \right] \quad (4.98)$$

where $G = 0.67 \times 10^{-7} \text{ cm}^3/\text{gm}/\text{sec}^2$. Typical values follow:

$$M_1 = 500 \text{ lb} \quad L_1 = 30 \text{ ft} \quad a_1 = 2.5 \text{ ft} \quad M_1/L_1 = 16.7 \text{ lb/ft}$$

$$M_2 = 250 \text{ lb} \quad L_2 = 4 \text{ ft} \quad a_2 = 2 \text{ ft} \quad M_2/L_2 = 60.25 \text{ lb/ft}$$

$$M_3 = 400 \text{ lb} \quad L_3 = 3 \text{ ft} \quad a_3 = 1 \text{ ft} \quad M_3/L_3 = 133.3 \text{ lb/ft}$$

We assume the ball to be 1/2 ft inside Cylinder 2. We compute the r_{ij} as follows

$$\left. \begin{aligned} r_{21} &= (6.25 + 33.5^2)^{1/2} = 33.7 \text{ ft} ; & 1/r_{21} &= 0.0297 \\ r_{11} &= (6.25 + 3.5^2)^{1/2} = 4.3 \text{ ft} ; & 1/r_{11} &= 0.232 \\ r_{22} &= (4 + 3.5^2)^{1/2} = 4.03 \text{ ft} ; & 1/r_{22} &= 0.248 \\ r_{12} &= (4 + 0.25)^{1/2} = 2.06 \text{ ft} ; & 1/r_{12} &= 0.485 \\ r_{13} &= (1 + 0.25)^{1/2} = 1.12 \text{ ft} ; & 1/r_{13} &= 0.895 \\ r_{23} &= (1 + 2.5^2)^{1/2} = 2.7 \text{ ft} ; & 1/r_{23} &= 0.371 \end{aligned} \right\} \quad (4.99)$$

For these values we get for the specific force f

$$f = G [(16.7)(0.202) + (60.25)(0.237) - (133.3)(0.524)] \text{ ft/sec}^2 \quad (4.100)$$

giving

$$\left. \begin{aligned} f &= 1.7 \times 10^{-6} \text{ cm/sec}^2 \\ f &\cong 1.7 \times 10^{-9} \text{ g} \end{aligned} \right\} \quad (4.101)$$

which is a force on the ball toward M_3 and due mainly to mass M_3 . If this became critical then one could effect compensation by locating the ball further inside M_2 , or by shifting closely placed auxilliary masses. It is clear that the effect of M_3 is going to decrease rapidly with increase in r_{13} .

4.5.4 Perturbation Due to Vehicle Magnetic Fields

For certain mission considerations beyond the scope of this dissertation, the ball that will be flight-tested is made of a tungsten alloy which is para-magnetic. Thus the only magnetic force is a result of induction due to the divergence of whatever magnetic field is present.

The force due to the field induced in a sphere of radius r and susceptibility k at a distance d on the axis of a dipole of moment M is (see Ref. 1)

$$F = \frac{M^2 k r^3}{4\pi^2 d^7} \quad \text{for } d \gg r \quad (4.102)$$

For a sphere of density ρ , the specific force is

$$f = \frac{3F}{4\rho r^3} = \frac{3kM^2}{16\pi^2 \rho d^7} \quad (4.103)$$

For a magnetic dipole of moment

$$M = 8 \times 10^4 \text{ pole-cm} \quad (4.104)$$

a tungsten ball with $k = 10^{-6}$, $\rho = 18 \text{ g/cm}^3$, and $d = 50 \text{ cm}$ one gets

$$f = 10^{-11} \text{ cm/sec}^2 \cong 10^{-14} \text{ g} \quad (4.105)$$

A magnetic dipole with a net strength of 8×10^4 pole-cm is somewhat larger than is expected to be present.

4.5.5 Perturbations Due to Electric Forces

Since the ball is enclosed in a cage of metal rods further surrounded by a metal shield and since it has periodic contact with the side wall rods, no electrostatic charge should build up on the ball and it will also be partially shielded from the earth's field. Thus, for this configuration no net electric force should exist.

4.5.6 Perturbations Due to Misalignment of Attitude Control Jets

Vehicle attitude control is accomplished by a gas jet system of two T-shaped clusters of three jets each. The nozzles in one cluster are directed oppositely from those in the other. None of these points along the roll axis (i. e. , the plane of the T is normal to the roll axis). However, if the plane of a T is not quite normal to the roll axis, a net force along this axis will result. However it is important to note that since this force acts on the vehicle along its roll axis it will not exert a force on the ball but will merely aid or fight the drag-make-up thrusters.

For an attitude control system operating in a limit cycle mode governed by a minimum impulse of 0.01 lb-sec per jet per firing, then 6 jets misaligned by 0.02 rad would produce an impulse of 0.0012 lb-sec per firing along the roll axis. Now, the drag on the vehicle is about 10^{-2} lb which requires 10^{-2} lb-sec of impulse for compensation. Thus, if the attitude jets fired less frequently than once per hundred seconds, they would contribute less than 0.12% error to the determination of the impulse required for drag compensation (or equivalently the determination of the drag force by measuring fuel consumption). Furthermore, since a single firing would produce a ΔV in the roll direction of about

$$\Delta V = \frac{Ft}{M} = \frac{0.01 \times 0.02}{100} = 2 \times 10^{-6} \text{ ft/sec} \quad (4.106)$$

and since a firing lasts about 0.02 sec, the acceleration due to one firing is

$$a = \frac{2 \times 10^{-6}}{0.02} = 10^{-4} \text{ ft/sec}^2 \quad (4.107)$$

which is about equal to the drag specific force and thus would not saturate the thrust control system.

The above indicates that the current vehicle attitude system, which has a limit cycle period in excess of 5 min, should not compromise the drag make-up system.

Chapter 5

CONCLUSIONS AND RECOMMENDATIONS

The results of the work described in this dissertation have led to the following major conclusions:

- For systems whose coefficient matrix is K-symmetric the inverse of the solution matrix (matrizant) is easily obtainable by a direct multiplication involving only the transpose of the matrizant.
- Although no direct method is available for recognizing the K-symmetry of a matrix, aids to trial and error methods are available for finding an appropriate K. Once a K is known for a system, the K for any related system, which has a state vector expressible as a constant non-singular matrix times the original state vector, can be directly determined.
- The fundamental matrizant for the angular displacement expressed in Euler parameters of a free body having two equal principal moments of inertia has a very simple structure which allows direct computation of the displacement at any future time in terms of the initial conditions.
- The use of a control law based on "inertial" relative velocities in conjunction with on-off control is effective for controlling the translational motion of an arbitrarily tumbling satellite so as to keep it on a "drag-free" trajectory without the necessity of knowing or controlling the angular orientation of the vehicle.
- Of three different specific systems of control, namely, (1) lead-lag (for rate) with bang-bang control, (2) pseudo rate (for rate) with bang-bang control, and (3) lead-lag (for rate) with PWPF modulated on-off valves for control, investigated by computer simulation, all function well in the absence of noise but with the addition of noise into the position sensor signal the PWPF system was superior to the other two especially for dead band to rms noise ratios near 1. For ratios greater than about 1.5 the pseudo rate system was as efficient as the PWPF even in the case in which some terms were omitted in the process of deriving the pseudo rate.
- The concept of using the fact that the direction of the drag force remains nominally fixed in the body (of a satellite with attitude control which keeps one body axis nominally along the velocity vector) for synthesizing a simplified drag make-up sensing and control system appears feasible.

Principal errors arise from contact of the proof mass with the side walls of a cage which loosely constrains the proof mass in a direction transverse to the drag. Trajectory errors less than those arising from $1/500$ of the drag force appear achievable.

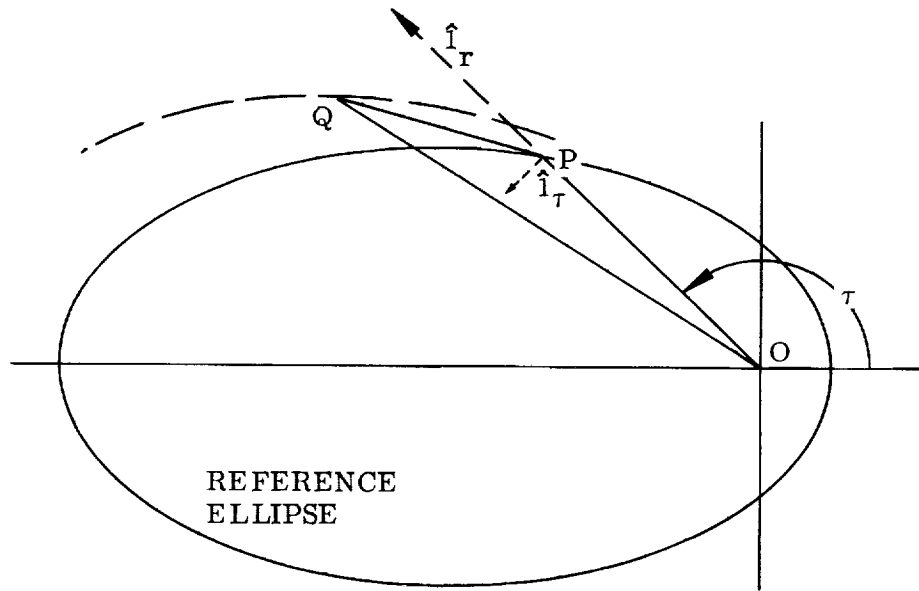
Further effort in the following areas would provide useful results, and thus, these recommendations for further investigation seem appropriate:

- (1) Find a direct method for either obtaining the K for a given matrix or prove that none exists.
- (2) Obtain the fundamental matrix for a free body of unequal inertias.
- (3) Solve exactly the problem of minimum limit cycle fuel consumption in the presence of noise.

Appendix A

LINEARIZED EQUATIONS OF RELATIVE MOTION FOR SATELLITES IN NEIGHBORING ELLIPTIC ORBITS

In this development, we choose the orbit of one satellite as the reference or nominal orbit and derive the equations of motion of the other relative to it. As a consequence of the linearization it is clear that the choice is arbitrary and either orbit could have been used as the reference. The geometry is shown in the accompanying figure:



$$\begin{aligned}\overline{OP} &= \vec{r} & \hat{i}_z &= \hat{i}_r \times \hat{i}_\tau \\ \overline{OQ} &= \vec{r}_q \\ \overline{PQ} &= \vec{\rho}\end{aligned}$$

The equations of motion of a mass point at P in the presence of gravitational attraction ($GM = \mu$) at O and a specific force F_p at P are

$$\frac{\Pi}{r} + \frac{\mu}{r^3} \vec{r} = \vec{F}_p \quad (A.1)$$

Similarly at Q we have

$$\frac{\Pi}{r} + \frac{\mu}{r_q^3} \vec{r}_q = \vec{F}_q \quad (\text{A.2})$$

We wish equations of relative motion,* i.e., in terms of

$$\vec{\rho} = \vec{r}_q - \vec{r} \quad (\text{A.3})$$

and

$$\vec{F} = \vec{F}_q - \vec{F}_p \quad (\text{A.4})$$

Taking the difference between Eqs. (A.2) and (A.1), we have

$$\frac{\Pi}{\rho} + \mu \left(\frac{\vec{\rho} + \vec{r}}{r_q^3} - \frac{\vec{r}}{r^3} \right) = \vec{F} \quad (\text{A.5})$$

Now

$$r_q^3 = r^3 \left(1 + 2 \frac{\vec{r} \cdot \vec{\rho}}{r^2} + \frac{\rho^2}{r^2} \right)^{3/2} \quad (\text{A.6})$$

Taking

$$\vec{\rho} = x\hat{1}_r + y\hat{1}_\tau + z\hat{1}_z = \vec{x} + \vec{y} + \vec{z} \quad (\text{A.7})$$

and letting

$$\vec{\rho} = r\vec{\delta} \quad (\text{A.8})$$

$$\vec{\delta} = \xi\hat{1}_r + \eta\hat{1}_\tau + \zeta\hat{1}_z \quad (\text{A.9})$$

*This course was first pursued by G. W. Hill in 1878.

we have

$$\frac{1}{r_q^3} = \frac{1 - 3\Delta}{r^3}, \quad \Delta \cong \hat{1}_r \cdot \vec{\delta} \cong \frac{x}{r} \quad (\text{A.10})$$

With these relations, Eq. (A.5) becomes

$$\frac{\Pi}{\rho} + \frac{\mu}{r^3} \vec{\rho} - \frac{3\mu\Delta(\vec{r} + \vec{\rho})}{r^3} = \vec{F} \quad (\text{A.11})$$

Following Tschauner and Hempel (Ref. 6), we shall investigate the above in terms of derivatives with respect to anomaly τ . The following relations apply

$$\dot{\tau} = \omega \quad (\text{A.12})$$

$$r = \frac{p}{1 + e \cos \tau} \quad (\text{A.13})$$

$$p = \frac{h^2}{\mu} \quad (\text{A.14})$$

$$h = r^2 \omega \quad (\text{A.15})$$

$$\frac{\mu}{r^3} = \frac{r\omega^2}{p} \quad (\text{A.16})$$

$$\frac{\vec{I}}{r} = \frac{d\vec{r}}{dt} = \frac{d\vec{r}}{d\tau} \cdot \frac{d\tau}{dt} \equiv \omega \vec{r}' \quad (\text{A.17})$$

$$\frac{\Pi}{r} = \omega(\omega' \vec{r}' + \omega \vec{r}'') \quad (\text{A.18})$$

$$\omega' = -2hr^{-3} r' = -\frac{2\omega r'}{r} \quad (\text{A.19})$$

$$\frac{\Pi}{\rho} = \omega^2 \left(\vec{\rho}'' - \frac{2\vec{\rho}' r'}{r} \right) \quad (\text{A.20})$$

we have

$$\vec{\rho}' = r' \vec{\delta} + r \vec{\delta}' \quad (\text{A.21})$$

$$\vec{\rho}'' = r''\vec{\delta} + 2r'\vec{\delta}' + r\vec{\delta}'' \quad (\text{A.22})$$

Equation (A.11) becomes

$$\vec{F} = \omega^2 \left[r''\vec{\delta} + 2r'\vec{\delta}' + r\vec{\delta}'' - \frac{2r'}{r} (r'\vec{\delta} + r\vec{\delta}') \right] + \frac{\mu}{r^2} \vec{\delta} - \frac{3\mu\Delta}{r^2} (\hat{1}_r + \vec{\delta}) \quad (\text{A.23})$$

Now

$$r' = \frac{er^2 s\tau}{p} \quad \sin \tau \equiv s\tau, \text{ etc.} \quad (\text{A.24})$$

$$r'' = \frac{er}{p} (rc\tau + 2r's\tau) \quad (\text{A.25})$$

and Eq. (A.23) becomes

$$\vec{F} = \omega^2 r \left[\vec{\delta}'' + \vec{\delta} \left(\frac{erc\tau}{p} + \frac{2er's\tau}{2} - \frac{2res\tau}{p} + \frac{r}{p} \right) - \frac{3r}{p} \Delta (\hat{1}_r + \vec{\delta}) \right] \quad (\text{A.26})$$

$$\frac{\vec{F}}{r\omega^2} = \vec{\delta}'' + \vec{\delta} - \frac{3\Delta(\hat{1}_r + \vec{\delta})}{1 + ec\tau} \quad (\text{A.27})$$

Now

$$\vec{\delta}' = \xi' \hat{1}_r + \eta' \hat{1}_\tau + \xi' \hat{1}_z + \xi \hat{1}_r' + \eta \hat{1}_\tau' + \xi \hat{1}_z' \quad (\text{A.28})$$

And for the situation in which $F_p = 0$ we have

$$\hat{1}_z' = 0, \quad \hat{1}_r' = +\hat{1}_\tau, \quad \hat{1}_\tau' = -\hat{1}_r \quad (\text{A.29})$$

so that

$$\vec{\delta}' = (\xi' - \eta) \hat{1}_r + (\xi + \eta') \hat{1}_\tau + \xi' \hat{1}_z \quad (\text{A.30})$$

and

$$\vec{\delta}'' = (\xi'' - 2\eta' - \xi) \hat{1}_r + (\eta'' - 2\xi - \eta) \hat{1}_\tau + \xi'' \hat{1}_z \quad (\text{A.31})$$

Neglecting product terms like ξ^2 , $\eta\xi$, etc., we have $\Delta \cong \xi$ and on collecting terms, Eq. (A.27) becomes

$$\frac{\vec{F}}{\omega^2 r} = \left(\xi'' - 2\eta' - \frac{3\xi}{1 + ec\tau} \right) \hat{1}_r + (\eta'' + 2\xi') \hat{1}_\tau + (\xi'' + \xi) \hat{1}_z \quad (\text{A.32})$$

If we break up \vec{F} into components such that

$$\frac{\vec{F}}{\omega^2 r} \equiv f_r \hat{1}_r + f_\tau \hat{1}_\tau + f_z \hat{1}_z \quad (\text{A.33})$$

we can write three component equations:

$$\xi'' - 2\eta' - \frac{3\xi}{1 + ec\tau} = f_r(\tau) \quad (\text{A.34})$$

$$\eta'' + 2\xi' = f_\tau(\tau) \quad (\text{A.35})$$

$$\xi'' + \xi = f_z(\tau) \quad (\text{A.36})$$

where the f 's can be thought of as specific forces measured in "orbit g's." For cases in which $f(z)$ is not an explicit function of ξ or η , it is clear that Eq. (A.36) is uncoupled from Eqs. (A.34) and (A.35) and represents harmonic motion (into and out of the nominal orbit plane.)

To solve the coupled set, Eqs. (A.34) and (A.35), which describe the in-plane relative motion, we start with the homogeneous equations (i.e., $f_r = f_\tau = 0$). Equation (A.35) can be directly integrated giving

$$\eta' + 2\xi = \alpha \quad (= \text{constant}) \quad (\text{A.37})$$

Eliminating η' from Eq. (A.34) gives

$$\xi'' + \frac{1 + 4ec\tau}{1 + ec\tau} \xi = 2\alpha \quad (\text{A.38})$$

Setting $\alpha = 0$ in Eq. (A.38) gives

$$\xi'' + \frac{1 + 4ec\tau}{1 + ec\tau} \xi = 0 \quad (\text{A.39})$$

The fact that this equation has a closed form solution in terms of simple functions* is the key to the closed form solution to the set, Eqs. (A.34) and (A.35). No general method exists for obtaining a solution to Eq. (A.39). Because of the $(1 + e c \tau)$ in the denominator of the second term we are tempted to look for a product solution of the form

$$\xi = x(1 + e c \tau) \quad (\text{A.40})$$

with

$$\xi' = x'(1 + e c \tau) - x e s \tau \quad (\text{A.41})$$

$$\xi'' = x''(1 + e c \tau) - 2x' e s \tau - x e c \tau \quad (\text{A.42})$$

Putting this into Eq. (A.39) gives

$$x'' + x'' e c \tau - 2x' e s \tau - x e c \tau + x + 4e x c \tau = 0 \quad (\text{A.43})$$

Regrouping gives

$$x'' + x + e[c \tau(x'' + 3x) - 2x's \tau] = 0 \quad (\text{A.44})$$

Now if this is to be a solution it must be good for all e including $e = 0$. For $e = 0$ we have from Eq. (A.44)

$$x'' + x = 0 \quad (\text{A.45})$$

If we put this constraint into the term in e in Eq. (A.44) it becomes

$$e[2x c \tau - 2x's \tau] = 0 \quad (\text{A.46})$$

We see that $x = k s \tau$ is clearly a solution to both Eqs. (A.45) and (A.46) which yields the result

$$\xi = u_1(\tau) = s \tau(1 + e c \tau) \quad (\text{A.47})$$

as a solution to Eq. (A.39).

Since Eq. (A.39) is second-order, there is clearly another solution. Having one solution to a set of equations allows us to reduce the order of the set by one.

*Tschauner and Hempel (Ref. 6).

For the case of a second-order system this allows the second solution to be found in general. This turns out to be

$$u_2 = u_1 \int \frac{d\tau}{u_1^2} \quad (\text{A.48})$$

which is easily verified as follows:

$$u_2' = u_1' \int \frac{d\tau}{u_1^2} + \frac{1}{u_1} \quad (\text{A.49})$$

$$u_2'' = u_1'' \int \frac{d\tau}{u_1^2} + \frac{u_1'}{u_1^2} - \frac{u_1'}{u_1^2} = u_1'' \int \frac{d\tau}{u_1^2} \quad (\text{A.50})$$

Putting this into Eq. (A.39) gives

$$\left[u_1'' + \frac{1 + 4ec\tau}{1 + ec\tau} u_1' \right] \int \frac{d\tau}{u_1^2} = 0 \quad (\text{A.51})$$

which is identically satisfied since u_1 is a solution to Eq. (A.39).

We get u_2 explicitly from Eq. (A.48):

$$u_2 = s (1 + ec\tau) \int \frac{d\tau}{s^2 \tau (1 + ec\tau)^2} \quad (\text{A.52})$$

which is most easily evaluated by changing the independent variable to the eccentric anomaly E . Carrying out the integration gives for u_2

$$u_2(\tau) = \frac{1}{\epsilon^4} \left[\frac{3e}{2} - \epsilon^2 c \tau - \frac{e}{2} (1 + 2e^2)(c^2 \tau - s^2 \tau) - \frac{3e^2}{\epsilon} Eu_1 \right] \quad (\text{A.53})$$

where $\epsilon^2 \equiv 1 - e^2$, E is the eccentric anomaly, and the constants are chosen such that the Wronskian determinant (cf. the discussion on p. 23)

$$u_1 u_2' - u_2 u_1' = 1 \quad (\text{A.54})$$

Using the same approach of Eq. (A.39) on Eq. (A.38), we have corresponding to Eq. (A.44)

$$x'' + x + e [c \tau (x'' + 3x) - 2x' s \tau] = 2\alpha \quad (\text{A.55})$$

For $\alpha = ek$ where k is a constant, we have for the same constraint

$$x'' + x = 0 \quad (\text{A.56})$$

and

$$2x c \tau - 2x' s - 2k = 0 \quad (\text{A.57})$$

and we see that for $k = 1$, $x = c \tau$ is a solution to this set so that $c \tau (1 + e c \tau)$ is a solution to Eq. (A.38) for $\alpha = e$.

Equivalently the function

$$u_0(\tau) = \frac{c \tau}{e} (1 + e c \tau) \quad (\text{A.58})$$

is a solution Eq. (A.38) for $\alpha = 1$.

We will also have need of the derivatives:

$$u_1'(\tau) = c \tau + e(c^2 \tau - s^2 \tau) \quad (\text{A.59})$$

$$u_2'(\tau) = \frac{1}{\epsilon^4} \left[(1 - 4e^2) s \tau + 2e(1 + 2e^2) s \tau c \tau - \frac{3Ee^2}{\epsilon} (c \tau + e c^2 \tau - e s^2 \tau) \right] \quad (\text{A.60})$$

$$u_0'(\tau) = -\frac{1}{e} s \tau - 2s \tau c \tau = -\frac{s \tau}{e} (1 + 2e c \tau) \quad (\text{A.61})$$

As a check we note for $\tau = 0$

$$u_1(0) u_2'(0) - u_2(0) u_1'(0) = - \left(- \frac{1}{1+e} \right) (1+e) = 1 \quad (\text{A.62})$$

Now from Eq. (A.37) we have that

$$\eta = \int (\alpha - 2\xi) d\tau \quad (\text{A.63})$$

defining $\eta = V_1$ when $\xi = u_1$ we have

$$V_1(\tau) = -2 \int u_1 d\tau = \frac{1}{e} (1 + e c \tau)^2 \quad (\text{A.64})$$

$$V_2(\tau) = -2 \int u_2 d\tau = \frac{2}{e^4} \left[\left(1 + \frac{e^2}{2} \right) s \tau + \frac{e}{2} (1 + 2e^2) s \tau c \tau - \frac{3e^2}{2e} V_1 E \right] \quad (\text{A.65})$$

$$V_0 = \int (1 - 2u_0) d\tau = \tau - \frac{2s\tau}{e} - (s \tau c \tau + \tau) \quad (\text{A.66})$$

$$V_0 = - \frac{s\tau}{e} (2 + e c \tau) = - \frac{1}{e} [u_1(\tau) + s \tau] \quad (\text{A.67})$$

The choice of integration constants for the indefinite V-integrals was chosen to simplify the K-orthogonality relations on the matrix P (see Chapter I).

Note also that $\eta = 1, \xi = \xi' = \eta' = \alpha = 0$ is an independent solution to Eqs. (A.34) and (A.35) corresponding to the mass point Q leading P by a constant angle.

If we now form the state vector

$$x^\dagger = (\xi, \eta, \xi', \alpha) \quad (\text{A.68})$$

Then for $\vec{f} = 0$, Eqs. (A.34) and (A.35) can be written as

$$x' - Fx = 0 \quad (\text{A.69})$$

where

$$F = \begin{bmatrix} 0 & 0 & 1 & 0 \\ -2 & 0 & 0 & 1 \\ q & 0 & 0 & 2 \\ 0 & 0 & 0 & 0 \end{bmatrix} \quad \text{and} \quad q = \frac{3}{1 + e c \tau} - 4 \quad (\text{A.70})$$

From the results above we see that we have 4 linearly independent x 's which satisfy Eq. (A.69)*

$$\begin{aligned} x_0^\dagger &= (u_0, V_0, u'_0, 1) \\ x_1^\dagger &= (u_1, V_1, u'_1, 0) \\ x_2^\dagger &= (u_2, V_2, u'_2, 0) \\ x_3^\dagger &= (0, 1, 0, 0) \end{aligned} \quad (\text{A.71})$$

Thus the matrix P having these x 's as columns

$$P = \begin{bmatrix} 0 & u_0 & u_1 & u_2 \\ 1 & V_0 & V_1 & V_2 \\ 0 & u'_0 & u'_1 & u'_2 \\ 0 & 1 & 0 & 0 \end{bmatrix} \quad (\text{A.72})$$

satisfies the equation

$$P' = FP \quad (\text{A.73})$$

We now restate Eqs. (A.34) and (A.35) in matrix form

$$x' = Fx + Df \quad (\text{A.74})$$

*It should be pointed out that these solutions can be obtained by other means. For example by varying the (orbital) parameters, one finds that variation of perigee time (δt_p) produces a solution corresponding to y_1^\dagger [see Eq. (2.78) for relation between x and y], variation of eccentricity (δe) produces y_0^\dagger , etc.

where

$$f^{\dagger} = (f_r, f_{\tau}) \quad , \quad D = \begin{bmatrix} 0 & 0 \\ 0 & 0 \\ 1 & 0 \\ 0 & 1 \end{bmatrix} \quad , \quad \text{and} \quad Df = \begin{bmatrix} 0 \\ 0 \\ f_r \\ f_{\tau} \end{bmatrix} \quad (\text{A.75})$$

The solution to Eq. (A.74) is

$$x(\tau) = X(\tau, \tau_0) \left[x(\tau_0) + \int_0^{\tau} X^{-1}(t, \tau_0) Df(t) dt \right] \quad (\text{A.76})$$

where X is the fundamental matrix satisfying the equation

$$X' = FX \quad , \quad X(\tau_0, \tau_0) = I \quad (\text{A.77})$$

That Eq. (A.76) is a solution to Eq. (A.74) can be verified by direct multiplication.

The matrix X can be obtained from P in Eq. (A.73) and is simply

$$X(\tau, \tau_0) = P(\tau) P^{-1}(\tau_0) \quad (\text{A.78})$$

since

$$\frac{dP^{-1}(\tau_0)}{d\tau} = 0 \quad \text{and} \quad P(\tau_0) P^{-1}(\tau_0) = X(\tau_0, \tau_0) = I \quad (\text{A.79})$$

we have

$$X' = P'(\tau) P^{-1}(\tau_0) = FP(\tau) P^{-1}(\tau_0) = FX \quad (\text{A.80})$$

Note there is no requirement that $P(\tau) = I$ for some value of the argument τ . That it will not necessarily be is explicitly clear from Eq. (A.72).

Another interesting factorization of X is the Floquet factorization. For systems in which the coefficient matrix $F(\tau)$ is periodic [i.e., $F(\tau + T) = F(\tau)$], the following factorization is valid:

$$X = R(\tau, \tau_0) e^{B(\tau - \tau_0)} \quad (A.81)$$

where R is periodic with the (same) period T , and B is a constant matrix.

By substituting Eq. (A.81) into Eq. (A.77) one gets the following relation between B and R

$$R' = FR - RB \quad (A.82)$$

which is known as the Lyapunov reduction. Although B and R are not unique but only related, the real part of the eigenvalues of B are unique (for a given F) and determine the stability of the system. Since R is periodic and in particular has the property

$$R(\tau_0 + T, \tau_0) = R(\tau_0, \tau_0) = I \quad (A.83)$$

the following relation applies

$$X(\tau_0 + T, \tau_0) = e^{BT} \quad (A.84)$$

Additional insight into a given system may be gained by using the Jordan form of B

$$\Lambda = N^{-1}BN \quad (A.85)$$

where N is a constant matrix. We thus find that

$$X = R e^{N\Lambda N^{-1}(\tau - \tau_0)} = RN e^{\Lambda(\tau - \tau_0)} N^{-1} \quad (A.86)$$

Letting

$$RN \equiv Q \quad (A.87)$$

Note Q is also periodic with period T .

we have

$$X = Q e^{\Lambda(\tau-\tau_0)} N^{-1} \quad (A.88)$$

Now for $\tau = \tau_0$ we have $X = I$ giving

$$Q(\tau_0) = N \quad (A.89)$$

Thus in this form we see that

$$X(\tau, \tau_0) = Q(\tau) e^{\Lambda(\tau-\tau_0)} Q^{-1}(\tau_0) = Q(\tau) e^{\Lambda\tau} \left[Q(\tau_0) e^{\Lambda\tau_0} \right]^{-1} \quad (A.90)$$

which is known factorization and expresses very elegantly the structure and symmetry of the fundamental matrizant. We note also the relation between Q and A which corresponds to that in Eq. (A.82)

$$Q' = FQ - QA \quad (A.91)$$

If we call $Q e^{\Lambda\tau} = \varphi(\tau)$, we note that $\varphi' = F\varphi$ and thus φ is a solution to the matrix Eq. (A.73). Like P it does not necessarily have the boundary condition that $\varphi(\tau_0) = I$. We shall call integral matrices such as $\varphi(\tau)$ a matrizant solution to Eq. (A.73) and reserve the term "fundamental matrix" (FM) for the quantities of the form

$$X(\tau, \tau_0) = \varphi(\tau) \varphi^{-1}(\tau_0) \quad (A.92)$$

From this relation it is explicitly clear that $X(\tau_0, \tau_0) = I$, the identity.

Having the constant matrix in Jordan form provides the potential for gaining insight into the basic system structure since the normal modes are laid bare in this representation.

We also note the following property of these solutions: Multiplying Eq. (A.77) from the right by a constant matrix C gives

$$X'(\tau, \tau_0) C = F(\tau) X(\tau, \tau_0) C ; \text{ i.e., } [XC]' = F[XC] \quad (A.94)$$

Since F is periodic we have

$$X'(\tau, \tau_0) = F(\tau) X(\tau, \tau_0) \quad (\text{A.95})$$

$$X'(\tau + T, \tau_0) = F(\tau) X(\tau + T, \tau_0) \quad (\text{A.96})$$

This implies (due to uniqueness of solutions with the same boundary conditions) that

$$X(\tau, \tau_0) C = X(\tau + T, \tau_0) \quad (\text{A.97})$$

which by virtue of the fact that $X(\tau_0, \tau_0) = I$ gives

$$C = X(\tau_0 + T, \tau_0) \quad (\text{A.98})$$

By repeated application of this process one can verify that for any integer k

$$X(\tau_0 + kT, \tau_0) = C^k = X^k(\tau_0 + T, \tau_0) \quad (\text{A.99})$$

Thus

$$X(\tau + T, \tau_0) = X(\tau, \tau_0) X(\tau_0 + T, \tau_0) \quad (\text{A.100})$$

and

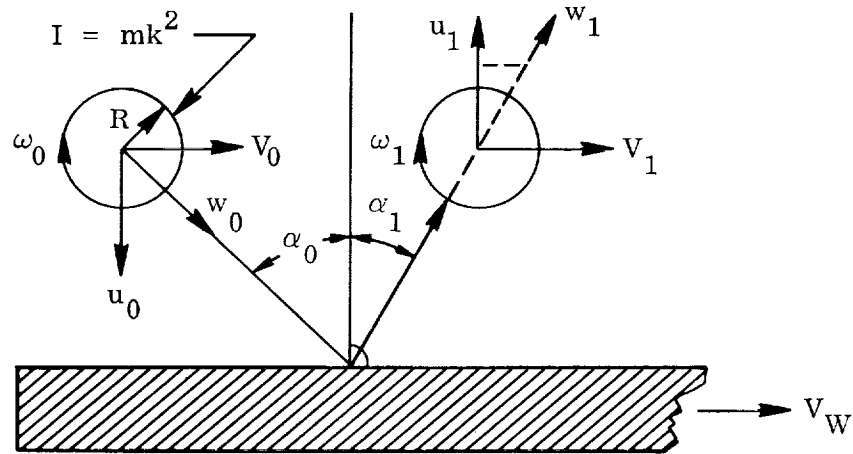
$$X(\tau + kT, \tau_0) = X(\tau, \tau_0) X^k(\tau_0 + T, \tau_0) \quad (\text{A.101})$$

This relation is exploited by Lange and Smith (Ref. 7) to avoid integration over more than one period for the case of periodic inputs.

Appendix B

FOLLOW THE BOUNCING BALL

When a ball impacts against a wall one recognizes intuitively that some angular momentum is imparted to the ball in the course of the impact. The question that appears new is what is the effect including relative magnitudes on a ball bouncing between two closely spaced walls with (initially) appreciable down-wall velocity. To gain insight into the problem we first develop the detail dynamics of a ball impacting at an angle against a single wall. We postulate a spherical ball of mass m , inertia I , and radius R impacting with a total linear velocity w_0 , with components u_0 normal to the wall and V_0 along the wall. The component w_0 makes an angle $\alpha_0 = \tan^{-1}(V_0/u_0)$ with the normal to the wall; the ball is assumed to have an angular velocity ω_0 normal to the plane of the trajectory (i.e., the paper); see the accompanying figure.



Now the velocity of the rim of the ball (at the instant and point of contact) along the wall is $V_{T0} = V_0 - R\omega_0$. The velocity normal to the wall is $u_0 = w_0 \cos \alpha_0$.

If we assume that the velocity of the wall during impact is V_W , we recognize the following interaction. The impact will cause the normal velocity to change

sign and, if there is energy loss, to decrease in magnitude. For a coefficient of restitution e_1 the normal velocity after impact will be

$$u_1 = -e_1 u_0 \quad (\text{B.1})$$

and the impulse given to the ball by the wall in the direction normal to the wall will be

$$I_m = m(u_0 - u_1) = m(1 + e_1)u_0 \quad (\text{B.2})$$

This impulse is equal to the integral of the normal force through the impact, i.e.,

$$I_m = \int_{\Delta t} F_N dt = m(1 + e_1)u_0 \quad (\text{B.3})$$

In the direction along the wall we have two possibilities for the type of interaction. If $V_{T0} = V_w$, there is no relative velocity between the wall and the rim of the ball and the ball either does not move along the wall or it rolls without slipping. In either case there is no tangent force on the ball and thus, for zero rolling friction, no change in the angular velocity or tangent velocity of the ball, and the ball leaves the wall such that the rim velocity of the point of contact equals the wall (in plane) velocity.

If $V_{T0} \neq V_w$, there is a tangent force in a direction which opposes the relative velocity so as to force $V_{T0} - V_w$ to zero. The magnitude of the tangent force is $F_T = \mu F_N$ where μ is the coefficient of sliding friction between the wall and the ball. If during the impact $V_T - V_w$ goes to zero, then F_T becomes zero. In this case, as before, the ball then leaves the wall with a rim speed equal to the wall speed.

From this fact we can determine the velocity of the ball after impact. We investigate these two cases:

Case I. The ball leaves the impact with rim velocity equal to the wall velocity, i.e., $V_{T1} = V_w$. For $V_{T0} > V_w$, the change in linear momentum in the "V" direction (i.e., along the wall) during impact is

$$\int_{\Delta t} F_T dt = m(V_0 - V_1) \quad (\text{B.4})$$

The change in angular momentum is

$$R \int_{\Delta t} F_T dt = I(\omega_1 - \omega_0) \quad (B.5)$$

Thus

$$mR(V_0 - V_1) = I(\omega_1 - \omega_0) \quad (B.6)$$

We also have after impact

$$V_w = V_{T1} = V_1 - R\omega_1 \quad (B.7)$$

From this we may solve for V_1 in terms of V_w and the initial conditions:

$$mR^2V_0 + IR\omega_0 = mR^2V_1 + I(V_1 - V_w) \quad (B.8)$$

$$V_1 = \left[mR^2V_0 + I(R\omega_0 + V_w) \right] / (I + mR^2) \quad (B.9)$$

In terms of the radius of gyration k where $I = mk^2$ we have

$$V_1 = \left[R^2V_0 + k^2(V_w + R\omega_0) \right] / (R^2 + k^2) \quad (B.10)$$

For the case in which $V_w > V_{T0}$ we have

$$\int_{\Delta t} F_T dt = m(V_1 - V_0) \quad (B.11)$$

and

$$R \int F_T dt = I(\omega_0 - \omega_1) \quad (B.12)$$

giving as before

$$mR(V_1 - V_0) = I(\omega_0 - \omega_1) \quad (B.13)$$

which leads to the identical result.

From the condition that $V_{T1} = V_w$ we can solve for $R\omega_1$

$$R\omega_1 = V_1 - V_w = \left[R^2(V_0 - V_w) + k^2 R\omega \right] / (R^2 + k^2) \quad (B.14)$$

We can solve for the initial conditions that allow this result. We have

$$m(V_0 - V_1) = m[k^2/(R^2 + k^2)](V_0 - V_w - R\omega_0) = \int_{\Delta t} F_T dt \quad (B.15)$$

Now for F_T we have

$$|F_T| = \begin{cases} \mu |F_N| & \text{for } V_T \neq V_w \\ 0 & \text{for } V_T = V_w \end{cases} \quad (B.16)$$

Thus

$$\int_{\Delta t} F_T dt \leq \mu \int_{\Delta t} F_N dt = \mu m(1 + e_1)u_0 \quad (B.17)$$

and since $e_1 \leq 1$ we can write the inequality

$$[k^2/(R^2 + k^2)] |V_0 - V_w - R\omega_0| \leq 2\mu |u_0| \quad (B.18)$$

or since $V_0 = u_0 \tan \alpha_0$ we have

$$\left| \tan \alpha_0 - \frac{V_w + R\omega_0}{|u_0|} \right| \leq 2\mu \left(1 + \frac{R^2}{k^2} \right) \quad (B.19)$$

Thus we see that we will always have rolling without slipping before the end of impact if before impact we have

$$\left| \tan \alpha_0 - \frac{V_w + R\omega_0}{u_0} \right| \leq 2\mu \left(1 + \frac{R^2}{k^2} \right) \quad (B.20)$$

For the case of a solid homogeneous sphere we have

$$I = \frac{2}{5} mR^2 = mk^2 \quad (B.21)$$

and

$$k^2 = \frac{2}{5} R^2 \quad (\text{B.22})$$

Thus, for the case of the solid sphere we get

$$\text{for} \quad \left| \tan \alpha_0 - \frac{V_w + R\omega_0}{|u_0|} \right| \leq 7\mu \quad (\text{B.23})$$

that

$$V_1 = [5V_0 + 2(V_w + R\omega_0)]/7 \quad (\text{B.24})$$

$$R\omega_1 = [5(V_0 - V_w) + 2R\omega_0]/7 \quad (\text{B.25})$$

and

$$\Delta V = V_0 - V_1 = \frac{2}{7} [V_0 - V_w - R\omega_0] \quad (\text{B.26})$$

velocity imparted to ball during impact.

Case II. We can now clearly define and investigate a second case, namely, when

$$\left| \tan \alpha_0 - \frac{V_w + R\omega_0}{|u_0|} \right| > 7\mu \quad (\text{B.27})$$

In this situation we have

$$\begin{aligned} V_1 &= V_0 - \frac{1}{m} \int F_T dt = V_0 - \frac{\mu}{m} \int F_N dt \\ &= V_0 - \mu(1 + e_1)u_0 \\ &= u_0 [\tan \alpha_0 - \mu(1 + e_1)] \end{aligned} \quad (\text{B.28})$$

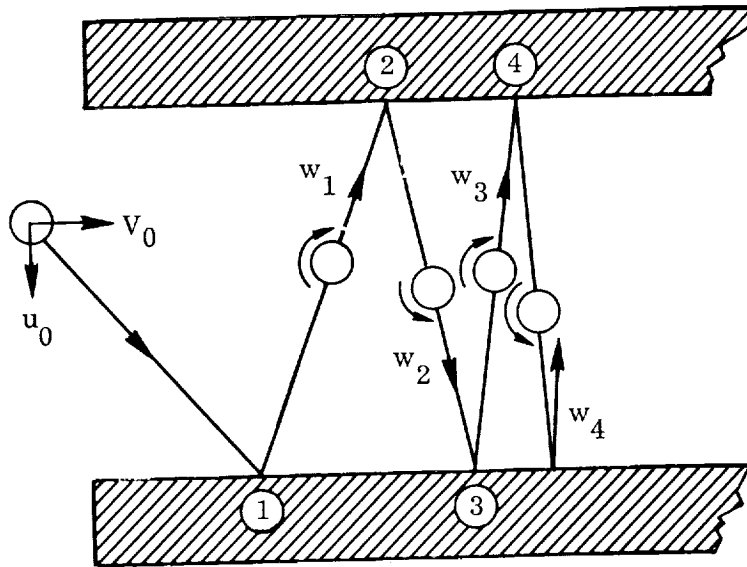
and we see that V_1 is a function of the initial velocity and the coefficient of friction. In this case the ball is still sliding at the end of the impact.

We now have the tools to investigate the problem initially posed. It may be worthwhile noting that the phenomenon of a ball starting out bouncing "down"

a channel and rapidly transferring into a vertical bounce was confirmed experimentally before the theoretical explanation was developed in detail.

It turns out that the spin of the ball has a critical effect on the behavior and this combined with the process of hitting alternate walls is responsible for the observed phenomenon.

We now investigate the situation illustrated in the accompanying figure in which a ball enters a channel or box and proceeds down the channel by bouncing from wall to wall.



For this problem we adopt a coordinate system fixed in the box. Thus $V_w = 0$. From the preceding analysis we know for the case of rolling without slipping that after the first hit we have (since $V_w = 0$)

$$V_1 = \frac{R^2 V_0 + k^2 R \omega_0}{R^2 + k^2} = R \omega_1 \quad (\text{B.29})$$

Assuming that we get rolling without slipping during the second hit, we have that the rim velocity of the ball at the point of impact is again zero, i.e.

$$V_2 + R \omega_2 = 0 \quad (\text{B.30})$$

Conservation of momentum yields

$$\int F_T dt = m(V_1 - V_2) \quad (B.31)$$

and

$$R \int F_T dt = I(\omega_1 - \omega_2) \quad (B.32)$$

giving

$$mR^2(V_1 - V_2) = I(R\omega_1 - R\omega_2) \quad (B.33)$$

which is different in sign from the result of the previous hit because the sense of the tangent force relative to the angular velocity is reversed.

Solving for V_2 in this case, we find that

$$V_2 = \frac{mR^2 V_1 - IR\omega_1}{mR^2 + I} \quad (B.34)$$

Applying the initial condition that after impact Number 1 we had

$$V_1 - R\omega_1 = 0 \quad (B.35)$$

gives

$$V_2 = \frac{mR^2 - I}{mR^2 + I} V_1 \quad (B.36)$$

It is clear that if the ball proceeds down the channel by rolling without slipping at each hit that in all hits after the first it will lose the same fraction of its down channel velocity. Thus in terms of V_1 , the velocity after the first hit, we have after the n^{th} hit

$$V_n = \left(\frac{mR^2 - I}{mR^2 + I} \right)^{n-1} V_1 \quad (B.37)$$

For a solid homogeneous sphere ($I = \frac{2}{5} mR^2$) this becomes

$$V_n = \left(\frac{3}{7} \right)^{n-1} V_1 \quad (B.38)$$

V_1 of course depends on the initial condition. For the case where the ball enters non-spinning (i.e., $R\omega_0 = 0$) we have

$$V_1 = \frac{R^2}{R^2 + k^2} V_0 \quad (\text{B. 39})$$

and for a solid homogeneous sphere this is

$$V_1 = \frac{5}{7} V_0 \quad (\text{B. 40})$$

Thus after six hits the down channel velocity of a solid sphere will have decreased to less than 1% of its initial value.

To determine the conditions under which the rolling without slipping will apply we look at the second hit, since it is typical (as regards initial conditions) of all subsequent hits.

We had

$$V_2 = \left[(R^2 - k^2) / (R^2 + k^2) \right] V_1 \quad (\text{B. 41})$$

We will get rolling without slipping if the following conditions are satisfied

$$V_2 - V_1 \leq \mu(1 + e) V_1, \quad u_1 = e_1 u_0 \quad (\text{B. 42})$$

or in terms of V_1

$$2\sigma V_1 \leq \mu(1 + e_1) u_1 \quad \text{where} \quad \sigma \equiv k^2 / (R^2 + k^2) \quad (\text{B. 43})$$

Now at the third hit we will get rolling without slipping if

$$V_3 - V_2 = 2\sigma V_2 < \mu(1 + e_1) u_2 \quad (\text{B. 44})$$

Now

$$V_2 = (1 - 2\sigma) V_1 \quad (\text{B. 45})$$

and

$$u_2 = e_1 u_1 \quad (\text{B. 46})$$

Thus we have

$$2\sigma(1 - 2\sigma) V_1 \leq e_1 \mu(1 + e_1) u_1 \quad (\text{B. 47})$$

or

$$2\sigma V_1 \leq \mu(1 + e_1) u_1 (e_1)/(1 - 2\sigma) \quad (\text{B. 48})$$

For rolling without slipping at the second hit we had

$$2\sigma V_1 \leq \mu(1 + e_1) u_1 \quad (\text{B. 49})$$

Thus we will have rolling without slipping on all subsequent hits if

$$e_1/(1 - 2\sigma) \geq 1 \quad (\text{B. 50})$$

or

$$e_1 \geq 1 - 2\sigma = (R^2 - k^2)/(R^2 + k^2) \quad (\text{B. 51})$$

For the solid homogeneous sphere this means we must have

$$e_1 \geq \frac{3}{7} \quad (\text{B. 52})$$

which is not a very high coefficient of restitution.

To recapitulate we will get rolling without slipping from the second hit on if the following are satisfied

$$\frac{V_1}{u_1} = \tan \alpha_1 \leq \mu(1 + e_1)/2\sigma \leq \frac{\mu}{\sigma} = \mu \left[1 + \frac{R^2}{k^2} \right] \quad (\text{B. 53})$$

and

$$e_1 \geq (R^2 - k^2)/(R^2 + k^2) \quad (\text{B. 54})$$

For the solid sphere these conditions are

$$\tan \alpha_1 \leq \frac{7\mu}{2} \quad (\text{B. 55})$$

$$e_1 \geq \frac{3}{7} \quad (\text{B. 56})$$

We can now determine the initial conditions under which the above conditions will follow.

We need to roll without slipping at the first hit which requires that

$$(V_0 - R\omega_0) \sigma \leq \mu(1 + e_1) u_0 \quad (\text{B. 57})$$

and also we need to roll without slipping at the second hit which requires that

$$2\sigma V_1 \leq \mu(1 + e_1) u_1 \quad (\text{B. 58})$$

Now

$$V_1 = (1 - \sigma) V_0 + \sigma R\omega_0 \quad (\text{B. 59})$$

and

$$u_1 = e_1 u_0 \quad (\text{B. 60})$$

In terms of these the second condition is

$$2\sigma[(1 - \sigma) V_0 + \sigma R \omega_0] \leq \mu(1 + e_1) e_1 u_0 \quad (\text{B. 61})$$

or

$$\sigma(V_0 - R \omega_0) \leq \frac{e_1}{2[1 - \sigma + R \omega_0 / (V_0 - R \omega_0)]} \mu(1 + e_1) u_0 \quad (\text{B. 62})$$

One additional fact of interest is the distance the ball will travel down the channel after the first hit.

We have for a channel of height h , that the distance d_1 between the first and second hits is

$$d_1 = V_1 t_1 = h \tan \delta_1 \quad (\text{B. 63})$$

Now

$$V_2 = (R^2 - k^2)/(R^2 + k^2) V_1 \equiv \rho V_1 \quad (\text{B. 64})$$

and

$$t_2 = \frac{h}{u_2} = \frac{h}{e_1 u_1} = t_1 / e_1 \quad (\text{B. 65})$$

Thus

$$d_2 = V_2 t_2 = \rho \frac{V_1 t_1}{e_1} = \frac{\rho d_1}{e_1} \quad (\text{B. 66})$$

and the total d after n hits is

$$d = \sum_{n=1}^n d_n = d_1 \left[1 + \frac{\rho}{e_1} + \left(\frac{\rho}{e_1}\right)^2 \dots + \left(\frac{\rho}{e_1}\right)^n \right] \quad (\text{B.67})$$

$$d = \frac{d_1 \left[1 - (\rho/e_1)^n \right]}{1 - \rho/e_1} \cong \frac{d_1}{1 - \rho/e_1} \quad \text{for } \frac{\rho}{e_1} < 1 \quad (\text{B.68})$$

For the solid sphere we have $\rho = \frac{2}{7}$. For a reasonably good e_1 say $e_1 = \frac{5}{7}$ we would then have

$$d = h \tan \alpha_1 / (1 - 2/5) = \frac{5}{3} h \tan \alpha_1 \quad (\text{B.69})$$

Clearly the better e_1 (i.e., the closer to 1) the smaller d . In the limit for a sphere with $e_1 = 1$ we would have

$$d = \frac{7}{5} h \tan \alpha_1 \quad (\text{B.70})$$

For the case of a hollow shell-like sphere with $I = \frac{2}{3} mR^2$

$$\rho = (1 - 2/3) / (1 + 2/3) = \frac{1}{5} \quad (\text{B.71})$$

We would have, for $e_1 \cong 1$

$$d = h \tan \alpha_1 / (1 - 1/5) = \frac{5}{4} h \tan \alpha_1 \quad (\text{B.72})$$

For a handball (hollow rubber ball) we have

$$I \cong \frac{1}{2} mR^2 \quad (\text{B.73})$$

$$\rho = \frac{1 - 1/2}{1 + 1/2} = \frac{1}{3} \quad , \quad e_1 = \frac{2}{3} \quad (\text{B.74})$$

$$d = 2h \tan \alpha_1 \quad (\text{B.75})$$

Appendix C

PSEUDO RATE LIMIT CYCLE PERFORMANCE

In the control of the drag-free satellite, we are primarily interested in the limit cycle performance. An important tool in the investigation of limit cycle performance is the phase plane diagram of the limit cycle. The drag free satellite limit cycle for the axis opposing drag is shown in Fig. C-1. The kinematic relations indicated follow directly from the parabolic nature of trajectories. This limit cycle strictly applies only to the single axis system. We know from steady-state symmetry that if a limit cycle is present it must look like this (in the x, \dot{x} plane) irrespective of the form of the switching line(s).

For a system using a linear combination of position and actual rate with hysteresis (HYS) and dead band (DB) the switching lines would be as indicated by the dashed lines in the figure. For the pseudo rate system of Chapter 4, the switching lines are not straight because switching is accomplished by position plus a pseudo rate which is not linearly related to the actual rate. As the following analysis shows, the pseudo rate is exponentially related to the actual rate which means that the switching lines (in the x, \dot{x}_p plane) would be segments of exponentials as indicated in Fig. C-1.

From the block diagram of Fig. 4-6 we have for \dot{x} and \dot{x}_p during thrust on:

$$\ddot{x} = f_d - f_c = (1 - \gamma) f_d \quad (C. 1)$$

$$\ddot{x}_p = -\frac{\dot{x}_p}{T_1} - f_c = -\frac{\dot{x}_p + \gamma T_1 f_d}{T_1} \quad (C. 2)$$

which gives

$$\dot{x} = \dot{x}_o - (\gamma - 1) f_d t \quad (C. 3)$$

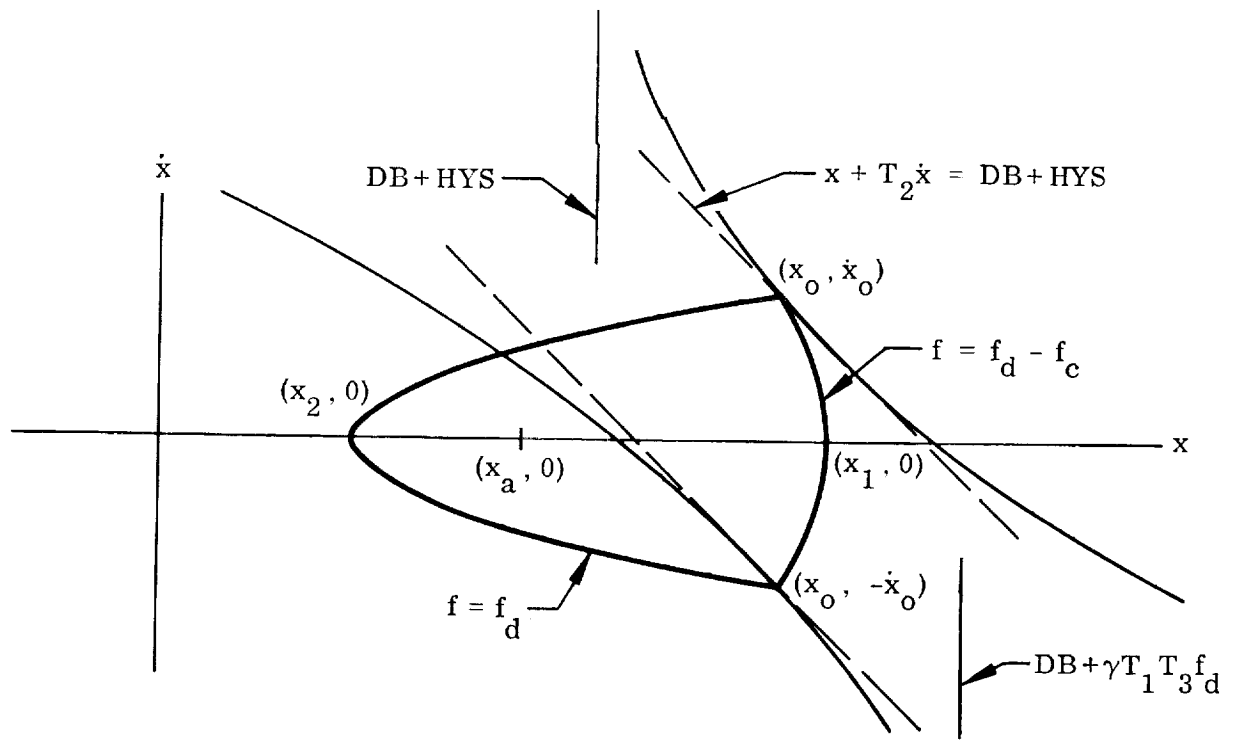
$$\dot{x}_p = (\dot{x}_{po} + \gamma T_1 f_d) \exp(-t/T_1) - \gamma T_1 f_d \quad (C. 4)$$

and

$$\dot{x}_p = (\dot{x}_{po} + \gamma T_1 f_d) \exp[(\dot{x} - \dot{x}_o)/(\gamma - 1) f_d T_1] - \gamma T_1 f_d \quad (C. 5)$$

during thrust off:

$$\ddot{x} = f_d \quad (C. 6)$$



f_d Causes \dot{x} to increase

\dot{x} Forward velocity of ball relative to vehicle

x Forward relative displacement of ball

$$x_{01} \triangleq |x_1 - x_0| \quad ; \quad t_{01} \triangleq |t_1 - t_0| \quad ; \quad \gamma \triangleq |f_c/f_d| \quad ; \quad T \triangleq 2(t_{01} + t_{02}) = \text{period}$$

$$x_0 = \text{Switching line intercepts} = DB + \frac{1}{2} HYS + T_1 T_2 f_d$$

KINEMATIC RELATIONS

$$x_{01} = \frac{1}{2} (\gamma - 1) f_d t_{01}^2 = \frac{1}{2} f_d t_{01} t_{02} = \frac{x_0^2}{2(\gamma - 1) f_d} = \frac{1}{2} \dot{x}_0 t_{01}$$

$$x_{02} = (\gamma - 1) x_{01} = \frac{x_0^2}{\gamma f_d} = \frac{1}{2} f_d t_{02}^2 = \frac{1}{2} \dot{x}_0 t_{02}$$

$$x_{13} = \gamma x_{01} = \frac{1}{2} \gamma (\gamma - 1) f_d t_{01}^2 = \frac{1}{2} \dot{x}_0 t_{12} = \frac{1}{2} f_d t_{01} t_{02}$$

$$\dot{x}_0 = (\gamma - 1) f_d t_{01} = f_d t_{02} = \sqrt{2 f_d x_{02}} = \sqrt{2(\gamma - 1) f_d x_{01}} = \frac{2x_{01}}{t_{01}} = \frac{4x_{12}}{T}$$

$$x_a = \text{time average value of } x = x_0 - \frac{2}{3} (\gamma - 2) x_{01}$$

Fig. C-1 Limit Cycle Phase Plane Diagram

$$\ddot{x}_p = -\frac{\dot{x}_p}{T_1} \quad (C.7)$$

giving

$$\dot{x} = -\dot{x}_o + f_d t \quad (C.8)$$

$$\dot{x}_p = \dot{x}_{pf} \exp(-t/T_1) \quad (C.9)$$

$$\dot{x}_p = \dot{x}_{pf} \exp[-(\dot{x} + \dot{x}_o)/f_d T_1] \quad (C.10)$$

Now \dot{x}_{po} , the initial value of \dot{x}_p at thrust on, is equal to the final value of \dot{x}_p during thrust off (i.e., at $\dot{x} = \dot{x}_o$ in steady state). Thus

$$\dot{x}_{po} = \dot{x}_{pf} \exp[-2\dot{x}_o/f_d T_1] \quad (C.11)$$

Similarly \dot{x}_{pf} , the initial value of \dot{x}_p at thrust off is equal to the final value of \dot{x}_p during thrust on (i.e., at $\dot{x} = -\dot{x}_o$). Thus

$$\dot{x}_{pf} = (\dot{x}_{po} + \gamma T_1 f_d) \exp[-2\dot{x}_o/(\gamma - 1) f_d T_1] - \gamma T_1 f_d \quad (C.12)$$

Solving for \dot{x}_{pf} and \dot{x}_{po} in Eqs. (C.11) and (C.12) gives

$$\dot{x}_{pf} = -\gamma T_1 f_d \frac{1 - \exp[-2\dot{x}_o/(\gamma - 1) f_d T_1]}{1 - \exp[-2\gamma\dot{x}_o/(\gamma - 1) f_d T_1]} \quad (C.13)$$

from which

$$-\gamma T_1 f_d < \dot{x}_{pf} < 0 \quad (C.14)$$

and

$$-\gamma T_1 f_d \exp(-2\dot{x}_o/f_d T_1) < \dot{x}_{po} < 0 \quad (C.15)$$

During thrust on the switching line that applies (to turn the thrust off) is

$$x + T_2 \dot{x}_p = DB \quad (C.16)$$

By putting the value of \dot{x}_p from Eq. (C.5) into Eq. (C.16) we get the turn-off switching line in the $x-\dot{x}$ plane, viz.

$$x + T_2(\dot{x}_{po} + \gamma T_1 f_d) \exp [(\dot{x} - \dot{x}_o)/(\gamma - 1) f_d T_1] = DB + \gamma f_d T_1 T_2 \quad (C.17)$$

For $\dot{x} \ll 0$, x approaches $DB + \gamma f_d T_1 T_2$ asymptotically. From Eq. (C.15) we know $\dot{x}_{po} + \gamma T_1 f_d > 0$. Thus for $\dot{x} \gg 0$, $-x$ grows exponentially with \dot{x} .

During thrust-off the switching line that applies (to turn thrust-on) is

$$x + T_2 \dot{x}_p = DB + HYS \quad (C.18)$$

Putting the value of \dot{x}_p from Eq. (C-10) we get the turn-on switching line in the $x-\dot{x}$ plane, viz.

$$x + T_2 \dot{x}_{pf} \exp [-(\dot{x} + \dot{x}_o)/f_d T_1] = HYS + DB \quad (C.19)$$

For $\dot{x} \gg 0$, x approaches $HYS + DB$ asymptotically. Since $\dot{x}_{pf} < 0$, x increases exponentially with $-\dot{x}$. These lines are indicated in Fig. C-1.

The implication of the values of the asymptotes is that, since the off-line asymptote must be to the right of the on-line asymptote for a stable limit cycle, we have that

$$\gamma T_1 T_2 f_d > HYS \quad (C.20)$$

This may be viewed as the requirement that the rate gain must be large enough to overcome the delay of the hysteresis.

By taking the average of Eqs. (C.5) and (C.10) we can find that the average value of \dot{x}_p is

$$[\dot{x}_p]_{av} = -f_d T_1 \quad (C.21)$$

and for the linear approximation in which the limit cycle period is small compared to the integration time constant T_1 i.e., for

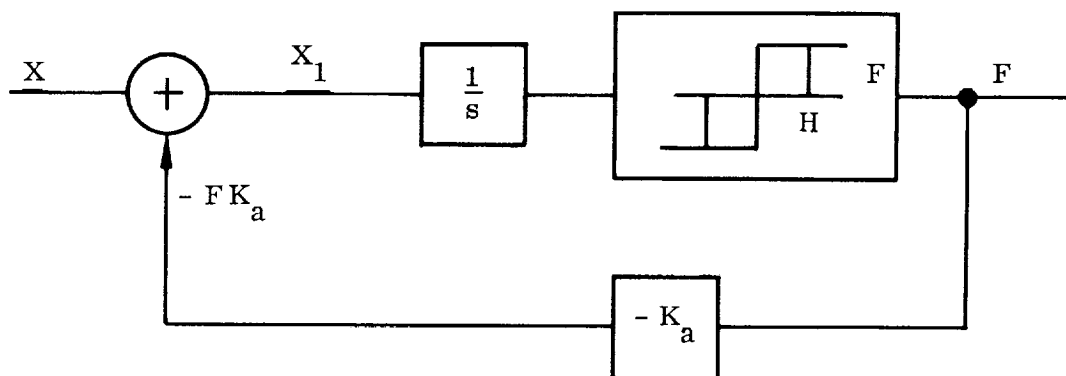
$$\frac{2\gamma\dot{x}_o}{(\gamma - 1)f_d} \ll T_1 \quad (C. 22)$$

we find that \dot{x}_p goes from $(\dot{x}_{po} \cong -T_1 f_d + \dot{x}_o)$ to $(\dot{x}_{pf} \cong -T_1 f_d - \dot{x}_o)$ as \dot{x} goes from (\dot{x}_o) to $(-\dot{x}_o)$. Thus in steady state $\Delta\dot{x}_p \cong \Delta\dot{x}$ and we observe that the effect of the pseudo rate is to provide a rate \dot{x}_p which tracks the true rate \dot{x} , but with an offset equal to $-T_1 f_d$. This is equivalent to increasing the dead band by the amount $T_2 T_1 f_d$.

In summary, to achieve stable limit cycle operation with pseudo rate we must choose the parameters such that $\gamma T_1 T_2 f_d > \text{HYS}$. We will get an effective dead band equal to $\text{DB} + T_1 T_2 f_d$, and the value of x_o the vertical line in Fig. C-1, will be $\text{DB} + T_1 T_2 f_d + 1/2 \text{HYS}$.

Appendix D PWPF CONTROL

The following analysis indicates the theory of operation of the PWPF control. A block diagram of the control is shown below



The following applies for input $X = \text{constant}$. Consider the system immediately after thrust turn on. At this time we have

$$X_1 = X - FK_a \quad (\text{D. 1})$$

The duration of thrust (T_T) is given by

$$T_T(FK_a - X) = H \quad (\text{D. 2})$$

At thrust off we have

$$X_1 = X \quad (\text{D. 3})$$

and the time between thrusts (T_0) is given by

$$T_0 X = H \quad (\text{D. 4})$$

The total period is

$$T = T_0 + T_T \quad (D. 5)$$

$$T = H \left(\frac{1}{X} + \frac{1}{FK_a - X} \right) = \frac{HFK_a}{X(FK_a - X)}$$

and the frequency is $1/T$, i.e.,

$$f = \frac{X(FK_a - X)}{HFK_a} \quad (D. 6)$$

Thus the frequency is parabolic in X , the value of the input.

The thrust factor F_T is given by

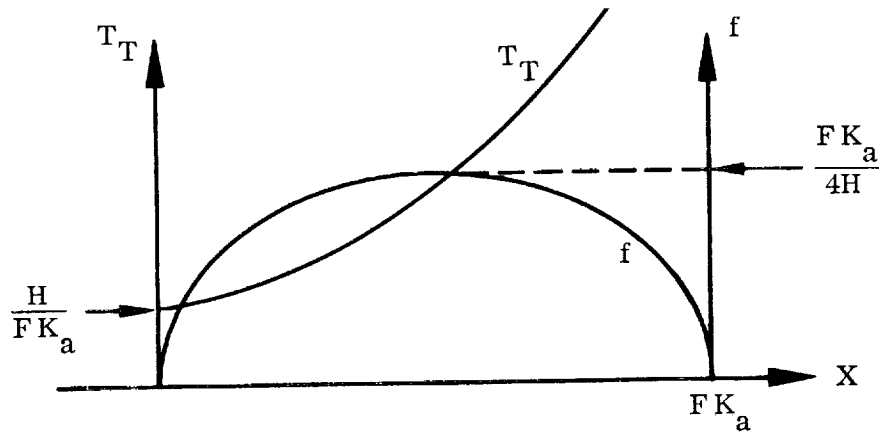
$$F_T = \frac{T_T}{T} = \frac{X}{FK_a} \quad (D. 7)$$

which is clearly linear in X .

The maximum frequency, from $\frac{df}{dX} = 0$, is $f_{\max} = \frac{FK_a}{4H}$. The minimum thrust time corresponds to $X = 0$ and is

$$T_{T_{\min}} = \frac{H}{FK_a}$$

The characteristic is shown below:



REFERENCES

1. Lange, B., "The control and use of drag-free satellites," Department of Aeronautics and Astronautics, Stanford University, SUDAER No. 194, June 1964.
2. Danby, J. M. A., "Matrix Methods in the Calculation and Analysis of Orbits," AIAA J., 2, 13-19, 1964.
3. deVries, J. P., "Elliptic Elements in Terms of Small Increments of Position and Velocity Components," AIAA J., 1 No. 11, 2626-29, (1963).
4. Clohessy, W. H. and R. S. Wiltshire, "Terminal Guidance System for Satellite Rendezvous," J. Aerospace Sci., 27, 653-658 (1960).
5. Battin, R. H., Astronautical Guidance (McGraw-Hill Book Co., Inc., New York, 1964), p. 304.
6. Tschauner, J. and Hempel, P., "Rendezvous with a target in an elliptic orbit," Astronaut. Acta, 11, 104-109 (1965).
7. Lange, B. and Smith, R. G., "The application of Floquet theory to the computation of small orbital perturbations over long time intervals using the Tschauner-Hempel equations," Department of Aeronautics and Astronautics, Stanford University, SUDAER No. 241, August 1965.
8. Wintner, A., The Analytic Foundations of Celestial Mechanics, (Princeton University Press, Princeton, 1947), Chap. I.
9. Synge, J. L., Handbuch der Physik, Vol. III, "Classical Dynamics," (Springer-Verlag, Berlin, 1960).
10. Siegel, C. L., Vorlesungen Uber Himmels Mechanik, (Springer-Verlag, Berlin, 1956), Chap. I.
11. Garfinkel, B., "Variation of elements," Notes of the 1961 Yale Summer Institute in Dynamical Astronomy (to appear).
12. Pease, M. C., Methods of Matrix Algebra, (Academic Press, Inc., New York, 1965), Chap. XV.
13. Pars, L. A., Analytical Dynamics (John Wiley & Sons, New York, 1965), p. 490-494.

14. Goldstein, H., Classical Mechanics, Addison Wesley, Reading, Mass. 1959.
15. Webster, A. G., The Dynamics of Particles, Hafner, New York, 1949
16. Weiten, E. F., "A Four Vector Method of Describing the Rotational Motion of Rigid Bodies," Lockheed Missiles & Space Company, Internal Report, February 14, 1964.
17. Gaylord, R. S. and Keller, W. N. "Attitude Control System Using Logically Controlled Pulses," ARS Guidance and Control Conference, Stanford University, August 1961.
18. Kunkle, J. L., "The Agena Pneumatic System," Lockheed Missiles & Space Company, A313082, December 1962.
19. Pistiner, J. S., "On-Off Control System for Attitude Stabilization of a Space Vehicle," ARS J. 29, No. 4, 283-289 (1959)
20. Kalman, R. E. and Bertram, J. E., "Control System Analysis and Design," Trans. ASME, J. Basic Eng., June 1960, pp. 371-393. (Aizerman's paper, in Russian, is referenced and discussed.)
21. Luenberger, D. G., "Observing the State of a Linear System," IEEE Trans. Mil. Elec. MIL-8, No. 2, (1964)
22. Leonard, B. S., "Analysis and Modification of the Derived Rate System for Long Life Attitude Control of Space Vehicles," Lockheed Missiles & Space Company, LMSC/577639, October 2, 1964.
23. Nicklas, J. C. and Vivian, H. C., "Derived Rate Increment Stabilization: Its Application to the Control Problems," JPL Technical Report 32-69, July 1961.
24. Trimmer, H. D., "Pulse Modulation Circuit Studies," Lockheed Missiles & Space Company, November 1959.
25. Coddington, E. A. and N. Levinson, Theory of Ordinary Differential Equations, (McGraw-Hill Book Co., 1955) Ch. 3.
26. Parzen, E., Modern Probability Theory and its Applications, (Wiley & Sons, New York 1960) p. 334.